EBERHARD KARLS
UNIVERSITÄT
TÜBINGEN

Physics-based numerical modeling of surface-groundwater flow and transport at catchment scale

Dissertation

der Mathematisch-Naturwissenschaftlichen Fakultät
der Eberhard Karls Universität Tübingen
zur Erlangung des Grades eines Doktors der Naturwissenschaften
(Dr. rer. nat.)

vorgelegt von

MSc. Aníbal Pérez García
aus Sincelejo, Kolumbien

Tübingen
2011

Tag der mündlichen Qualifikation: 24.06.2011

Dekan: Prof. Dr. Wolfgang Rosenstiel

1. Berichterstatter: Prof. Dr.-Ing Olaf Cirpka

2. Berichterstatter: Prof. Dr. Peter Grathwohl

Contents

List of Figures

List of Tables

Acknowledgements

I would like to take this opportunity to express my gratitude to the people who have provided support throughout my Ph.D. journey. I was very lucky to have them around me.

I feel very happy to have had Dr. Claudius Bürger guide through my Ph.D. study. I am truly grateful for his support. It has been a pleasure working with you Claudius.

I would like to thank Prof. Dr. Olaf Cirpka for his support and the discussions that we always had. I am very happy to have worked with him at this point of my life.

I would like to thank Dr. Jesús Causapé and Dr. Raphael Abrahao for providing ideas and field data I have used in this thesis. They have provided me with a different perspective for looking at things in my Ph.D. work.

I would like to thank my defense committee members Prof. Dr. Peter Grathwohl, Prof. Jens Bange and Prof. Paul Bons for taking time to review my thesis.

I want to thank also all of the Center of Applied Geosciences (ZAG) staff for their help. Also I would like to thank all my friends from the ZAG and especially from the Hydrogeology group. I want also thank Ashutosh for the very constructive discussions and for being a great office partner. Nelson, Fernando and Jozsef for the wonderful discussions and talks. Leonardo, Richy, Katrin, Lorena and Monica for all the help.

I would like to express my gratitude to my family for their support and love. My dad and mom who have devoted their life to making their children happy, my sister and brother for bringing joy to my life.

Finally, I would like to make a very special mention to my wife, Carolina, who has been an essential part of my Ph.D. journey, for her endless love, support and patience.

Abstract

Agriculture representing the main user of water and one of the largest anthropogenic sources of nitrate pollutants, understanding irrigation and fertilization impacts has become a priority issue in water management. The land-use transformation and the intensification of irrigation and fertilization involves spatially distributed changes affecting the hydrological fluxes across the surface and subsurface interface. Hence, the simulation of this transformation requires a model that can deal with complexity in both surface and subsurface.

Empirical and conceptual hydrological models do not explicitly consider physical processes taking place within the catchment so that their ability to evaluate the impact of land-use changes and the evolution of irrigation and fertilization may be questionable. Furthermore, they also fail to provide detailed description of fluxes of solutes in the surface and subsurface.

Physics-based models arises as the best alternative to simulate catchment transition into irrigation agriculture. This type of models use a set of coupled partial differential equations derived from the principles of conserving mass and momentum of water to describe the flow and transport processes at catchment scale. A review of previous studies reveals that they are either associated with natural watersheds without anthropogenic influence, only investigate surface response, or do not account for land-use changes. Their methodologies, that commonly widely differ from each other, typically hold only for their particular case studies and cannot be extrapolated to other studies.

In this investigation, I propose a general methodology for the use of physics-based models. The methodology is applied to investigate the effects of land-use change in the semi-arid Lerma basin (Ebro valley, Spain), which underwent a transition from rainfed towards irrigation agriculture. For four consecutive years, this transition of formerly uncultivated land to irrigated farmland was intensively monitored. A computationally efficient hillslope equivalent is introduced to identify catchment controlling factors, set up an adequate calibration problem and speed-up the validation of complex surface-subsurface models. The method is successfully tested, and used in the calibration of the physics-based model of the Lerma basin.

The calibrated and validated, physics-based, 3-D fully-coupled model is used to study the effect of the transition into agriculture on the hydrological functioning of the basin

for this case study, where spatio-temporal data on cropping patterns, irrigation and fertilizer amounts, and the associated catchment response are available with considerably high resolution. Validation results show that the physics-based model is able to simulate and predict the impact of the land-use transformation and irrigation on surface and subsurface flow dynamics with high accuracy. Sensitivity and correlation analyses about the calibrated model parameter vector indicate that the set of calibrated parameters is identifiable and locally unique for the parameter zonation defined using information on lithological units and texture data.

In order to indicate changes in the runoff generation process and catchment functioning, the evolution of the total stream length and the average infiltration capacity provided by the model were studied. The results show that irrigation agriculture has raised the base level of the water table of the Lerma aquifer causing new portions of the drainage network to become perennial. An approximate infiltration capacity is introduced to study the evolution of the runoff-generation processes during the transformation. Yet, spatially distributed values of exfiltrating fluxes are directly obtained from the model. Both the approximate infiltration capacity curve and the contribution of exfiltration to stream flow are consistent in indicating a shift from Hortonian towards Dunne flow runoff generating processes triggered by the land-use change and the intensification of irrigation.

A conservative transport model is integrated to the validated flow model of the Lerma basin in order to simulate the impact of the transformation also on water quality, and to predict concentrations under different water management scenarios. Validation results indicates that despite the lack of data to describe the nitrogen transformation processes and many simplifying assumptions, it is possible to simulate transport at catchment systems with a parsimonious physics-based approach.

Chapter 1

Introduction

1.1 Motivation

In the last century, irrigated agriculture has expanded around the world by 480% (from 47.3 MHa in 1900 to 276.3 MHa in 2000). Nowadays it represents 18% ($\sim$ 280 MHa) of the global croplands and projections - focusing exclusively on developing countries - claim a further increase of 20% (up to a total of $\sim$ 330 MHa) by 2030 (Scanlon et al., 2007). In semi-arid areas, irrigation fosters crop productivity and allows for intensification and diversification of agriculture. As a backdrop, irrigation consumes 90% of global freshwater (Shiklomanov, 2000) and degrades water quality by flushing nutrients into soils and aquifers.

In the central Ebro valley (northern Spain), agriculture represents the main use of water and the majority of agricultural production relies on irrigation. The immense amount of water needed is supplied by a well-structured man-made channel network, which is fed by reservoirs located up to 100 kilometers north in the higher Pyrenees. In recent years, the total irrigation amount has increased constantly, which has led to increased efforts to study the effectiveness of irrigation practices. Spanish researchers have begun to monitor larger irrigation districts in detail. Studies in the Bardenas irrigation district, (Causapé et al., 2004; Causape et al., 2006) suggest that the intensification of irrigation has caused a considerable increase in nitrate within the drainage network. This may put the sustainability of these agricultural practices at risk. Despite the ongoing efforts, more comprehensive studies to improve the understanding of the impact of irrigation and land-use change on the surface-subsurface flow dynamics are still missing. One way to gain better insight in the latter could be by detailed modeling, where flow and transport processes are quantitatively described to a level consistent with available data series.

The Lerma basin ($7.5 km^2$ in size) is a semi-arid, formerly fallow land, whose transformation into an irrigation agriculture catchment was closely monitored by Spanish researchers. Since October 2005 pre-defined plots were gradually opened to local farmers

for cropping and irrigation agriculture. In conjunction with the transformation, irrigation water amounts, crop pattern, and fertilizer application was documented plot-wise and stream-discharge measured in 15-minute intervals at the basin outlet. Nitrate concentrations were measured at first in daily intervals and since 2008 also in 15-minute intervals at the basin outlet. Field observations comparing the hydrological year 2006 with subsequent years show that the intermittent main creek in Lerma basin has become a perennial stream due to irrigation. Considerable groundwater exfiltration is therefore evident. This indicates a shift in runoff generation processes during the monitoring period.

The goal for the Lerma basin study is the development of a model for the evaluation of the sustainability of current agricultural practices. In this context, the fate and transport of nitrate is of primary importance. The determination of surface-subsurface velocity fields and/or time variant travel-time distributions are a prerequisite for transport simulation. Also the explicit consideration of the spatial distribution of transport parameters along different transport paths becomes important.

Empirical models based on the estimation of a functional relationship between concurrent input and output datasets have been typically used in most catchment scale studies. Per definition, this type of models fail when the input signal presented to the model does not follow the statistics of the datasets used to obtain the relationship. Indeed, the output could even be physically impossible, such as a negative discharge.

Conceptual hydrological models have been posed as an alternative to empirical models. They rely on a network of interconnected storages, and the routing of water and solutes between these storages is accounted for by semi-empirical relationships. The groundwater domain is often extremely simplified in these models. Hence, they fail to provide details of water flows, soil moistures distributions and descriptions of fluxes of solutes. Additionally, the ability of a conceptual model to evaluate the impact of land-use changes and hypothetical water management scenarios would be questionable due to the semi-empirical nature of the process description.

To assure reliability and predictive power of the model at the Lerma basin, it is important to accurately represent the natural system in question. It implies the use of a model able to account adequately for all spatially distributed surface-subsurface interactions and provide detailed descriptions of solute fluxes. In that respect, I believe that the ongoing land-use change where hydrosystems are forced by increasingly larger amounts of irrigation water and cropping area expansion could be tackled best in a surface-subsurface physics-based approach.

Surface-subsurface, physics-based hydrological models solve the coupled partial differential equations that describe water movement at the surface and in the unsaturated and saturated subsurface. For the solution of (the partial differential) equations, the catchment area and its boundaries are discretized by a grid of points. In that respect, a physics-based model is also a distributed one.

A distributed model requires several thousands of grid nodes to represent the catchment. This increases both the number of parameters and the computation time. Hence, in the context of physics-based models finding a reasonable equilibrium between the number of calibration parameters and the goodness-of-fit represents an additional challenge as any decision may affect the model predictions. This process is referred to in the literature as parameterization. In the parameterization one should be able to identify which parameters can be defined from available field data and which parameters need to some kind of fitting. Eventually, one should also be able to identify potential problems due to high correlation between calibration parameter, and to define an appropriate initial set of parameter values, i.e. the initial guess.

Sensitivity studies methods may be used in the parameterization as they quantify the influence of parameters on model outputs. A common choice to evaluate sensitivities in distributed models is the direct numerical differentiation method. It is performed by repeating the simulations with slightly different parameters. While the evaluation of sensitivity at one point of the parameter space (i.e. local sensitivities) is typically enough for simple cases, for surface-subsurface coupled models repetitions of this local method at many points of the parameter space (i.e. global sensitivities) are required. Such analysis implies huge computation times in physics-based models due to the fairly high spatial resolution that they need. In that respect, model geometrical simplification would be desirable to speed-up the parameterization.

Obviously, sole reliance on computer modeling is not a wise choice for predicting the coupled hydrologic response of complex hydrosystems. Unfortunately, enough data do not exist to rigorously validate uncalibrated deterministic models at catchment scale. Therefore, the inference of model parameters is performed using measurements of dependent quantities, such as hydraulic heads, flow discharge or solute concentrations. In this respect, it would be possible to find more than one parameter set providing an equally good representation of overall hydrologic response. However, in a physics-based model the space of possible parameter values and their combinations can be constrained. Without the physics, the definition of such constraints may become cumbersome and any combination could be valid.

A review of previous studies reveals that they are either associated with natural watersheds without anthropogenic influence, only investigate the surface hydrological response, do not account for land-use changes, or are exclusively focused on flow dynamics disregarding water quality issues. Additionally, they fail to present a general methodology that may be extrapolated to other studies. This study differs from others physics-based approaches because: (1) it presents a general methodology that holds for any physics-based model at catchment scale, (2) considers the ongoing land-use transformation, (3) account for the strong influence of irrigation on the whole hydrosystem, and (4) simulates the flow and transport integrated response of the basin.

1.2 Objectives

The main goal of this thesis is to improve our understanding how the transformation of rainfed basin towards irrigation agriculture impacts the hydrological functioning and water quality. For this purpose, a fully-integrated surface-subsurface, physics-based model is used. The pursuit of this goal is performed in a three-step procedure. The first step aims to investigate the ability of physics-based flow models to simulate catchment systems under land-use change and strong anthropogenic influence. To address it the following research questions are formulated:

- How can we develop a surface-subsurface physics-based flow model at catchment scale? How can we validate such a model?
- How can we determine the influence of catchment controlling factors from typically available observations? To what extent can a geometrical simplification be used to parameterize a physics-based model? What are the factors that control the surface-subsurface hydrological response at catchment scale?
- To what extent can surface-subsurface spatial and temporal flow dynamics be explained by a physics-based model? What are field data and spatial resolution requirements to reproduce adequately those dynamics at catchment scale?

The second step aims to investigate the effect of the intensification of agricultural activities on the basin hydrological functioning. This step give rise to two more research questions:

- How can spatially and temporal resolved variables obtained from a physics-based model be used to define the impact of the transformation from rainfed into irrigation agriculture at catchment scale? What are the benefits of using a surface-subsurface physics-based model?
- What are the hydrological processes affected by such transformation? How does this transformation influence the surface-subsurface dynamics?

In the third step, the ability of a parsimonious physics-based nitrate transport model coupled to the flow model is investigated to simulate the measured concentrations. To address the latter the following research question is formulated:

- To what extent can a conservative physics-based model reproduce the nitrate fate and transport at catchment scale? How can this model be used to predict local impacts of the ongoing change?

To answer these research questions, the available dataset at the Lerma basin is used, which includes precipitation, stream discharge, nitrate concentrations and irrigation measurements; estimation of reference evapotranspiration; and records of crop patterns and fertilization.

1.3 Thesis Outline

The thesis is organized as follows: In Chapter 2, the different components of the hydrological cycle are briefly presented. Typical approaches, formulations and assumptions for each component are also introduced. A brief introduction to hydrological models is also given. Finally, an overview of previous applications of flow and transport models in the context of physics-based approaches is presented. In Chapter 3, the governing equations that describe flow and transport processes at the surface and subsurface and their interaction are briefly reviewed.

In Chapter 4, a model protocol to be used in the construction of distributed, physic-based model is presented. Following, in Chapter 5, a novel geometrical simplification is introduced that allows us to identify catchment controlling parameters in physics-based models. Later in this chapter, the simplification is tested using the well-known Borden site experiment dataset.

In Chapter 6, the model application to the Lerma basin is presented. First, the available datasets are presented. Boundary conditions are defined and an appropriate initial condition for the flow model is generated. A formal parameterization of the flow model which makes use of the simplification presented in Chapter 5 is discussed. Following, findings of the parameterization are used to define the set of calibration parameters and the calibration parameter space. Calibration and validation of the flow model are presented. Performance measures, uniqueness and identifiability of the set of calibrated parameters are also discussed. The flow model is then used to analyze more spatially and temporally resolved variables. Finally, the construction of a nitrate transport model is presented. The results obtained with the transport model are also discussed in this section.

Chapter 7 summarizes the content of this investigation. Results are discussed in a broad perspective. A critical assessment of the present investigation is performed. Also, future applications of the model are briefly discussed.

Chapter 2

Physics-based Models

In this chapter, I review different approaches for physics-based model. Section 2.1 discusses the hydrological cycle and its different components. Formulations and assumptions for each component are introduced. Section 2.2 presents a brief introduction to hydrological models. Finally, section 2.3 gives an overview of previous applications of flow and transport models in the context of physics-based approaches.

2.1 Components of the Hydrologic Cycle

In order to study the hydrologic cycle, the drainage basin (watershed or catchment) is used as the control volume. Basic conservation equations can be applied. The basin or catchment is defined as the area that topographically appears to contribute all the water that passes through a given cross-section of a stream (Dingman, 2002). The conventional method of basin delineation requires a topographic map or a digital elevation model (DEM). DEMs are data files of land-surface elevations at grid points and they are commonly obtained via radar systems (e.g. Shuttle Radar Topography Mission (SRTM)).

The hydrologic cycle as illustrated in Figure 2.1 is a complex network of inflows and outflows that may be conveniently expressed as:

$$I - O = \Delta S \tag{2.1}$$

This equation is usually called the water balance or the hydrologic equation, where I represents the sum of all inflows, i.e. precipitation, irrigation, groundwater inflows; and O represents the outflows, i.e. evapotranspiration, groundwater outflows and stream discharge (surface runoff). Over a reasonably long time period without significant trends in climate and anthropogenic inputs or outputs, one could neglect net changes of storage, so that for such period $\Delta S = 0$. Unfortunately, this idealized condition is rarely found in reality and more complex approaches are needed.

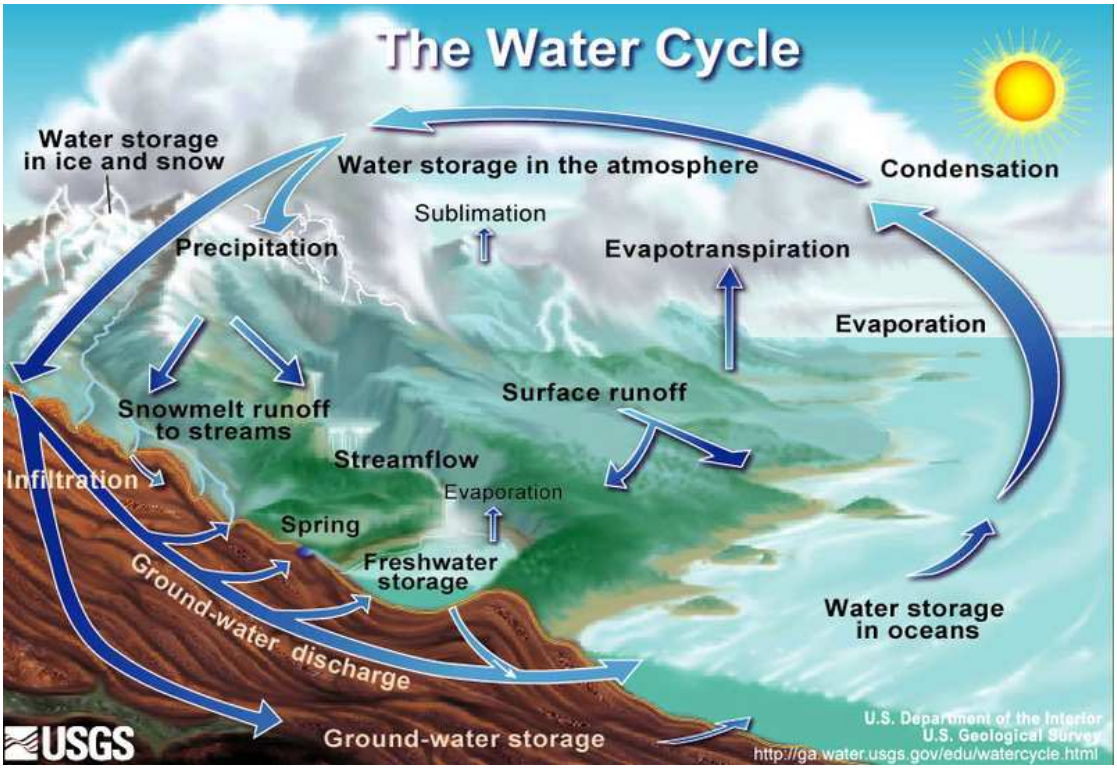

Figure 2.1: Hydrological cycle (Source: http://ga.water.usgs.gov/edu/watercycle.html)

Most hydrological studies aim to understand the hydrological response of the drainage basin. For this goal, it is important to comprehend the interactions between the components of the hydrological cycle. In the following, this chapter will be focus on the discussion of different features regarding the main components of the hydrological cycle: precipitation, evapotranspiration, surface runoff, infiltration and groundwater flow.

2.1.1 Precipitation

All water enters the land phase of the hydrologic cycle as precipitation. Hence, its temporal and spatial distribution controls the basin hydrologic response. Commonly, the measurement of precipitation is performed using a vessel open to the air at the point of observation, and periodically (pluviometer) or continuously (pluviograph) record the quantity of water it collects. Recorded point values are used to estimate regional precipitation. In small basins, the point values are taken as representative for the whole basin or averaged values -weighted or arithmetically- are calculated from close-by pluviometric stations. In larger areas, Thyssen polygons or interpolation methods (e.g. Kriging, Spline or IDW) are employed to estimate the spatial distribution of precipitation.

The transient behavior of precipitation is another important aspect of the hydrological response of a catchment, as it largely determines the seasonality of other hydrologic quantities such as streamflow and groundwater recharge. In arid and semiarid regions, such influence is enhanced due to huge differences between dry and wet periods, and because

of the rapid and intense character of the precipitation events. In this respect, temporal resolution of the available precipitation measurements becomes a controlling factor when studying the catchment hydrological response.

2.1.2 Evapotranspiration

Evapotranspiration is a collective term to account for all processes by which water at or near the surface becomes atmospheric water vapor. The term includes evaporation from rivers, lakes, bare soil and vegetative surfaces and from within the leaves of plants (transpiration). Direct measurement of evapotranspiration is very difficult and expensive, therefore various models have been developed to estimate evapotranspiration based on more easily measured quantities.

A free-water evaporation theoretical concept was introduced to group general methods for estimating evapotranspiration, that neglect advection and changes in heat storage. Different approaches have been used to calculate evaporation from free water: water-balance, mass transfer, Eddy-correlation, energy balance and the so-called Penman or combination approach can be mentioned. Among them, the Penman approach (Penman, 1956) is the most extensively used method to estimate evapotranspiration from free surface water. It relies on the combination of the mass transfer concept and energy-balance approaches. The conceptual idea of the method could be expressed as:

$$E \propto \frac{\triangle \times \text{net radiation} + \gamma \times \text{mass transfer}}{\triangle + \gamma} \tag{2.2}$$

From this, it can be stated that the evaporation rate, E, is proportional to a weighted sum of a rate due to net radiation and a rate due to mass transfer. The weighting is given by the psychometric constant, γ; and the derivative of the saturation pressure e_{sat} curve with respect to temperature T at the air temperature T_a, expressed as:

$$\triangle = \left.\frac{\partial e_{sat}}{\partial T}\right|_{T_a} \tag{2.3}$$

The net radiation can be expressed based on the energy balance as:

$$\text{net radiation} = \frac{K + L - G + A_w - \Delta Q/\Delta t}{\rho_w \lambda_v} \tag{2.4}$$

where net radiation is expressed in the volume of water transferred by unit of time and area. K $[EL^{-2}T^{-1}]$ is the net short-wave radiation which depends on the solar radiation and the reflectivity of the water surface (albedo); L $[EL^{-2}T^{-1}]$ is the net long-wave radiation; G $[EL^{-2}T^{-1}]$ is the net conduction to the ground; A_w $[EL^{-2}T^{-1}]$ is the net water advected energy (inflows and outflows); and $\Delta Q/\Delta t$ $[EL^{-2}T^{-1}]$ is the change in the

amount of heat stored in the body during the time Δt. ρ_w $[ML^{-3}]$ is the mass density of water, and λ_v $[EM^{-1}]$ is the latent heat of evaporation.

In the combination approach, the mass transfer relation is assumed to depend on the difference between the actual vapor pressure e_a and the saturation vapor pressure at the air temperature $e_{sat}(T_a)$ $[ML^{-2}]$ rather than at the water surface. Thus, the mass transfer can be written as:

$$\text{mass transfer} = f(\upsilon_a)(e_{sat}(T_a) - e_a) \tag{2.5}$$

where $f(\upsilon_a)$ $[L^3M^{-1}T^{-1}]$ is a function of the wind speed υ_a $[LT^{-1}]$ that represents the aerodynamic conductance (inverse of the aerodynamic resistance) of the transport of water vapor from the surface to a reference height.

The relative humidity, W_a $[-]$, which can be directly measured at a representative location is expressed as:

$$W_a = \frac{e_a}{e_{sat}(T_a)} \tag{2.6}$$

So that, the equation 2.5 can be re-written as:

$$\text{mass transfer} = f(\upsilon_a)e_{sat}(T_a)(1 - W_a) \tag{2.7}$$

By replacing Equations 2.7 and 2.4 in Equation 2.2 and neglecting the water-advected energy A_w, and the change in heat storage ($\Delta Q/\Delta t$), the generalized Penman equation is obtained:

$$E = \frac{\triangle(K + L - G) + \gamma\rho_w\lambda_v[f(\upsilon_a)e_{sat}(T_a)(1 - W_a)]}{\rho_w\lambda_v(\triangle + \gamma)} \tag{2.8}$$

with E $[LT^{-1}]$ being the evaporation from a wet surface.

Transpiration is a two-step process, in which water molecules pass (1) from the stomatal cavity to the leaf surface and (2) from the leaf surface into the atmosphere. The latter results in a system of two resistances in series: the leaf and aerodynamic resistances, respectively. In analogy to electric-circuit, a vegetated surface like grass or crop can be thought as a large number of leaf resistances in parallel. The total resistance may be calculated as the reciprocal of the sum of the reciprocals of the individual resistances. From this perspective, it is reasonable to represent a relatively uniform vegetated surface as single *big leaf* whose total resistance is the multiplicative inverse of the sum of the reciprocal of individual leaves resistances (Dingman, 2002) called the *canopy resistance*.

The well-known approach presented by Monteith (1965) introduced a modified version of Penman equation to represent not just the evaporation but also the transpiration from a vegetated surface. This relation has become known as the *Penman-Monteith* equation, and is derived by incorporating the canopy resistance in the Penman equation. Mon-

teith (1965) proved that a leaf can be treated as a free water surface by modifying the psychometric constant in the denominator of the original Penman-equation. The *modified psychometric constant* can be expressed after Monteith (1965) as:

$$\gamma^* = \gamma(1 + r_c * f(\upsilon_a)) \tag{2.9}$$

Replacing γ by γ^* in the denominator of equation 2.8, Penman-Monteith formulation to calculate evapotranspiration ET $[LT^{-1}]$ is obtained:

$$ET = \frac{\triangle(K + L - G) + \gamma\rho_w\lambda_v[f(\upsilon_a)e_{sat}(T_a)(1 - W_a)]}{\rho_w\lambda_v(\triangle + \gamma(1 + r_c * f(\upsilon_a))} \tag{2.10}$$

where r_c is the canopy resistance, which is expected to be a function of the stomatal resistance of individual leaves. Under wet-canopy conditions $r_c = 0$ and the equation 2.10 reduces to equation 2.8.

Over a bare land surface with no standing water, the soil moisture is the only source of water for evaporation. Therefore, the rate of evaporation must depend on the moisture content of the topmost layer of the soil. When the soil surface is fully saturated and the soil moisture content is not a limiting factor of evaporation, this maximum rate of evaporation for the given surface weather conditions is called the potential evaporation rate ET_p that can be calculated by the Penman equation (Eq. 2.8). Nevertheless, very often the potential evaporation rate needs to be reduced, i.e. the actual evaporation rate ET_a need to be calculated. For the estimation of the actual evaporation, the availability of soil moisture needs to be considered. For this purpose, the Penman-Monteith approach can be used since it accounts for transition resistivity within the surface near air layer using the wind speed function $f(\upsilon_a)$ and within the soil, via the canopy resistance r_c.

From the original Penman-Monteith equation and the equations of the aerodynamic and canopy resistance, the Food and Agriculture Organization of the United Nations (FAO) derived the so-called FAO-Penman-Monteith equation (Allen et al., 1998) as:

$$ET_o = \frac{0.408\triangle R_n + \gamma\frac{900}{T_2+273}\upsilon_2(1 - W_a)}{\triangle + \gamma(1 + 0.34\upsilon_2)} \tag{2.11}$$

where ET_o is a reference evapotranspiration in mmd^{-1}, R_n is the net radiation at the crop surface in $MJm^{-2}d^{-1}$ calculated as $K - L$, T_2 is the air temperature at 2 m height $[^\circ C]$ and υ_2 is the wind speed at 2 m height in ms^{-1}.

The FAO Penman-Monteith equation (Eq. 2.11) determines the evapotranspiration from the hypothetical grass reference surface and provides a standard to which evapotranspiration in different periods of the year or in other regions can be compared and to which the evapotranspiration from other crops can be related. To calculate evapotranspiration for a particular crop pattern, the FAO Penman-Monteith equation (Eq. 2.10), in conjunction with meteorological and crop data, can be used.

By adjusting the albedo, and the aerodynamic and canopy surface resistances to the growing characteristics of the specific crop, the evapotranspiration rate can be directly estimated. However, the albedo and resistances are difficult to estimate accurately as they may vary continuously during the growing season due to change of climatic conditions, crop growth, and changes of the soil surface moisture. The canopy resistance will further be influenced by the soil water availability, and it would strongly increase if the crop is subjected to water stress (Allen et al., 1998).

The FAO presented a crop coefficient approach to calculate the *crop* evapotranspiration which would be equivalent to the actual evapotranspiration ET_a from the reference evapotranspiration ET_o that relies upon a crop coefficient k_c:

$$ET_a = k_c ET_o \tag{2.12}$$

k_c integrates the effect of characteristics that distinguish a typical field crop from the grass reference. Such characteristics include crop height, reflectance (albedo) and canopy resistance. Differences in soil evaporation and crop transpiration between field crops and the reference surface are also integrated within the crop coefficient k_c.

The crop height directly influences the aerodynamic conductance (i.e. the wind speed function $f(\upsilon_a)$), and consequently the turbulent transfer of vapor from the crop into the atmosphere. The albedo of the crop/soil surface influences the net radiation of the surface R_n which is the primary source of the energy exchange for the evaporation process. The canopy resistance r_c is affected by leaf area (number of stomata), leaf age and condition, and the degree of stomatal control. Consequently, different surfaces will have different k_c coefficients. Different factors like crop type, crop growth stages, climate may also affect k_c value.

2.1.3 Surface Runoff

Surface runoff (or overland flow) is a sheet flow defined as the precipitation excess that moves over the land surface to stream channels after infiltration. There are two distinct surface-runoff generation processes:

Hortonian overland flow (HOF) The mechanism is named after Robert Horton who described the process in a series of papers in the 1930s (i.e. Horton, 1931, 1933, 1936). HOF occurs when the water-input rate, Q_i, exceeds the infiltration capacity of the surface soil for a period long enough to generate ponding in excess of depression storage (Loague et al., 2010). In the HOF, the surface soil becomes saturated by infiltrating water from above because it is unable to transmit water downward into the profile fast enough.

Horton (1933) stated that overland flow due to infiltrating water from above would occur virtually from the entire upland catchment. This view was modified by Betson (1964), who proposes the *partial-area concept*: the event response originates from Hor-

tonian overland flow on a limited area that varies from basin to basin. Furthermore, his results indicated that the size of the Hortonian-runoff contributing area is controlled by the water saturation of the soil and the water-input intensity. However, these two factors appear to cause large variations only under transition scenarios or unusual conditions, e.g. land-use change, irrigation intensification, climate change.

Saturation or Dunne overland flow (DOF) This process was first studied by Dunne and Black (1970). It occurs when the water-input rate is less than the infiltration capacity of the surface soil, the initial water table/perched water table position is shallow, and the duration of the water-input event is sufficient for the saturated zone to reach the surface (Loague et al., 2010). In this mechanism, the surface soil becomes saturated from below, it consists of direct water input to the saturated zone. When the water input occurs over the basin, all or part of it infiltrates and some of this infiltration percolates to recharge the groundwater raising the water table. Since the water table is close to the surface it reaches relatively quickly the surface and all subsequent rainfall becomes runoff.

Overland unsteady flow governing equations can be derived using the principles of continuity and momentum (e.g. Gottardi and Venutelli, 1993) that can be expressed for the two dimensional case as:

$$\bigtriangledown \cdot (\vec{u}H) + \frac{\partial h}{\partial t} + q^e + q_{og} = 0 \tag{2.13}$$

$$\frac{\partial \vec{u}H}{\partial t} + \bigtriangledown \cdot (\vec{u} \otimes \vec{u}H) + gH \bigtriangledown H + gH(\vec{S}_o - \vec{S}_f) = \vec{0} \tag{2.14}$$

where $\vec{u}$ indicate average flow velocities $[LT^{-1}]$; H is the water surface depth $[L]$; h is the hydraulic head $[L]$; g is the acceleration due to the gravity $[LT^{-2}]$. $\vec{S}_o$ and $\vec{S}_f$ are the bed slope of the channel and the friction slope $[-]$, respectively. q^e is the exchange flow with subsurface, q_{og} represents a source/sink term accounting for meteorological forcing. Equations 2.13 and 2.14 are the so-called *shallow water equations*. Terms of the equation of momentum (Eq. 2.14) are named according to the physical process they represent as follows:

$$\frac{\partial \vec{u}H}{\partial t} \quad \text{Local Acceleration} \tag{2.15}$$

$$\bigtriangledown \cdot (\vec{u} \otimes \vec{u}H) \quad \text{Convective Acceleration} \tag{2.16}$$

$$gH \bigtriangledown H \quad \text{Pressure force} \tag{2.17}$$

$$gH(\vec{S}_o - \vec{S}_f) \quad \text{Gravity and friction forces} \tag{2.18}$$

Where the *local acceleration* and the *convective acceleration* terms (called also inertial terms) describe the change in momentum due to change in velocity over time, and due to change in the specified direction, respectively. The *Pressure term* denotes a force

proportional to the change in water depth along the channel. The *gravity and friction term* express forces proportional to the bed and friction slope.

Commonly, the solution of the set of continuity and momentum equations represents a very complex problem, hence, simplifications are needed. Simplified approximations are achieved by neglecting some of the terms of the momentum equation, e.g. the *diffusive wave* approximation results from neglecting the inertial terms, while neglecting inertial and pressure terms leads up the so-called *kinematic wave* approximation.

2.1.4 Infiltration

The role of the infiltration process in the hydrological cycle was first recognized by Horton (1933). He defined infiltration as the process by which water enters the soil. The rate of infiltration is mainly determined by (1) the rate at which the water arrives from above, e.g. rainfall, snowmelt or irrigation; (2) the hydraulic conductivity at the near-surface soil layer, which is determined by the degree to which soil is filled with water (soil moisture); and (3) by soil hydraulic properties like the (air) entry pressure and pore-size (Dingman, 2002).

A common method to quantitatively estimate infiltration is the numerical solution of the Richards' equation (Richards, 1931), which describes the unsaturated flow in porous media. Richard's equation assuming an incompressible medium can be expressed as:

$$\frac{\partial \theta(\psi)}{\partial t} - \bigtriangledown \cdot (K(\psi) \bigtriangledown h) = 0 \tag{2.19}$$

in which θ is the volumetric water content $[-]$, ψ is the pressure head $[L]$, h is the total hydraulic head $[L]$ defined as $\psi + z$, with z being the elevation above the datum; K is the (unsaturated) hydraulic conductivity of the porous medium $[LT^{-1}]$;and t is the time.

The Richards' equation requires the definition of the soil water retention curve $\theta(\psi)$ and the unsaturated hydraulic conductivity function $K(\psi)$. For this purpose multiple approaches have been proposed in the literature, e.g. Brooks and Corey (1965); Mualem (1976); van-Genuchten (1980).

2.1.5 Groundwater flow

Groundwater is usually associated to water under pressure greater than the atmospheric in the saturated zone of the subsurface. It is fed by infiltrated water reaching the water table that represents the upper boundary of the groundwater zone at which pressure is atmospheric. Recharge of the groundwater can also occur by seepage from surface water bodies. Groundwater eventually may also discharge into rivers or streams. The flow of water in a saturated porous medium is governed by Darcy's law, that for an isotropic

medium may be defined as:

$$\mathbf{q} = -k_s \bigtriangledown h \tag{2.20}$$

in which **q** is the vector of specific discharge, k_s is the saturated hydraulic conductivity. The negative sign means that the water flows in the negative direction of the hydraulic gradient from higher to lower heads. The saturated hydraulic conductivity drives the groundwater flow calculations and depends on the size and shape of the pores, hence it changes for different type of soils. k_s can be measured in the field via pumping tests; or estimated using a grain-size analysis. Values of k_s based on estimations from soil texture can be also found in the literature (e.g. Carsel and Parrish, 1988; Schaap et al., 2001). Hydraulic conductivity of porous media may also depend on the the direction of flow (anisotropy), and it may varies in space (heterogeneity) (e.g. Zhang, 2002).

The groundwater flow equation is commonly expressed as:

$$S_s \frac{\partial h}{\partial t} - \bigtriangledown \cdot (k_s \bigtriangledown h) = 0 \tag{2.21}$$

where S_s $[-]$ is the specific storage coefficient that describes the relative change of mass of the water stored in the porous medium due to an absolute change of the hydraulic head h. In general, S_s represents the compressibility of both water and pore space.

The development of more efficient numerical methods has allowed the calculation of transient three-dimensional flow of water assuming the unsaturated and saturated zones as an integrated system. It is achieved by using a variably-saturated Richards' equation proposed by Cooley (1971), and later adapted by Huyakorn et al. (1984).

2.2 Approaches for flow and transport models

In this section, existing approaches for surface-subsurface models are reviewed. Section 2.2.1 gives an introduction to hydrological models and also briefly describes different types of models. Section 2.2.2 and 2.2.3 presents the state of art of fully-coupled physics-based flow and transport models, respectively.

2.2.1 Definition of Terms

Models are simplified representations of the real world. Models can be either physical, analogue or mathematical. The physical models have been very important in the past. However, the mathematical group of models is the most easily and universally applied, and the one with the most rapid development with regard to scientific basis and application (Refsgaard, 1997).

Hydrological models are composed of two main parts, namely, a conceptual and a computational model. *Conceptual model* is the scientific basis that describes the sys-

tem by variables, properties and the process relevant to explain the natural system. The *natural system* in hydrological models is the hydrological cycle or parts of it. The *computational model* is the piece of code able to simulate the hydrological processes based on the conceptual model. The computational model evaluates a function or a set of functions transforming model input into model output.

Model inputs are values introduced into the model function. They describe the model external forces that act onto the simulated system and include boundary and initial conditions. The *model parameters* are constant values that characterize properties of the natural system or processes. *Model outputs* are the resulting values of the model, they resemble the state of the modeled system as a response to the external forcing (model inputs) given a set of model parameters.

Hydrological models may be classified according to the spatial description of catchment processes as lumped and distributed, and according to the description of the physical processes as empirical, conceptual and physics based. A *lumped model* is a model where the catchment is regarded as a single unit. The variables and parameters represent average values for the entire catchment. A *distributed model* is structured to enable the spatial variation of different catchment characteristics to be represented by a network of grid points. Model applications require often several thousands of grid points, each of which is characterized by parameters and variables.

An *empirical model* is defined as a model developed without an explicit, spatially-distributed consideration of physical processes taking place within the catchment. Empirical models typically estimate a functional relationship between concurrent input and output time series based on statistical inference. A *conceptual model* usually combines physical structures and equations, with semi-empirical relationships. The physical significance is usually not clear, so that the parameter can not be assessed from direct measurements. Instead, it is necessary to calibrate the values using the concurrent input and output time series.

A *lumped conceptual model* attempt to describe flow and transport of solutes in a physically meaningful way, although in a simplified manner. These type of models often include multiple storages. The routing of water and solutes between these storages is accounted for by semi-empirical relationships. The groundwater domain is often neglected or extremely simplified in these models. Examples of lumped conceptual models include HBV (Lindstrom et al., 1997) and SWAT (Arnold et al., 1998) Commonly a conceptual model is also a lumped model, however a third group of models referred to in the literature as *conceptual distributed* (or process-based distributed) can be mentioned. TOPMODEL (Beven et al., 1995) and mHM (Kumar et al., 2010) are examples of this type of models.

A *physics-based model* describes the flow and transport processes from complex descriptions using mathematical representations. This type of model consists of a set of partial differential equations together with parameters which, in principle, have direct phys-

ical significance and can be evaluated (or estimated) from independent measurements. Physics-based catchment models are commonly also spatially distributed.

Lumped and distributed conceptual models appear very attractive if compared to more complex physically-based models because they are easier to operate and require less data. However, this type of models fail to provide details of water flows, soil moistures storages and descriptions of solute fluxes (Hansen et al., 2007). Furthermore, the ability of a conceptual model to evaluate the impact of land-use changes and alternative agricultural practices would be questionable due to the semi-empirical nature of the process descriptions (Refsgaard et al., 1999).

2.2.2 Surface-Subsurface Physics-based Flow Models

The systems approach to hydrologic investigation incorporates the measurement of observable variables in the hydrologic cycle and the development of explicit relationships between these parameters. Mathematical models of watershed hydrology can be derived from physically-based mathematical methods or by parametric or stochastic methods of system investigation, being the most important property of a mathematical model the degree of representation of spatial and temporal variations in the input and output parameters.

Physical hydrology involves the investigation of the mechanisms of the component processes within the hydrologic cycle. If each of these processes can be described by a physical law with an exact mathematical representation, it would be possible to model an entire catchment. This model would be expressed in the form of a composite boundary-value problem described by partial differential equations (Freeze and Harlan, 1969).

In a physics-based flow model, the transient hydrological processes are represented by a set of partial differential equations, interrelated by the concepts of continuity of mass and momentum. In particular, these are the shallow-water equations for flow at the land-surface and in streams and the Richards' equation for flow in the subsurface. These equations, together with the boundary conditions comprise the composite boundary value problem that represents the hydrological model. A boundary value problem of this complexity must be solved by numerical techniques. For the solution of partial differential equations, the real continuum of points making up the field and its boundaries is replaced by a finite set of points arranged in a grid over the region. Therefore, a physics-based model at catchment scale is in practice also a fully-distributed one.

The continuity of flow between surface and subsurface has been extensively proved in the literature (e.g. Furman, 2008; Panday and Huyakorn, 2004). Hence to investigate the basin hydrological response, it results appealing to consider the surface and the subsurface compartments as a coupled system. Two common approaches can be used for this purpose: the dual-node approach (e.g. VanderKwaak, 1999), and the common-node

approach (e.g. Brown, 1995; Dawson, 2008; Refsgaard and Storm, 1995).

The common-node approach is based on superposition (Therrien and Sudicky, 1996), where continuity of hydraulic head is assumed between the surface and the subsurface, which corresponds to instantaneous equilibrium between them. The matrix of contributions arising from the discretization of the surface nodes are superimposed onto those stemming from the discrete form of the porous medium equation. Continuity in pressure head is therefore ensured between the different domains, which avoids the need for a direct evaluation of the exchange fluxes between the porous medium elements and the other domains. A scheme of this type of coupling was presented by Weill et al. (2011). In this, the partitioning between surface and subsurface flow processes is controlled by the subsurface model since the atmospheric forcing input is treated as a boundary condition. The land surface boundary condition is handled by a switching algorithm that determines for any given surface node whether a Neumann (i.e., prescribed flux) or Dirichlet (i.e.,prescribed head) condition is to be imposed. The type of boundary condition is dictated by the saturation state of the node. A Neumann boundary condition is imposed when the surface node is not saturated, in the case of rainfall, or if it is not dry beyond a minimum threshold moisture content, in the case of evaporation. If the surface node becomes saturated during rainfall or dry during evaporation, the surface boundary condition is switched to Dirichlet and the surface–subsurface partitioning becomes soil-limited. Under Dirichlet conditions the infiltration or exfiltration flux is calculated from the head solution. This check for boundary condition switching at the land surface is performed at every nonlinear iteration of the subsurface solution procedure.

The dual-node approach uses an exchange flux term to couple the surface and the subsurface domains. The flow depends upon the gradient across the domains and a first-order exchange coefficient as expressed by:

$$q_{ex} = \lambda(\psi - H) \tag{2.22}$$

where λ is a first-order exchange coefficient which is a measure of the hydraulic connectivity between the two domains, ψ is the pressure head, and H the surface water depth. λ depends on the relative permeability of the porous medium and the thickness of an interface between the two domains, usually called *coupling length*. Apart from the advantages of the dual-node method related to numerical stability and efficiency, it also helps to decrease the effect of the vertical resolution of the near-surface node, which has been posed as a common concern on the use of the common-node approach (e.g. Downer and Ogden, 2004; Vogel and Ippisch, 2008).

Concerns regarding the unphysical nature of the coupling length and the consequent problems on the definition of this parameter from direct field measurements have been risen in the past. Kollet and Zlotnik (2003) pointed out the poor performance of the model

when an inadequate value of the coupling length is used. In particular, they demonstrated how a very small value of coupling length may lead to a physically unrealistic pressure disequilibrium between surface and subsurface. However, Ebel et al. (2009) presented a methodology to find a reasonable coupling length value which enforces near-continuity condition in pressure between the surface and subsurface. The choice of a reasonable coupling length minimize the influence of the first-order coupling coefficient and allows to preserve the underlying physics-based nature of the model. The dual-node scheme is employed in many fully-coupled surface-subsurface models, e.g. InHM (VanderKwaak, 1999), MODHMS (Panday and Huyakorn, 2004), HydroGeosphere (Therrien et al., 2008).

Fully-coupled surface-subsurface flow modeling approaches were first introduced by Freeze and Harlan (1969), who presented a blueprint for a physics-based mathematical model of a complete hydrological system. Since then, many studies have used this concept to simulate rainfall-runoff relationships. VanderKwaak and Loague (2001) applied the Integrated Hydrology Model (InHM) to the R-5 catchment ($\sim$0.1 km^2). In particular, they simulated two "Horton type" rainfall events (i.e. rainfall rates are greater than the infiltration capacity of the soil) with duration of 1.6 and 1.9 hours. To evaluate the goodness-of-fit, simulated hydrographs at the outlet were compared to the observed hydrographs by calculating the root mean squared error. The subsurface response could not be evaluated as the data set of the R-5 catchment did not include hydraulic heads in the unsaturated or saturated zones. Despite the "Horton type" forcing of the system, they found that both, Horton and Dunne (i.e. saturation excess overland flow) streamflow generation processes, are important for the R-5 catchment. The Dunne mechanism dominates along the channel axis, while the Horton mechanism is dominant in areas of low permeability. Using InHM the authors could track dynamic wetting and drying histories of partial-source (a single streamflow generation process dominant) and variable-source areas (where both mechanisms play a role).

Panday and Huyakorn (2004) presented a physics-based spatially-distributed model with additional capabilities to account for agricultural features at the catchment scale, namely the *storage exclusion* based on the definition of an obstruction height term and the *depression storage* related to rill heights. They successfully tested their implementation on the so-called tilted V-catchment by direct comparison to solutions obtained with two traditional hydrological simulation codes: HSPF (Bicknell et al., 1993) and HEC-1 (US Army Corps of Engineers, USACE).

Kollet and Maxwell (2006) presented an alternative coupling approach where overland flow is simulated as a free-surface boundary condition of the physics-based model. It is based on the assumption of pressure continuity across the surface-subsurface interface (i.e. common-node approach). This approach was used by Maxwell and Kollet (2008) to quantify the effect of subsurface heterogeneity on Hortonian runoff generation and to

identify settings where groundwater flow dynamics directly feed back to the land-surface-atmosphere energy exchange (Ferguson and Maxwell, 2011; Maxwell et al., 2007).

Studying lake-groundwater interaction in a glacial outwash terrain (area=$\sim$ 4 km^2; Boreal Plains of northern Alberta, Canada), Smerdon et al. (2007) reported a successful application of a physics-based model at the watershed scale. They found that, due to the transition from the frozen to the thawed state of riparian peat in summer, a seasonal time-dependence of saturated hydraulic conductivity and storage coefficient had to be incorporated in their model.

Kolditz et al. (2007) presented a regional hydrologic soil model (RHSM) and applied it to simulate groundwater recharge patterns at a regional scale for the Beerze-Reusel drainage basin (Netherlands). This investigation evolved into the proposal of an object-oriented concept for the numerical simulation of multi-field problems in coupled hydrosystems, the so-called *compartment approach* (Kolditz et al., 2008).

Li et al. (2008) studied the hydrological response of the Duffin creek watershed (area= $\sim$ 286.6 km^2) honoring eight different hydrostratigraphic subsurface units with the physics-based, surface-subsurface model HydroGeosphere (Therrien et al., 2008). Subsurface hydraulic head observations, taken during a reference period, were used to constrain the initial condition for the simulated three-dimensional hydrological response driven by daily precipitation as measured from April to December of the years 1986 and 1987. Calibrating seasonally variable parameters controlling evapotranspiration based on Hargreaves and Samani (1985) and Kristensen and Jensen (1975) for the year 1986, they found that their simulated stream-flow matched the measured one for 1987 at four different gauging stations within the catchment reasonably well. The subsurface response was not assessed due to the lack of concurrent hydraulic head time-series data.

Considering both, surface and subsurface hydrological response at the watershed scale, Jones et al. (2008) applied the physics-based InHM model to simulate the response of the Laurel Creek watershed (Ontario,CA) (area=75 km^2) to two discrete rainfall events with 420 and 900 hours duration. Their results show moderate agreement in simulated and measured runoff as well as subsurface hydraulic heads, and demonstrate the dynamic nature of the interaction occurring between the surface and the subsurface hydrological regimes. Their overall conclusion is that fully-coupled, surface/variably-saturated subsurface models are applicable at the watershed scale and possibly at larger scales. Nevertheless, they emphasize the need for more studies with more comprehensive data in order to improve the state of the art of coupled surface-subsurface modeling.

Goderniaux et al. (2009) studied the impact of climate change on groundwater at the Geer-basin (Belgium) using a physics-based surface-subsurface model. They investigated the evolution of the groundwater levels under different climate change scenarios generated using six regional climate model(RCM) assuming SRES A2 emission (medium–high) scenario (e.g Fowler and Kilsby, 2007). Their results suggested that the use of an sur-

face–subsurface modeling approach and sophisticated climate change scenarios improves the correspondence of the model with the real system. Furthermore, they indicated that the use of a spatially distributed evapotranspiration model together with the physics-based model represents a step forward in order to understand the impact of climate change on groundwater resources.

Despite the above mentioned successful applications of physics-based models, objections to these types of models are widely discussed in the hydrological literature. Apart from the question of parameter identifiability, uniqueness, and the need for effective parameter values at larger scales, (e.g. Beven, 1993, 2001, 2002), the range of validity of Richards' equation has been posed as a problem of physics-based models: Downer and Ogden (2004); Vogel and Ippisch (2008), among others, have pointed out that consistency with the assumptions underlying Richards equation requires a high spatial resolution that also depends on soil type and the scale of heterogeneities. Recent work of Kollet et al. (2010) has shown, however, that such a refined resolution is possible even at catchment scale by the use of high-performance computing. Commonly, in physics-based models, Richards' equation is handle as an effective law leading to appropriate system behavior rather than a fundamental soil-physical law.

2.2.3 Nitrate Transport Models

The pollution of surface water and groundwater by nitrate is a well-known worldwide problem. Inorganic nitrogen fertilizers represents one of the most common source of nitrate. In fact, agricultural activities represents the most significant anthropogenic source of nitrate contamination in the subsurface. In this respect, the conversion of natural to agricultural systems may affect water quality by adding considerable amounts of nitrate to the system. This concern has led to increased efforts to better understand the fate of nitrogen at agricultural catchments.

The nitrogen cycle in agricultural soils represents a very complex system (see Fig. 2.2). The common forms of inorganic nitrogen include nitrate (NO_3^-), nitrite (NO_2^-), nitrogen gas (N_2), ammonium (NH_4^+) and ammonia(NH_3). Nitrogen is also a major constituent of the organic matter in the form of proteins. The majority of the atmosphere is composed by nitrogen gas. Atmospheric nitrogen can be fixed or converted to nitrate, by cyanobacteria in lakes and the ocean; and by bacteria living on the root of plants such as legumes and lichens. Rainwater may also contain dissolved nitrate and ammonia. Nitrogen may also be released to the subsurface from sewage, animal wastes and fertilizers.

In the subsurface, oxidation and reduction of nitrogen species is accomplished by microorganisms. Under oxidizing conditions ammonium is converted to nitrite, which is converted to nitrate (*nitrification*). Nitrite is a very reactive ion and is almost immediately converted to nitrate, so that only little nitrite is found in the environment. Under

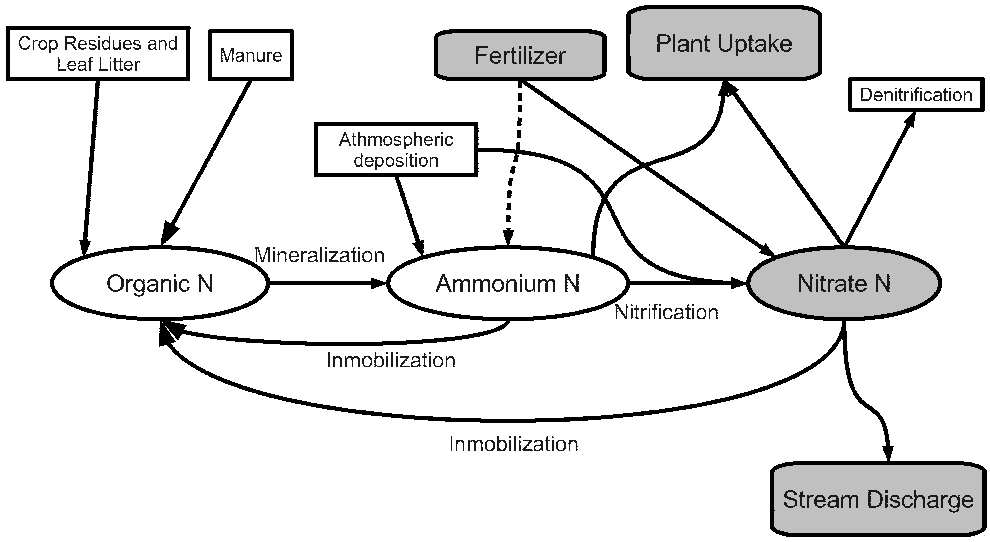

Figure 2.2: Nitrogen Cycle in Agricultural Soils

reducing conditions nitrate is converted primarily to nitrogen gas, a process known as *denitrification*. Organic matter will decay to ammonium under reducing conditions (*mineralization*). If the groundwater is under reducing conditions, the ammonium will remain in the ammonium form. If it is oxidizing, bacteria will convert the ammonium to nitrate (nitrification).

In agricultural areas, when fertilizer is applied to soil, some of the nitrogen may be taken up by microorganisms in the soil, a process known as *immobilization*. The immobilized nitrogen may be incorporated into proteins, nucleic acids, and other organic nitrogen constituents of microbial cells and cell walls; as such, it becomes part of the biomass. As the microbes may die and decay, some of the biomass nitrogen may be released as ammonium through the process of mineralization; the remainder undergoes conversion to more stable organic compounds, ultimately becoming a part of soil organic matter. The stabilized organic compounds are not readily available to plants; therefore, the net result of immobilization-mineralization is a decrease in the availability of the nitrogen added to soil as fertilizer, and also the partial conversion of this nitrogen to a form that is not subject to loss from most soils. Nitrogen loss during handling, storage and spreading of manure (organic matter used as fertilizer in agriculture) may also occur and it is known as *ammonia volatilization*.

The extent to which fertilizer is immobilized depends largely on the supply of carbon, which is used by soil microorganisms as an energy source. Of particular importance is the ratio of available carbon to mineral nitrogen or Carbon/Nitrogen (C/N) ratio. When this ratio is very low, mineralization exceeds immobilization, whereas at high ratios of C/N,

immobilization exceeds mineralization. Also of importance is the type of carbon source. In the presence of a simple substrate such as glucose, inorganic nitrogen is quickly consumed and disappears within a few days. With complex substrates, such as cellulose from plant residues, the process is slower, and the supply of inorganic nitrogen is never completely exhausted (Azam et al., 1993). The microorganisms responsible for immobilization utilize ammonium in preference to nitrate (Jansson, 1958), which is in agreement with reports that suggest that immobilization-mineralization is more extensive with ammoniacal fertilizers than with nitrate fertilizers. Immobilization-mineralization process may also be affected by environmental conditions, such as temperature, soil moisture content, and pH.

Nitrogen is the macronutrient more required by the plants and often limits growth. Plants have evolved multiple strategies for acquiring nitrogen, which range from the uptake of nitrate to nitrogen fixation and even carnivory. However, in soils with annual crops, nitrate is the most abundant source of nitrogen. In general, in a typical aerobic agricultural soil, both nitrate and ammonium are present but nitrate is the major form. For instance, optimal growth of tomatoes occurs in soil with a rate of nitrate to ammonium of 3:1 and it is inhibited if the concentration of ammonium is too high (Crawford and Glass, 1998).

Several models have been developed for modeling nitrogen transformation and nitrate leaching in the root zone, e.g. DAISY (Hansen et al., 1991), ANIMO (Rijtema and Kroes, 1991), LEACHN (Hutson and Wagenet, 1991), SOILN (Johnsson et al., 1987), EXPERT-N (Gayler et al., 2002)), but only a small number have the ability to simulate in an integrated way flow and transport at catchment scale.

In the last decades, the considerable advances made in physics-based models have encouraged the development of solute transport models which allow the detailed representation of a catchment, including the coupled 3-D surface-subsurface transport of a set of interacting solutes. Fully-integrated flow and transport model may be used to represent the transport of nitrate leached by irrigation practices through the unsaturated subsurface and its discharge to seepage areas and into surface water. Integration is very important as it ensures that the distributed parameters for the nitrogen transformation and nitrate transport are entirely consistent with very complex geological and climatological patterns.

Main solute transport processes to be accounted for in a nitrate model are advection, dispersion and plant uptake. Due to the complexity of the nitrogen cycle a nitrate transformation model able to simulate mineralization, immobilization, nitrification and denitrification coupled to the solute transport model may also be required in some cases. The latter can be expressed as:

$$\frac{\partial c_{NO_3}}{\partial t} = -\xi_{in} + \xi_n - \xi_d + I - U \tag{2.23}$$

where ξ is the rate of the process indicated by *in*, immobilization; *n*, nitrification; *d*, denitrification. I represents the rates of input of nitrate for wet and dry deposition, and fertilizers. U is the plant uptake of nitrate which depend on the plant requirements and the availability of nitrogen in the soil to meet those requirements.

In the literature, one can find a few attempts to simulate the nitrate transport at catchment scale using fully-integrated approaches for flow and transport. Styczen and Storm (1993) presented the modeling study of nitrogen at the Karup river agricultural catchment (425 km^2). They use an integrated approach that couple DAISY and the distributed physics-based flow and transport model MIKE-SHE (Refsgaard and Storm, 1995; Refsgaard et al., 1995). DAISY is a 1-D tool for the simulation of crop production and water and nitrogen balance in the root zone, and MIKE-SHE solves the coupled system of overland-flow(2-D), unsaturated zone (1-D) and saturated zone(3-D).

In a sequential scheme, DAISY first calculates water flow and nitrogen transport from the soil surface and through the root zone, subsequently the percolation at the bottom of the root zone (simulated by DAISY) is the input to MIKE-SHE calculations for the remaining part of the catchment. In this approach, the feedback from the groundwater zone is disregarded. As DAISY is one-dimensional, in principle a single run should be performed for each MIKE SHE horizontal grid cell (500 x 500 m). From a visual inspection the results show a relatively good agreement between measured and observed nitrate concentration in groundwater, nevertheless they fail to present nitrate concentrations at the river outlet. A statistical measurement of the performance is also missing.

Refsgaard et al. (1999) used the same framework as Styczen and Storm (1993) (i.e. DAISY and MIKE-SHE) to model flow and transport at two catchments in Denmark, Karup A and Odense A. They investigated the availability of the data required for such a model in the European context. Additionally, they tested the impact of the grid size on the performance of the model. Finally, they compared a distributed and a uniform agricultural representation of the crop patterns. Their results show that the influence of the resolution on the simulation of annual nitrate concentration statistical distribution is not very high. However, the effect on the temporal distribution is rather significant. Using a uniform crop type instead of distributed patterns, their results show that the model fails to simulate nitrate leaching and groundwater concentrations adequately. Finally, they concluded that in general, the DAISY-MIKE-SHE modeling system fails also to represent areas where the Hortonian overland flow is a dominant mechanism.

Birkinshaw and Ewen (2000b) presented a nitrogen transformation component(NITS) as an addition to SHETRAN (Ewen et al., 2000) which is a physics-based, spatially distributed river catchment modeling system so that it can be used to simulate integrated flow and transport in 3-D models. NITS is able to account for mineralization, immobilization, nitrification and denitrification. The nitrogen transformation model gives SHETRAN the ability to simulate nitrate generation and leaching and the subsequent subsurface transport

through combinations of confined, unconfined and unsaturated systems to seepage points and streams, and transport through stream networks. Birkinshaw and Ewen (2000a) validated NITS in the Slapton Wood agricultural catchment (0.94 km^2). The application of SHETRAN at the Slapton Wood catchment involves simulating the application of fertilizer, the generation of nitrate, leaching and subsurface transport to and along the Slapton stream, and comparing the simulated and measured nitrate concentration at the catchment outlet. Nitrate groundwater concentrations are not available. The simulated concentrations at the outlet of the Slapton Wood catchment correlates well with the observed values, i.e. R=0.62 for individual values and R=0.822 for monthly means.

Conan et al. (2003) proposed the combined use of SWAT (Arnold et al., 1998), MODFLOW (Harbaugh et al., 2000) and MT3DMS (Zheng and Wang, 1998) to simulate nitrate concentrations in surface water and the fate of leached nitrate in groundwater with the use of a reaction/transport model at a sub-catchment within Brittany (France). SWAT is a conceptual semi-distributed watershed model with a GIS interface able to outline sub-basins and stream networks from a digital elevation model and calculate daily water balances from meteorological, soil and land-use data. It also has the ability to simulate the movement and the transformation of nitrogen in the catchment. Basic processes simulated by SWAT includes mineralization, denitrification, volatilization and plant uptake. MODFLOW is a well-known 3-D fully distributed model that calculates groundwater flow from aquifer characteristics. MT3DMS is a 3-D groundwater solute transport model that can simulate advection, dispersion and chemical reactions of dissolved constituents in groundwater. The goal of this investigation was to validate the integrated use of these models in a heavily fertilized region using monthly data. Alternative scenarios were also evaluated. The authors compared the results obtained using SWAT alone with respect to the results from the coupled system SWAT-MODFLOW-MT3DMS. Recharge was distributed according to SWAT simulation outputs for each month. Stream-aquifer interactions are calculated using a stream-routing package of MODFLOW. The coupled flow model was calibrated in a two-step procedure: First, it was calibrated under steady state conditions adjusting river conductance and hydraulic conductivity. Second, specific yield and evaporation were adjusted under transient conditions. The MT3DMS model was based on the grid and results of MODFLOW. The distributed nitrate concentrations calculated by SWAT were the input for each month. Only nitrate reduction which is controlled by oxygen availability and/or pyrite (FeS_2) was accounted for. The latter was modeled by a first-order irreversible reaction. First-order rate constants for each geological formation, and initial nitrate concentration were calibrated. For the scenarios analysis, they kept the calibrated physical and hydrological conditions. Three scenarios were tested. The first two were dedicated to test the effect of the improvement of agricultural practices. For this goal, they decreased the annual amount of fertilizer application by 20%. Another scenario was dedicated to simulate the effect of changing practices on the nitrogen cycle.

Their results were relatively good when using the coupled system. The Nash-Sutcliffe coefficient for monthly nitrate load in the surface at the outlet and at an upstream station were 0.87 and 0.60, respectively. Conversely, the nitrate load using SWAT exclusively was always underestimated. The future scenarios generated with the coupled model, confirms that a reduction of fertilization would lead to a reduction of nitrate that percolates to the groundwater in up to 35%. However, nitrogen soil content would not change so dramatically. In the long-term, the beneficial impact of more efficient agricultural practice is more evident.

Nitrogen transformation models have numerous parameters which are very difficult to estimate from direct measurements since some of the formulations describing processes (i.e. mineralization, immobilization, nitrification, denitrification and plant uptake) are based on semi-empirical relationships. In that respect, the develoment of an approach that is able to simulate the evolution of the concentrations at catchment scale without the abandonment of the physics nature of the model would be very helpful. Also, due to the large uncertainty on the definition of nitrogen transformation processes parameters, a parsimonious approach would be preferred. As suggested by some authors mentioned above, nitrate appear to be the most abundant nitrogen form in agricultural catchment, hence in a agricultural catchment model it would be reasonable to investigate the nitrate fate.

Chapter 3

Governing Equations

HydroGeoSphere is chosen as the computational code to be used in the development of the fully-integrated flow and transport model of the Lerma basin. It is based on a rigorous conceptualization of the hydrologic system comprising surface and subsurface flow regimes with interactions. The code is designed to take into account all key components of the hydrologic cycle, i.e. precipitation, evapotranspiration, surface runoff, infiltration and subsurface flow.

For each time step, the model solves surface and subsurface flow and mass transport equations simultaneously and provides complete water and solute budgets (Therrien et al., 2008). To perform the integrated analysis, the model uses a mass conservative modeling approach that couples the surface flow and solute transport equations with the 3-D variably saturated subsurface flow and solute transport equations. In the following, the governing equations that describe the flow and transport dynamics are presented.

As a starting point, the basin scale water balance equation (Eq. 2.1) considering the difference of input and output flows per unit time can be expressed as:

$$\left[(PA_T) + \left(\sum_{j=1}^{N} I_j A_j\right) + Q_g - \left(\sum_{j=1}^{N} ET_j A_j\right) - Q_s\right] = (\Delta w_s + \Delta w_g) \tag{3.1}$$

where N is number of surface units (one for each land-use category); P is the total precipitation $[L/T]$; A_T is the total area of the basin $[L^2]$, I is the irrigation rate $[L/T]$ for each plot j with area A_j $[L^2]$, Q_g is the groundwater inflow $[L^3/T]$, Q_s is the discharge at the basin outlet $[L^3/T]$, ET_j is the evaporation rate from the soil surface and subsurface along with plant transpiration $[L/T]$ associated to each plot j, Δw_s and Δw_g are changes in surface water and groundwater storage $[L^3/T]$. The components listed in Eq. 3.1 are calculated implicitly within the model by integrating the local, spatially-distributed quantities over each finite element grid block at each time step.

3.1 Flow equations

Surface water flow is represented by the two-dimensional diffusive wave approximation to the shallow water equations. Richards' equation is used to approximate three-dimensional flow in both the saturated and unsaturated zones. Subsurface and surface water regimes are coupled using a physics-based exchange flux relationship.

3.1.1 Overland Flow

In the diffusive wave approximation of the the shallow water equations for overland flow, inertial terms are neglected and a hydrostatic vertical pressure distribution is assumed. By this, the flow velocity value corresponds to a vertical average. The approximation is generally applicable to mildly sloping streambeds. The diffusive wave equation can be written as follows (Gottardi and Venutelli, 1993):

$$\frac{\partial \phi_s h}{\partial t} - \frac{\partial}{\partial x_i}\left(Hk\frac{\partial h}{\partial x_i}\right) = -q^e \pm q_{og} \qquad \text{with } i \in \{1,2\} \tag{3.2}$$

in which Einstein's index notation is used, implying repeated summation about each index appearing at least twice in a product. H is the water depth $[L]$, h is the hydraulic head $(H+z)$ $[L]$, z is the bed elevation $[L]$, q_{og} is a volumetric flow rate per unit area representing external sources and sinks (i.e. rainfall/evaporation)$[LT^{-1}]$ and q^e is the surface-to-subsurface exchange rate $[LT^{-1}]$, defined positive from the surface to the subsurface. ϕ_s $[-]$ is the surface "porosity" introduced by Panday and Huyakorn (2004) to account for the effect of depression storage and obstructions on overland flow. To achieve this, the authors defined the height of depression storage (h_{ds}) and the obstruction height (h_{os}), which are physical parameters that can be interpreted as the mean spacing (equivalent void space) within the respective storage elements as a function of flow depth. k $[LT^{-1}]$ is the surface conductance, here assumed isotropic, which can be approximated using Manning's equation after Gottardi and Venutelli (1993):

$$k = \frac{H^{2/3}}{n_m\left[\left(\frac{\partial h}{\partial x_1}\right)^2 + \left(\frac{\partial h}{\partial x_2}\right)^2\right]^{1/4}} \tag{3.3}$$

in which $n_m[TL^{-1/3}]$ is Manning's friction coefficient. Eq. (3.2) is subject to appropriate combinations of boundary conditions (no flow, fixed head, critical depth, normal depth).

3.1.2 Subsurface Flow

Flow in both the unsaturated and saturated zones is simulated using a variably-saturated Richards' equation expressed after Huyakorn et al. (1984) as:

$$S_w S_s \frac{\partial \psi}{\partial t} + \phi \frac{\partial S_w}{\partial t} - \frac{\partial}{\partial x_i}\left(k_{s_{ij}} k_{rw}(S_w)\frac{\partial h}{\partial x_j}\right) = 0 \qquad \text{with } i,j \in \{1,2,3\} \tag{3.4}$$

subject to:

$$n_i k_{s_{ij}} k_{rw}(S_w)\frac{\partial h}{\partial x_j} = \begin{cases} q^e & \text{at} \quad z = z_{surf} \\ \pm q_g & \text{at} \quad \text{lateral and bottom flux boundaries} \end{cases} \tag{3.5}$$

in which h is the total head of subsurface water, $k_{s_{ij}}$ is the saturated hydraulic conductivity tensor for the porous medium $[LT^{-1}]$, k_{rw} is the relative permeability of the medium as function of water saturation (S_w) $[-]$, ϕ is the effective porosity $[-]$, q^e is the subsurface-surface exchange flux $[LT^{-1}]$, q_g is the fluid exchange with the outside of the simulated domain through the bottom and lateral boundaries $[LT^{-1}]$; S_s is the specific storage $[L^{-1}]$, ψ is the pressure head of water $[L]$ given as $\psi = h - z$ where z is the elevation $[L]$. n_i is the normal vector at the land surface pointing upwards, and z_{surf} is the elevation of the ground surface. Eq. (3.4) may also be subject to Dirichlet or Cauchy boundary conditions with respect to hydraulic head.

In order to solve the non-linear Richards' equation for unsaturated flow, a relationship must be established between the primary unknown ψ and the secondary variables S_w and k_r, so that both can be expressed in terms of the pressure head (ψ). In this study, we use the van-Genuchten functions (van-Genuchten, 1980):

$$S_w(\psi) = S_{w_r} + \frac{1 - S_{w_r}}{(1 + (\alpha\psi)^n)^m} \tag{3.6}$$

with S_{w_r} being the residual water saturation $[-]$, α the inverse air-entry pressure $[m^{-1}]$, n the pore distribution factor $[-]$ and m defined as $m = 1 - 1/n$, $n > 1$. The relative permeability, k_{rw}, can be calculated as:

$$k_{rw}(S_w) = (S_e)^{1/2}[1 - (1 - S_e^{1/m})^m]^2 \qquad \text{with} \qquad S_e = \frac{S_w - S_{w_r}}{1 - S_{w_r}} \tag{3.7}$$

3.1.3 Surface-Subsurface Coupling

The surface flow equation is solved on a triangular 2-D finite element mesh on top of a matching subsurface prism grid, i.e. all x_1 and x_2 coordinates of the individual surface elements are the same for the corresponding subsurface elements. The surface flow equation Eq.(3.2) is coupled to the 3-D subsurface equation Eq.(3.3) via leakage through an interface layer. The surface nodes are connected to the first active subsurface flow nodes via a first-order relationship (i.e. the dual node approach) which can be expressed according to VanderKwaak (1999) as:

$$q^e = \frac{k_r k_{33}}{l_e}(\psi - H) \tag{3.8}$$

in which k_r is the relative permeability for the exchange flux $[-]$, k_{33} is the vertical saturated hydraulic conductivity $[LT^{-1}]$ of the underlying porous medium and l_e is the interface layer thickness $[L]$. The relative permeability term k_r is the same as the relative permeability of the porous medium (k_{rw}) when water flows from the subsurface to the surface, while in the opposite direction, k_r is determined by the ratio of the water depth H at the surface to the total obstruction height ($h_s = h_{os} + h_{ds}$) (Panday and Huyakorn, 2004).

3.2 Solute transport

The solute transport is simulated using a two-dimensional advection-dispersion equation for the surface domain, and the 3-D advection-dispersion equation for the subsurface domain. The surface-subsurface transport coupling is performed using a 1-D advection term.

3.2.1 Surface domain

The equation for two-dimensional transport of solutes in the surface domain can be written after VanderKwaak (1999) as:

$$\frac{\partial c_s}{\partial t} + \vec{u}\overline{\overline{\nabla}} c_s - \overline{\overline{\nabla}}\left(H\mathbf{D}^s\overline{\nabla} c_s\right) - q_m^e + q_m^s = 0 \tag{3.9}$$

where $\mathbf{D}^s$ is a two dimensional hydrodynamic dispersion tensor of the surface flow domain representing diffusion and spreading due to turbulent mixing $[L^2T^{-1}]$. c_s is the surface concentration $[ML^{-3}]$. Concentrations represent depth-averaged quantities because rapid vertical mixing in shallow water is assumed. q_m^e represents the solute exchange rate between the subsurface and the surface $[ML^{-3}T^{-1}]$, and q_m^s a source/sink solute rate for the surface $[ML^{-3}T^{-1}]$.

3.2.2 Subsurface domain

Three-dimensional transport of solutes in a variably-saturated porous matrix is described by the following equation:

$$\phi S_w \frac{\partial c}{\partial t} + \vec{v} \bigtriangledown c - \bigtriangledown \left(\phi S_w \mathbf{D} \bigtriangledown c \right) - r = 0 \tag{3.10}$$

subject to:

$$n_i v \frac{\partial c}{\partial x_i} = \begin{cases} q_m^e & \text{at} \quad z = z_{surf} \\ \pm q_m^g & \text{at} \quad \text{lateral and bottom flux boundaries} \end{cases} \tag{3.11}$$

where c is the subsurface solute concentration $[ML^{-3}]$; v is the seepage velocity $[LT^{-1}]$, r accounts for the chemical reactions $[ML^{-3}T^{-1}]$. q_m^e is the surface-subsurface solute exchange rate $[ML^{-3}T^{-1}]$, and q_m^g is the solute exchange rate with the outside of the simulated domain through the bottom and lateral boundaries $[ML^{-3}T^{-1}]$. D_{ij} is the hydrodynamic dispersion tensor $[L^2T^{-1}]$ expressed after Bear (1979) as:

$$\phi S_w D_{ij} = (\alpha_l - \alpha_t) \frac{v_i v_j}{|\mathbf{v}|} + (\alpha_t |q| + \phi S_w D_e) \delta_{ij} \tag{3.12}$$

where α_l and α_t are the longitudinal and transverse dispersivity $[L]$, respectively. D_e is the effective diffusion coefficient $[L^2T^{-1}]$; and δ_{ij} is the Kronecker delta.

3.2.3 Surface-Subsurface Coupling

The surface-subsurface solute exchange can be expressed with a 1-D advection term:

$$q_m^e = q^e c_{ups} \tag{3.13}$$

where c_{ups} is the concentration upstream of the flow $[ML^{-3}]$. It equals c_s when the flow is from the surface to the subsurface and equals c when the flow is from the subsurface to surface. q^e is the flow exchange rate calculated by Eq. 3.8 $[LT^{-1}]$.

Chapter 4

Model Protocol

In physics-based model applications, one may pretend to know the relations between the quantities of interest well enough to perform predictions. Using parameter values from different sources, we predict the outcome of the physical interactions by calculating state variables. In fully-coupled, surface-subsurface models, we may calculate the flow velocity field of the coupled system based on parameter values for the saturated hydraulic conductivity, van-Genuchten parameters and surface roughness coefficients. These calculations never give exact predictions because of conceptual and parameter uncertainties, and measurement and computational errors (Cirpka, 2010).

In order to demonstrate that a given site-specific model is capable of making accurate predictions while honoring realistic hydrological stresses and material properties, we need to perform a model validation. A modeling protocol to validate fully-coupled physics-based models at catchment scale adapted from the presented by Anderson and Woessner (1992) is proposed in Figure 4.1. It includes establishing the purpose of the model, the conceptual model construction, the computer code selection -or development-, the model design, parameterization, calibration, sensitivity analysis and the validation or definition of prediction capabilities of the model.

4.1 Establish the purpose of the model

It is very important to define the purpose of the modeling effort. In that respect, the questions that the model will address and the best way to answer them should be defined. According to the purpose, the model may be classified as predictive, interpretative or generic. The definition of the purpose of the model should be the very first step in every model application as it may help to define if the model is necessary after all or a more parsimonious approach would be enough to answer more effectively the questions posed as the heart of the investigation. In this step, modelers must decide whether an analytical model provides an acceptable solution of the question or a numerical model is needed.

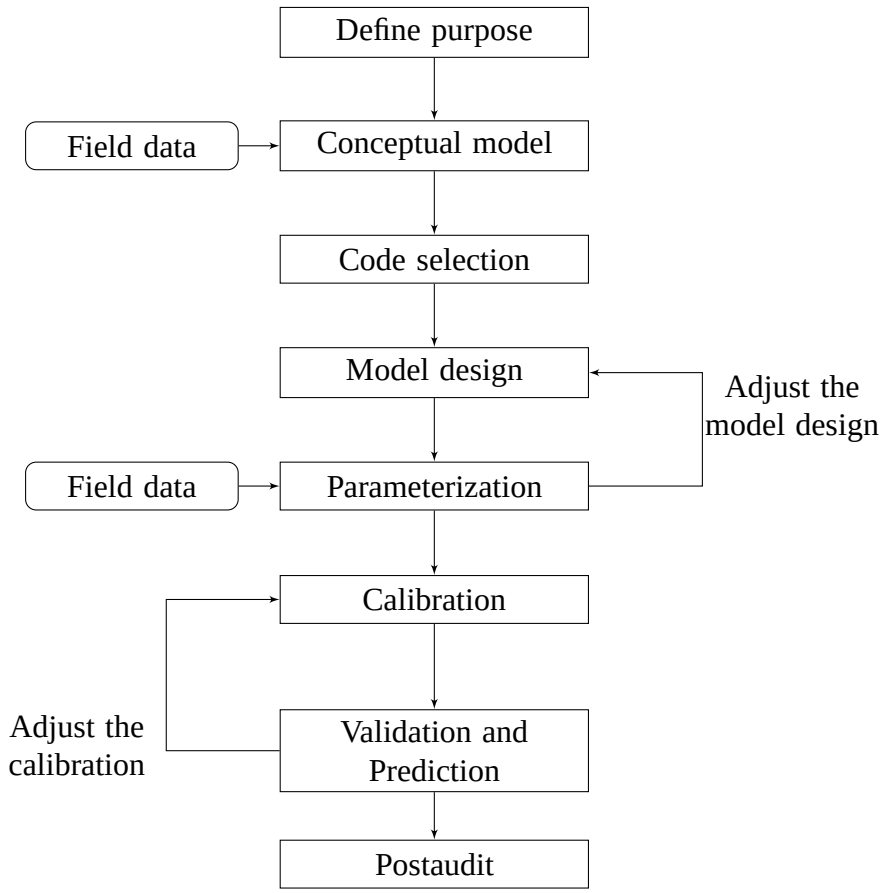

Figure 4.1: Catchment model protocol

After we decided that a numerical model is required to address our research questions, the purpose of the model will indicate us what governing equations should be used, and eventually what code will be the more suitable (Anderson and Woessner, 1992).

4.2 Develop a conceptual model of the system

The purpose of the construction of the conceptual model is to simplify the field problem and organize the available field data so that the system can be better understood. Field data and prior information is processed and assembled including hydrological stresses, topographic and geological maps, management information (e.g. irrigation volumes, fertilization registers, land-use maps) and expert information (e.g. farmer interviews, geological interpretations).

Theoretically, the closer the conceptual model is to the real system, the more accurate is the numerical model. However, in practice it is desirable to strive for *parsimony* (Anderson and Woessner, 1992). The principle of parsimony, or Occam's razor, calls for keeping a model as simple as possible while accounting for system processes and characteristics that are important to predictions (e.g. Hill, 2006).

The development of the conceptual model for physics-based surface-subsurface mod-

eling includes the definition of: (1) the area of interest and the boundaries of the model; (2) surface and subsurface units in order to account for forcing and material properties variability; and (3) the flow system that allows to understand the movement of water between surface and subsurface, identify surface and subsurface discharge areas, and aquifer connections.

4.3 Selecting the system of governing equations and a suitable computer code

The computer code is the algorithm able to solve the mathematical model numerically. The computer code and the governing equations should be verified. Computer code verification refers to the comparison of the numerical solution generated by the model with one or more analytical solution or with other numerical solutions. Most of the more common codes used for surface and subsurface modeling, e.g. MODFLOW (Hill, 1992), InHM (VanderKwaak and Loague, 2001), HydroGeosphere (Therrien et al., 2008), have already been tested.

Governing equations verification refers commonly to the comparison of the theoretical results to laboratory experiments. However, the verification of the applicability of a set of governing equations to a particular catchment can only be accomplished by applying the model to the catchment and comparing the model simulations to field measured data. For this purpose, the following steps are proposed.

4.4 Model design

The conceptual model is expressed in a suitable form to be modeled. This step includes: (1) the design of the grid; (2) the definition of the boundary conditions; and (3) the definition or generation of an appropriate initial condition.

The design of the grid consists of the construction of a discretized domain which is an array of nodes commonly associated to finite difference cells or finite elements. The nodes (and elements) form the framework of the numerical model. The overall dimensions of the grid are determined by the extension of the domain and the numerical technique used, i.e. finite difference or finite elements.

In the finite difference method, the solution domain is discretized as a rectangular grid. The intersections of the grid lines are the nodes at which the difference equation that will be derived is written. Finite differences grids types include the block-centered grid and the mesh-centered grids. In the former, flux boundaries always are located at the edge of the block, and in the latter the boundary coincides with a node (Anderson and Woessner, 1992).

Applying the finite element method, the domain is divided into a number of elements making up a grid. The point where the element corners meet are the nodes. In general, finite elements allow more flexibility in designing a grid. One-dimensional elements can be one-dimensional line or curve elements; two-dimensional elements can be either triangular, rectangles or quadrilaterals; and three-dimensional elements can be prisms, pyramids or bricks. The key of the finite element method is a minimization principle that allows to solve the nodal values so that the numerical error is minimized on average over the domain.

In a surface-subsurface fully-coupled model, we typically need to define multiple boundary conditions: subsurface flow boundary conditions include Dirichlet (first-type) boundaries of prescribed hydraulic head, source/sinks, evaporation or open-exit boundary. These boundary conditions may also vary in time.

For the surface flow, boundary conditions includes climatological (e.g. rainfall, evapotranspiration) and anthropogenic direct inputs (e.g. irrigation) and Dirichlet of prescribed water elevation. Boundary conditions at the divide of the surface domain should be also defined. Types of this boundary includes critical depth and zero-depth gradient (Therrien et al., 2008). Boundary conditions for solute transport can be defined as Dirichlet boundaries of prescribed concentrations, prescribed mass flux or Cauchy boundary conditions.

Ideally, the initial condition would be established from a comprehensive data collection campaign that provides the modeler with a snapshot of the system state at the beginning of the simulation period. Unfortunately, such a true initial condition is hardly available for any catchment. Therefore, typically an initial condition needs to be generated. Some methodologies used for this purpose include:

1. **Long-term average forcing ("spin-up")**. An initial condition is generated by forcing repeatedly the system with historical-average values until a quasi-steady state is reached (Jones et al., 2008). Measured data (i.e. hydraulic heads and/or stream discharge) at the beginning of the simulation period may be used to estimate the goodness-of-fit of the initial condition (Li et al., 2008).

2. **Draining of the system**. An initial condition of the coupled surface-subsurface system is generated by simulating the drainage of the catchment from an initial saturated state until a good agreement between simulated and observed values is achieved (e.g. VanderKwaak and Loague, 2001).

3. **Dynamic water balance**. The system is forced with meteorologic input data until the head distribution in the entire catchment does not change anymore when comparing a certain day of the current year with the same day of the previous year. To force the system, we can use one-year rainfall and evapotranspiration from the year previous to the beginning of the simulation, or from a typical year when this is not

available (Perez et al., In review). In similar way to the previous cases, measured stream discharge and/or hydraulic heads may be used to test the goodness-of-fit of the initial condition.

A combination of more than one method has been also used in some previous studies (e.g. Sudicky et al., 2008).

4.5 Parameterization

In the case of physics-based models, before performing any calibration, the set of calibration parameters should be defined. This process has been referred to in the literature as parameterization (Refsgaard, 1997; Refsgaard and Storm, 1996) or pre-calibration (Doherty and Hunt, 2009). In the following, I will attached to the term proposed by Refsgaard and Storm (1996) and refer to this as *parameterization*

In the parameterization, calibration parameters and physically acceptable and sensitive ranges of values for these parameters, i.e. calibration parameter space, should be also defined. The bigger the calibration parameter space is, the more computationally demanding the calibration is. We should also be able to define the spatial patterns of the parameter values so that a given parameter reflects the significant variation described in the available field data (e.g Abbott and Refsgaard, 1996; Refsgaard and Storm, 1996). Vegetation types, soil types and geological layers are examples of the use of representative parameter values. An adequate starting set of parameter values would also be very useful, as it would help to reduce the number of iterations towards the optimal solution.

An adequate calibration parameter should have an important effect on the model output. More specifically, the available observed data should be sensitive enough with respect to the parameter, so that the parameter value can be identified. Sensitivities are typically used in parameterization as they quantitatively indicate the influence of the parameters on the model outputs. For simple models, it is easy to derive closed-form expressions of the sensitivities, however for most models it is more complicated and the sensitivities must be evaluated numerically.

Numerical differentiation may be used for the evaluation of sensitivities in physics-based models. To evaluate sensitivities with this method, we consider the model output at location $\mathbf{x}$ and time t given a vector of parameter values $\mathbf{p}$ with a total of n_{par} values, defined as $f = f(\mathbf{x},t,\mathbf{p})$. Hereby, $f(\mathbf{x},t,\mathbf{p})$ represents the simulated model output at the same location using model parameter vector $\mathbf{p}$. For surface-subsurface models, $f(\mathbf{x},t,\mathbf{p})$ can be a simulated hydraulic head for the subsurface domain and a simulated discharge for the surface domain.

For the calculation of sensitivities only model outputs at observation locations and times are considered. An approximation of the sensitivity $\partial f/\partial p_i$ can be computed nu-

merically using a forward-difference scheme:

$$\frac{\partial f(\mathbf{x},t,\mathbf{p})}{\partial p_i} \approx \frac{f(\mathbf{x},t,\mathbf{p}+\vec{e}_i\Delta p_i) - f(\mathbf{x},t,\mathbf{p})}{\Delta p_i} \tag{4.1}$$

where $\vec{e}_i$ represents an all zeros vector with a one at position i and Δp_i is a small perturbation.

In linear problems, a small perturbation will generate the same effect on the model output no matter the original parameter value. Hereby if we have n_{par} parameters, $n_{par}+1$ simulations will be needed: one with the original set of parameter values and n_{par} changing each parameter value by a small increment. This analysis is referred to in the literature as local sensitivity (e.g. Saltelli, 2008; van Griensven et al., 2006).

In nonlinear problems, sensitivities may change significantly for different parameter values as the effect of the perturbation on model outputs depend on the original parameter value. For this case, we may need to calculate (local) sensitivities at s different parameter values for each parameter i, $i = 1,2..n_{par}$, i.e. global sensitivity. This procedure leads to a much larger number of required simulations: $2(s_1+s_2+...s_{n_{par}})$.

In surface-subsurface models, due to the nonlinearity associated with the unsaturated zone, sensitivities may be affected as parameter value change. If within the course of parameterization, parameters sensitivities evaluated at different parameter values are very similar, the nonlinearity causes no problem. In contrast, inconsistencies may occur when the sensitivity of one or more parameters change drastically. A given parameter may be locally considered unimportant in terms of the hydrological response but it could be very important globally. This situation may lead to lump important parameters based on incomplete information and in this way affect the predictive capability of the model. From this perspective, in physics-based coupled model we would require the calculation of global sensitivities for each parameter to ensure the adequate design of the calibration problem.

The quantitativeness of the measure of sensitivity for a given parameter p may also be affected by the nominal values chosen for the remaining parameters (van Griensven et al., 2006). Consequently, it results appealing to repeat the experiment for several sets of nominal values of the $n_{par}-1$ remaining parameters for each of the s values of the n_{par} parameters. Thus, many partial global sensitivities can be integrated in an *absolute* global sensitivity measure. This procedure increases the required simulations up to $(n_{par}+1)(s_1 \times s_2 \times s_3 \times ...s_{n_{par}})$. The computational effort required to complete the large number of simulations required to calculate an absolute global sensitivity is hardly feasible in complex fully-coupled, physics-based models due to the associated computational effort.

Parameter correlation is an additional concern in the calibration of hydrological models. In particular, in the case of high parameter correlation between two or more param-

eters, changes in one parameter can be offset by changes in other parameter(s), with the result that they can be varied in certain ratios with virtually no effect on any model output for which a corresponding field measurement exists (Doherty and Hunt, 2009). In that respect, high parameter correlation may result in a non-unique set of calibrated parameters. Hence, parameter correlation should be studied in the parameterization. For this purpose, we may calculate the covariance matrix of parameters $\mathbf{C_{pp}}$ at random location of the parameter space. The latter would allow us to assess the model parameterization in terms of parameter correlation (Anderman et al., 1996). $\mathbf{C_{pp}}$ about a given $\mathbf{p}$ can be calculated from the covariance matrix of error $\mathbf{C_{yy}}$ by linearized error propagation:

$$\mathbf{C_{pp}} = (\mathbf{J}^T \mathbf{C_{yy}}^{-1} \mathbf{J})^{-1} \tag{4.2}$$

with $\mathbf{J}$ being the $n_{obs} \times n_{par}$ sensitivity matrix containing all terms of the form $\partial f / \partial p_i$ calculated at observation locations and according observation times. n_{obs} is the total number of observations considered in the calculation of $\mathbf{C_{pp}}$.

From $\mathbf{C_{pp}}$ with entries c_{ij}, correlation coefficients r_{ij} can be calculated (after Sun et al., 2001) as:

$$r_{ij} = c_{ij} / \sqrt{c_{ii} c_{jj}} \tag{4.3}$$

Standard statistics text books, e.g. Navidi (2008), consider a correlation coefficient r larger than 0.75 as indicative of a high linear correlation.

Composite scaled sensitivities (*CSS*) were introduced by Hill (1992) as a statistic quantity that allows grouping all available observations in order to define which parameters are more important to reproduce the observations. *CSS* can be expressed after Hill and Osterby (2003) as:

$$(CSS_i)^2 = diag\left(\frac{1}{n_{obs}} [\mathbf{P}\mathbf{J}^T \omega \mathbf{J}\mathbf{P}]\right) \tag{4.4}$$

where P is an $n_{par} \times n_{par}$ diagonal matrix with the values of $\mathbf{p}$ on the main diagonal. ω is an $n_{obs} \times n_{obs}$ diagonal matrix with weighting values for each observation that can be assumed as the inverse of the errors covariance matrix $\mathbf{C_{yy}}^{-1}$.

In summary, an adequate parameterization of a physics-based surface-subsurface model should include a global sensitivity analysis and a correlation study of the parameter space. Global sensitivity analysis may help identifying which parameters are important in the model fitting, i.e. calibration set of parameters; and in what ranges they are sensitive, i.e. definition of the calibration parameter space. In general, an adequate parameterization process would allow speeding-up the calibration process by identifying poorly identifiable parameters, and narrowing down the calibration parameter space. As high parameter correlations may mislead the calibration, a correlation study would also help to recognize

potential problems in complex models, and to set-up an adequate calibration problem. In case that high parameter correlations are calculated, results would allow either fixing parameter values, adjusting the model design, incorporating prior information or collecting additional field data, before starting the calibration.

4.6 Calibration

The purpose of the calibration is to establish that the model can reproduce field measurements, i.e. heads and discharge, and to estimate parameter values based on measured quantities. In surface-subsurface models, such measurements are typically stream discharge, hydraulic heads, surface and subsurface concentrations. The calibrated values are achieved by modifying systematically the parameter values until the agreement between measured and simulated values is maximal.

Calibration can be performed *manually* or *automatically*. While manual calibration is deemed to be subjective due to the arbitrary decision of the modeler about the goodness-of-fit, automatic calibration may imply significant computation times not affordable in very complex applications. The choice of the calibration method relies on the modeler and is conditioned by the model running time.

Although the number of parameters depends largerly on the resolution of the spatio-temporal parameter fields. Transient fully-coupled models have been commonly dealt as an overdetermined problem as they have much more measurements, i.e. daily discharge and hydraulic heads, than parameters, i.e. soil hydraulic properties of a few geological zones. Hence, we can not expect the fitted model to meet all measurements perfectly. Instead, the aim is to optimize an overall model performance statistic such as the root squared mean error (RMSE) or the Nash-Sutcliffe coefficient (N_r). Calibration helps also to identify conceptual errors: if we cannot tune the parameters so that the model simulations are within the expected range of error, the underlying assumptions must be wrong. Unfortunately, the opposite does not hold, that is, a perfectly calibrated model does not ensure a correct conceptual model (e.g. Bredehoeft, 2003).

The uncertainty in measured data (measurement and aleatoric error) and in boundary conditions and model assumptions (epistemic error) can be expressed by the covariance matrix $\mathbf{C_{yy}}$. Then, a weighted least-square criterion χ^2 for the goodness of a fit can be expressed after Cirpka (2010) as:

$$\chi^2(\mathbf{p}) = \varepsilon^T \mathbf{C}_{\mathbf{yy}}^{-1} \varepsilon \tag{4.5}$$

where ε_i is the vector of errors consisting of n_{obs} entries $\varepsilon_i = o(\mathbf{x},t) - f(\mathbf{x},t,\mathbf{p})$, with $o(\mathbf{x},t)$ being the observation at location $\mathbf{x}$ and time t, and $f(\mathbf{x},t,\mathbf{p})$ the simulated model output at the same location using model parameter vector $\mathbf{p}$.

In the calibration then we seek a set of parameters **p** which minimizes χ^2. Additionally, for a good model χ^2 should approximately equal the degrees of freedom, i.e. $n_{obs} - n_{par}$.

The calibrated model may be influenced by uncertainty owing to the inability to define the exact spatial distribution of parameter values. Non-uniqueness and identifiability of the calibrated set of parameter values are deemed to affect the capability of the model to reproduce the natural system. Such problems in physics-based models have been widely discussed in the literature (e.g. Beven, 1989; Ebel and Loague, 2006). Due to high parameter correlation between parameters, it remains difficult to obtain a unique set of parameter values in calibration. As reported by Maier et al. (2009), this is particularly problematic for van-Genuchten parameters.

In this study, I follow the definition of Ebel and Loague (2006) and distinguish between uniqueness and identifiability. A set of parameter values is called identifiable if each individual parameter has an influence on the model output, i.e. the model output is sensitive to changes in each parameter, evaluated about the set of calibrated parameter values. A set of parameter values is called unique, if the same optimal model performance can not be achieved with another set of (different) parameter values. Uniqueness and identifiability can, but do not need to be related.

To evaluate identifiability and non-uniqueness about the set of calibrated parameter values, the covariance matrix of the parameters $\mathbf{C_{pp}}$ may be calculated after Eq.4.2. The main diagonal of $\mathbf{C_{pp}}$ contains the estimation variance σ_p^2 of each parameter p. It expresses the uncertainty in the determination of the value of the calibration parameters. If σ_p^2 is small compared to the value of p then the observations contain enough information and are sensitive enough on p to identify the value of p, i.e. they are identifiable.

Alternatively, the composite scaled sensitivity (CSS) has also been used to study parameter identifiability (e.g Anderman et al., 1996; Foglia et al., 2009; Hill and Tiedeman, 2007). Non-uniqueness about the set of calibration parameters can also be studied by calculating the correlation coefficients r_{ij} from the entries c_{ij} of the covariance matrix of parameters $\mathbf{C_{pp}}$ as expressed in Eq. 4.3.

Traditional statistical measurements like the root mean squared error (RMSE) and the Nash-Sutcliffe coefficient(N_r) are typically used to evaluate the performance of the calibration in physics-based models (e.g Jones et al., 2008). These measures are further discussed in section 4.7.

4.7 Validation and Prediction

The purpose of validation and prediction is to establish greater confidence in the model by using the set of calibrated parameters to reproduce a second set of field data. Test-

ing schemes used to evaluate the predictive ability of hydrological models have been widely discussed in the literature (e.g Abbott and Refsgaard, 1996; Ebel and Loague, 2006; Kirchner, 2006; Klemes, 1986, 1987; Loague and VanderKwaak, 2004). In particular, the hierarchical testing scheme proposed by Klemes (1986, 1987) has been posed as the most adequate for testing the capability of a model to predict the hydrological effect of climate change, land use change, and other non-stationary conditions. Four basic categories of typical modeling tests proposed by Klemes (1986) and previously discussed by Refsgaard and Knudsen (1996) are presented below:

1. **The split-sample test** involves splitting the available dataset into two periods, commonly, of a similar length: one for calibration and other for validation.

2. **The differential split-sample test** involves calibration of a model based on data before a catchment change occurs, adjustment of model parameters to characterize the change (if required), and validation on the subsequent period. Differential split-sample tests have been commonly used to show the ability of a distributed model to reproduce different climatological conditions (Abbott and Refsgaard, 1996). A basic requirement of this test is a record of concurrent climatic forcing from which different periods can be chosen that have different historical conditions. For instance, if we want to model a transition to a wetter scenario, i.e. an increase in irrigation, the model should be calibrated using a dryer dataset and then validated for the wetter case. In general, a differential split-sample test is a simple split-sample test, that presents two segments with markedly different conditions.

3. **The proxy-basin test** involves no direct calibration as only information from other gauged catchments is used. In this respect, validation with this scheme comprises identification of a gauged catchment deemed to be of a similar nature to the catchment being validated; initial calibration with the gauged basin and transfer of parameter values to the model being validated, including adjustment of parameters to reflect actual conditions within the validation catchment; and finally validation.

4. **The proxy-basin differential split-sample test** involves again no direct calibration but information from other (gauged) catchment is used. With this scheme validation comprises initial calibration on the other catchment; transfer of the model parameter values to the catchment being validated; selection of one parameter dataset before and one after the change; and subsequent validation on both periods.

Among the schemes proposed *the split-sample* and *the differential split-sample* tests are deemed to be suitable for the case of gauged basins. The proxy-basin test can alternatively make use of results from an already calibrated basin deemed to be of similar nature

of the one being validated, in where the parameter values are directly transfered to the model being validated.

The evaluation of the predictive power of a physics-based model should include the estimation of maximum error (ME), the root mean squared error (RMSE), the coefficient of residual mass (CRM) and the Nash-Sutcliffe coefficient(N_r). These statistics have been previously used to estimate residual errors and characterize systematic under and over-predictions (Jones et al., 2008; Loague and Kyriakidis, 1997). RMSE represents an aggregated measure of model precision; CRM is the aggregated measure of the "deviation" of the predicted values in relation to the observed ones considering the sign of the deviation. The latter implies that both positive and negative deviations contribute to the calculation of CRM, thus in a well-balanced model the residual values should cancel out. In that respect, CRM represents a measure of model under- and overestimation. N_r is a typical statistic for assessing the goodness-of-fit of transient hydrological models.These performance measures are defined as:

$$\text{ME} = max|S_i - O_i|_{i=1}^{n_{obs}} \tag{4.6}$$

$$\text{RMSE} = \left[\frac{1}{n_{obs}} \sum_{i=1}^{n_{obs}} (S_i - O_i)^2\right]^{1/2} \tag{4.7}$$

$$\text{CRM} = \frac{\sum_{i=1}^{n_{obs}} \left(O_i - S_i\right)}{\sum_{i=1}^{n_{obs}} O_i} \tag{4.8}$$

$$N_r = 1 - \frac{\sum_{i=1}^{n_{obs}} (S_i - O_i)^2}{\sum_{i=1}^{n_{obs}} (O_i - O)^2} \tag{4.9}$$

Where S_i are the simulated values at measurement locations, O_i are the observed (i.e. measured) values, and n_{obs} is the number of observations. For ME, RMSE and CRM the ideal value would be 0, whereas for N_r it would be 1. Negative values of CRM indicate a tendency of the model to overestimate discharge and hydraulic heads. Negative N_r indicate that the model prediction is worse than simply using the mean of the observations as a predictor.

If it is required to significantly change the calibrated parameter values during the validation it may be impossible to match the calibration targets. In that case, it would be necessary to repeat the calibration process including both calibration and validation targets. Consequently, the validation dataset becomes part of the calibration and another independent dataset would be needed to perform a new validation of the model.

4.8 Post-audit

A post-audit is conducted several years after the modeling study is completed. New field data is collected to define whether the predictions of the model under climate and/or water management scenarios were correct. A post-audit process should ensure that there has been long adequate time for significant changes to occur. Typically, the post-audit lead to new insights into system behavior which may lead to changes in the conceptual model or changes in the model parameters.

In summary, in this chapter a model protocol to construct and validate a fully-coupled physics-based model is presented. The protocol includes a series of steps intended to ensure the adequate ability of the model to simulate the natural system. Among these steps, parameterization and calibration processes represent two critical points within the development of this type of models as they are constrained by computational times. Hence, in the following a novel methodology is discussed that helps to speed-up these procedures.

Chapter 5

Hillslope Equivalent (HE)

5.1 Geometrical simplification

The combination of sensitivity studies and parameter correlation analysis represents a formal parameterization process. Unfortunately, in physics-based models, this process is commonly avoided due the huge computation times required (months or years). Therefore, the relevant parameters are left to be decided by the modeler based on subjective criteria. In this respect, a model simplification that allows to speed-up the parameterization would be very helpful tool.

In this chapter, the hillslope equivalent (HE) is presented that represents a simplification of the realistic catchment. The 3-D geometrically realistic model (GRM) of the catchment is converted into a 2-D equivalent hillslope. The surface area A and the perimeter Pe of the GRM are preserved and the topographic structure is converted into a single hillslope keeping the hypsometric curve of the natural watershed. The hypsometric curve is an empirical cumulative distribution of the catchment elevations that can be expressed as:

$$F_n(z) = P(x \leq z) \approx \frac{1}{u} \sum_{i=1}^{u} I(x \leq z) \tag{5.1}$$

where u is the number of cells of the digital elevation model (DEM); I is an indicator random variable which is set to 1 when the property $x \leq z$ holds and 0 otherwise. The empirical distribution function $F_n(z)$ is calculated from the DEM of the basin and gives us the relative frequency of the elevations. The latter can be expressed in terms of an area a_i associated to an elevation z_i since the resolution (cell size) of the DEM is known.

A rectangle with length L and width w, that has the same area A and perimeter Pe of the geometrically realistic model, is then constructed picking any of the two valid solutions of the system:

$$\begin{aligned} wL &= A \\ 2(L+w) &= Pe \end{aligned} \tag{5.2}$$

The latter is similar to the concept of *equivalent rectangle* introduced by Roche (1963) to study the influence of the geometrical characteristic of a basin on its hydrological response.

Using the percentage hypsometric curve each elevation z_i is associated to its correspondent area

$$a_i = wl_i \qquad \text{with} \begin{cases} w\sum_{i=1}^{u} l_i = A \\ \sum_{i=1}^{u} l_i = L \end{cases} \tag{5.3}$$

Since the rectangle is uniform in the *y*-direction, w is set to be uniform and a 2-D hillslope equivalent is assumed. The subsurface domain can be incorporated into the hillslope equivalent by reproducing the hypsometric representation of the aquifer top and bottom surface in the same way as for the digital elevation model.

An alternative path that incorporates the use of the hillslope equivalent in the model protocol discussed in the previous section is presented in figure 5.1. The geometrical simplification help us to guarantee that the design of the calibration problem is based on a comprehensive study that includes a global sensitivity analysis and parameter correlation evaluation with the benefit of reduced computational times.

To test the usability of the hillslope equivalent in the context of physics-based models, it is used in the context of the well-known Borden experiment (Abdul, 1985).

5.2 Experiments with the Borden Site problem

The particular Borden experiment discussed here is a 0.001 km^2 plot located within the Canadian Forces Base Borden, 70 km away from Toronto (Canada) that has been intensively studied in the literature, e.g. by Abdul (1985); Abdul and Gillham (1989); Jones et al. (2006). The plot is covered by grass and overlies an aquifer made primarily of medium sand. A constructed drainage channel is about 0.6 m wide and grass-free. Here, we simulated one of the experiments. It involved applying water mimicking a single rainfall event at a rate of 20 mm/hr for 50 min and monitoring the associated discharge for 50 min more following the application of the rainfall. The initial water table elevation was set to 2.78 m. Boundary conditions were set to no-flow except for the outlet, which is defined as critical depth. The subsurface was assumed homogeneous and isotropic.

To test the usability of the hillslope equivalent during the parameterization and calibration of the Borden site, both the HE and the geometrically realistic model are used.

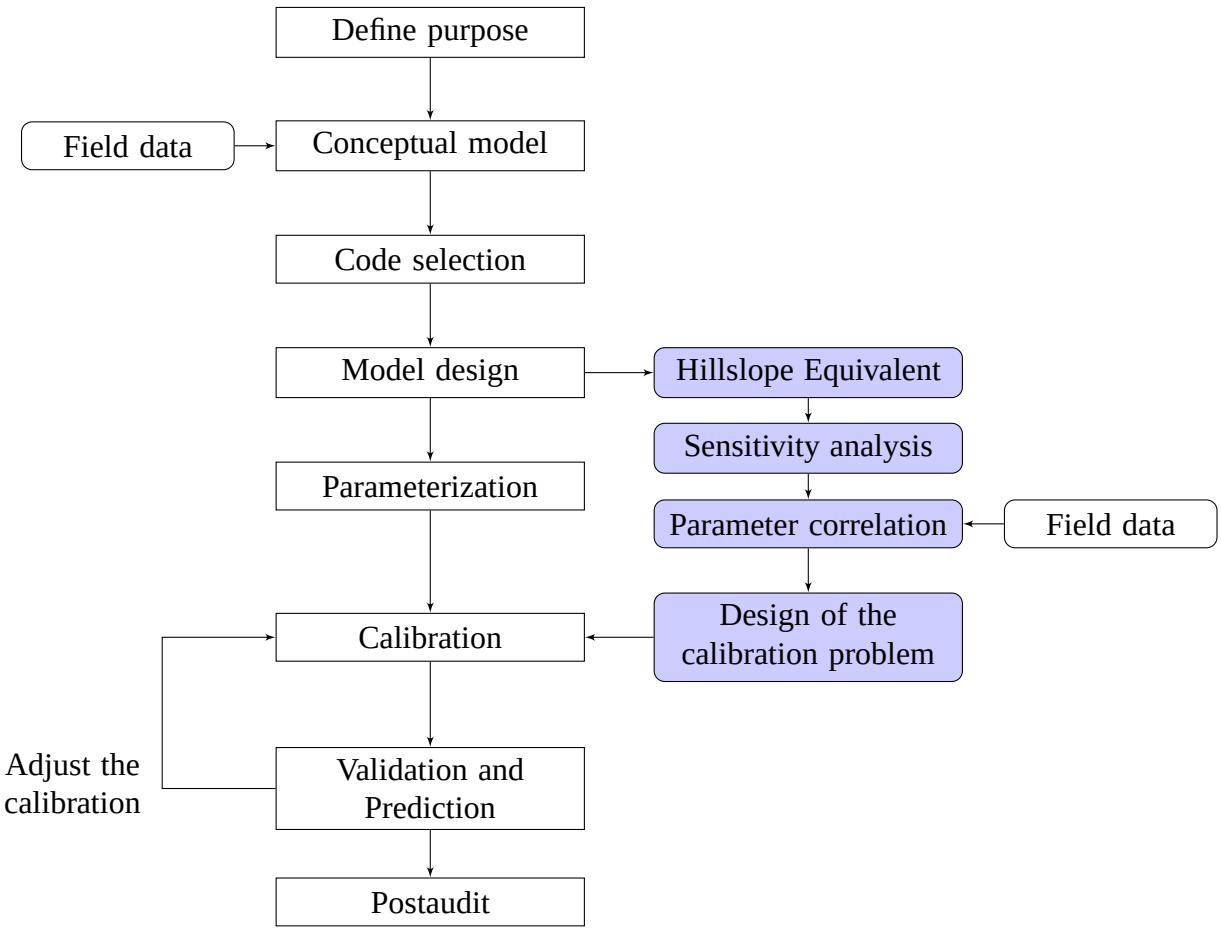

Figure 5.1: Alternative catchment model protocol - use of the hillslope equivalent

Figure 5.2 shows the hypsometric curve of the plot. From this, the hillslope equivalent is constructed following the methodology explained above.

The geometrically realistic 3-D representation of the Borden site and its 2-D hillslope equivalent are shown in Fig. 5.3. Climatological forcing, boundary and initial conditions from the original experiment were also imposed to the simplified model.

To investigate the effect of soil hydraulic parameters on the model outputs, the composite scaled sensitivities (*CSS*) were calculated for the saturated hydraulic conductivity (k_s), the inverse air-entry pressure (α) and the pore distribution factor (n) (number of parameters $n_{par} = 3$). Additionally, to study the variability of the sensitivities as the parameter value changes, we calculated the *CSS* of each of these parameters at 10 different values ($s_1 = s_2 = s_3 = 10$).

To study the effect of choosing nominal values of the remaining parameters on the sensitivity values, the experiment is repeated for 10 different nominal values of the 2 remaining parameters for each of the s_i values of the 3 parameters. Original $f(\mathbf{x},t,\mathbf{p})$ and perturbed case $f(\mathbf{x},t,\mathbf{p}+\delta_i\Delta p_i)$ simulations for each point are required. The latter leads to 4000 simulations.

The matrix of sensitivities **J** was used to calculate the correlation coefficient matrix at

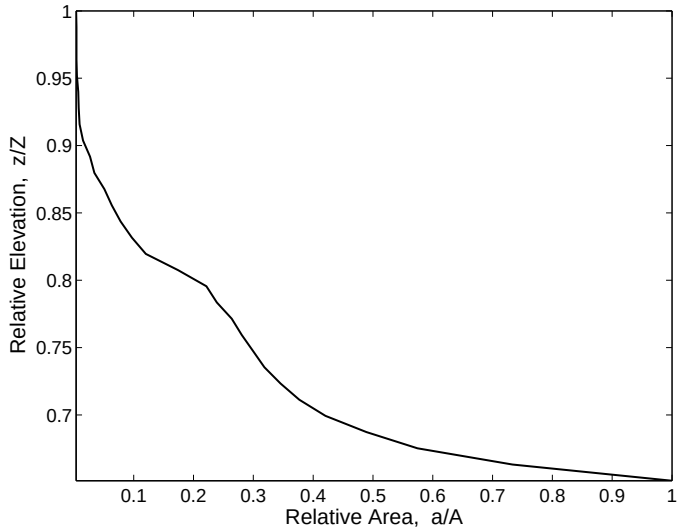

Figure 5.2: Percentage hypsometric curve of the Lerma Basin. a is the area associated to each elevation z. A is the total surface area (7.5 km^2) and Z the maximum elevation of the basin (527.9 m)

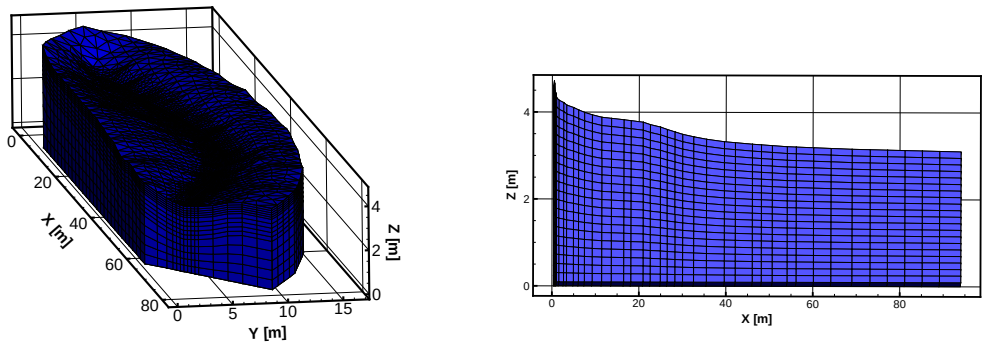

(a) GRM **(b)** HE

Figure 5.3: Geometrically Realistic Model (GRM) and Hillslope Equivalent (HE) for the Borden site experiment

five randomly chosen locations within the parameter space. Correlation values for α vs. k_s; α vs. n; and k_s vs. n are calculated. The measurement errors are assumed uncorrelated. Then $\mathbf{C_{yy}}$ simplifies to a diagonal matrix containing the variance of the measurement error for each observation. The latter was assumed as 10% relative error for all of the measured discharge values.

From the information provided by the 45 streamflow observations, values of *CSS* were calculated. We also evaluated the choice of different nominal values of the remaining parameters with both the GRM and the HE.

In figures 5.4 to 5.6, *CSS*s for the saturated hydraulic conductivity, k_s; and van-

Genuchten parameters, α and n using both the GRM and the HE are shown.

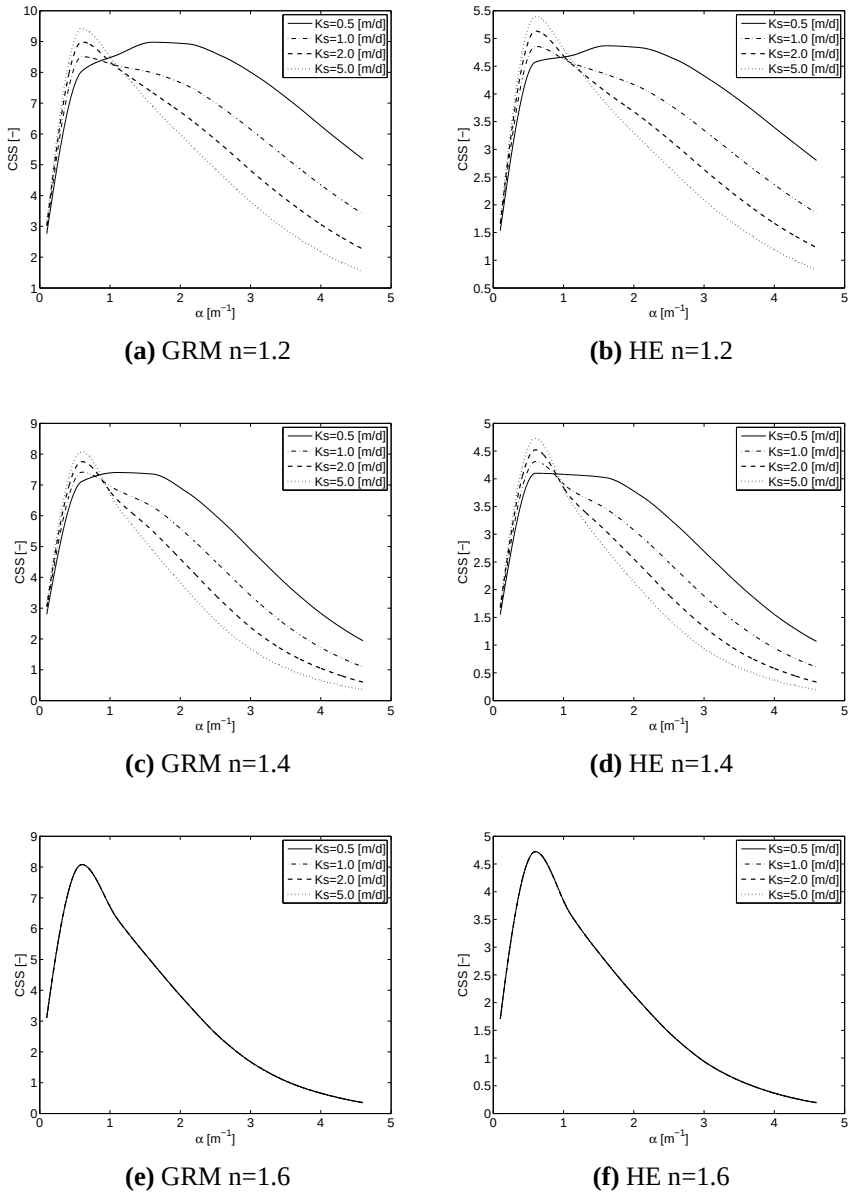

(a) GRM n=1.2 **(b)** HE n=1.2

(c) GRM n=1.4 **(d)** HE n=1.4

(e) GRM n=1.6 **(f)** HE n=1.6

Figure 5.4: Global *CSS* calculated for the geometrically realistic model (GRM) and for the Hillslope Equivalent(HE) for van-Genuchten α

A visual comparison between *CSS*s calculated with the GRM and the HE for α (Fig. 5.4) shows that they have a similar pattern. Both show a steep increase of sensitivity between $\alpha = 0.01$ and $\alpha = 0.7[m^{-1}]$ where a peak is reached, followed by a decrease of *CSS* for further increases in α. The choice of k_s-values appears to control the steepness of the decreasing portion of the curve as for higher values of k_s the decrease is steeper. Higher values of n seems to attenuate the effect of the choice of k_s.

For the van-Genuchten n, the curves of *CSS*s calculated for the GRM and HE show a very similar pattern (Fig. 5.5). Both present a steep increase from $n = 1.1$ to $n = 1.24$. A peak is observed at $n = 1.24$ followed by a slightly less steep decrease of *CSS*. For

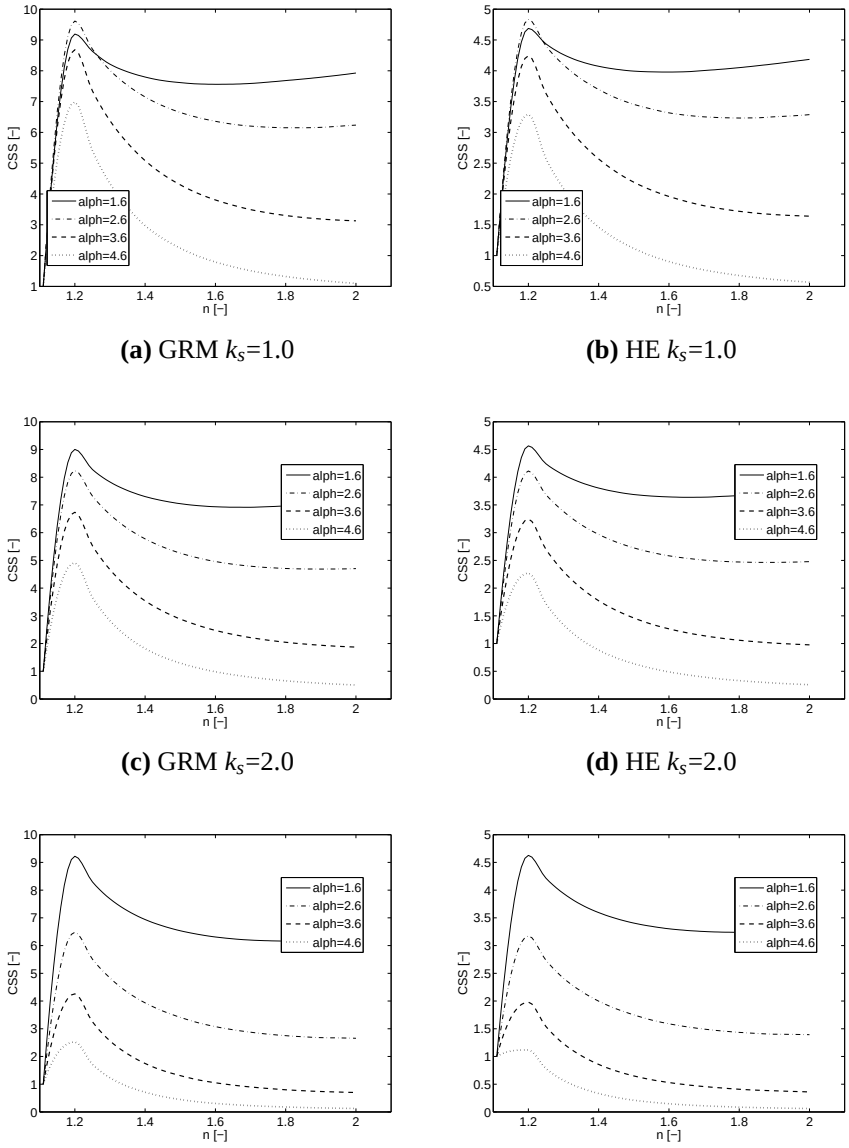

(a) GRM k_s=1.0 **(b)** HE k_s=1.0

(c) GRM k_s=2.0 **(d)** HE k_s=2.0

(e) GRM k_s=5.0 **(f)** HE k_s=5.0

Figure 5.5: Global *CSS* calculated for the geometrically realistic model (GRM) and for the Hillslope Equivalent(HE) for van-Genuchten *n*

$n > 1.8$, *CSS* values remain constant in both cases. The choice of α seems to affect the slope of the decreasing portion of the curve. Higher values of α appears also to reduce the width of the peak. The choice of higher values of k_s increases the differences between the curves generated for different values of α.

In the case of k_s (Fig. 5.6), for small values of α, *CSS* trends for both the HE and the GRM are very similar. In general, CSSs remain constant for any value of k_s. Besides, the effect of *n* appears to be negligible. Conversely, for larger values of α, the trends for the HE and the GRM become different. For increases in k_s, *CSS*s for the GRM shows a mild decrease; for the HE, on the other hand, *CSS*s remain almost constant for any value of k_s. For this case, the influence of the choice of *n* is minimum and appears to be further

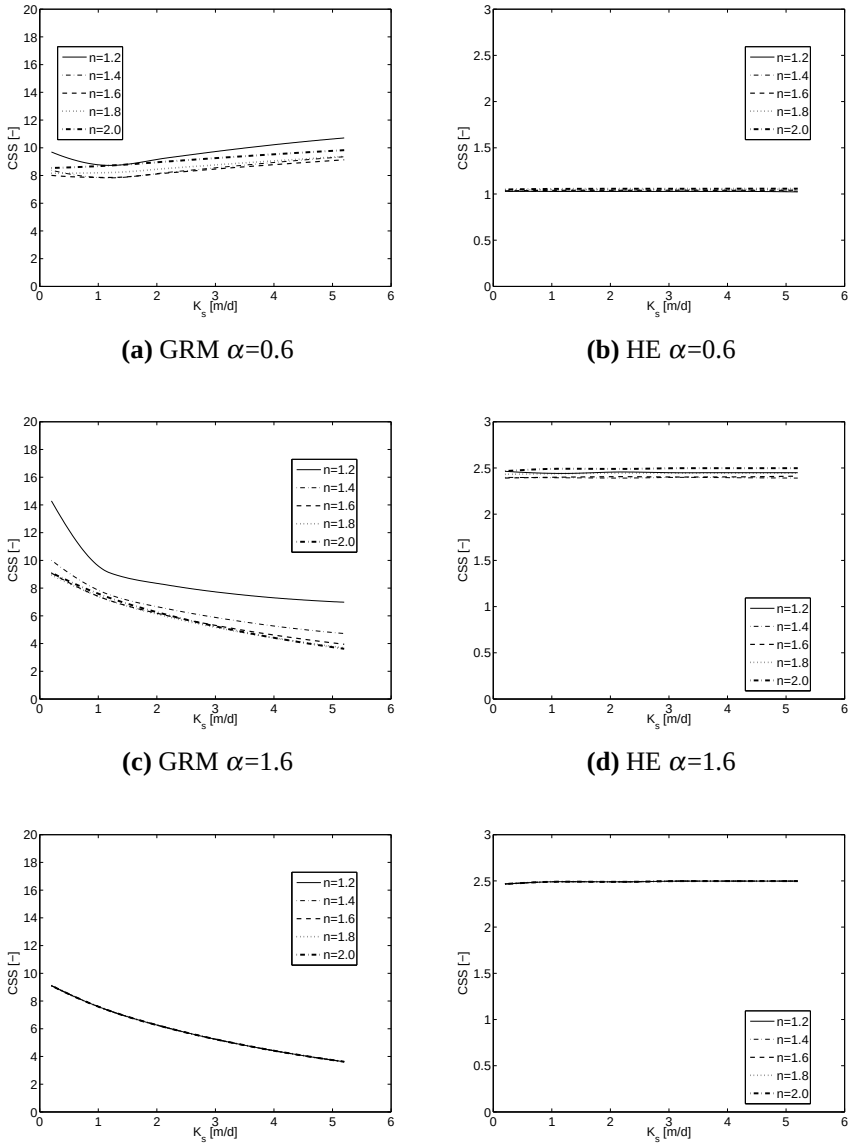

(a) GRM α=0.6 **(b)** HE α=0.6

(c) GRM α=1.6 **(d)** HE α=1.6

(e) GRM α=3.6 **(f)** HE α=3.6

Figure 5.6: Global *CSS* calculated for the geometrically realistic model (GRM) and for the Hillslope Equivalent(HE) for saturated hydraulic conductivity k_s

reduced by the increase of α. Differences in behavior between *CSS*s obtained using the HE and the GRM for k_s may be related to the fact that with considerable increases in α, the air-entry pressure is reduced so that the water-input starts infiltrating at smaller soil saturation. It results in a higher interaction of underlying layers. In this respect, the applicability of the HE may be reduced by increasing effect of deeper soil layers.

In the table 5.1, values of r obtained for both the HE and the GRM at five points of the parameter space are presented. An inspection of α-k_s correlations values obtained for both cases reveals that they are very similar. In both cases, r-values for α-k_s are very high ($r > 0.95$) at three of the points, while in the remaining two, the values are smaller but still very high.

Table 5.1: Correlation coefficients evaluated at different starting parameter values with the geometrically realistic model (GRM) and the hillslope equivalent (HE) of the Borden site. k_s: saturated hydraulic conductivity $[m/d]$; α:inverse air-entry pressure $[m^{-1}]$; and n: pore-distribution factor $[-]$

GRM

k_s=1.0, α=2.0, n=1.8			
	k_s	α	n
k_s	1.000		
α	-0.715	1.000	
n	-0.923	0.390	1.000
k_s=1.0, α=3.0, n=1.3			
	k_s	α	n
k_s	1.000		
α	-0.994	1.000	
n	-0.963	0.905	1.000
k_s=2.0, α=2.0, n=1.8			
	k_s	α	n
k_s	1.000		
α	-0.887	1.000	
n	-0.956	0.673	1.000
k_s=3.0, α=2.0, n=1.8			
	k_s	α	n
k_s	1.000		
α	-0.957	1.000	
n	-0.960	0.876	1.000
k_s=3.0, α=2.0, n=1.3			
	k_s	α	n
k_s	1.000		
α	-0.995	1.000	
n	-0.998	0.966	1.000

HE

k_s=1.0, α=2.0, n=1.8			
	k_s	α	n
k_s	1.000		
α	-0.727	1.000	
n	-0.994	0.651	1.000
k_s=1.0, α=3.0, n=1.3			
	k_s	α	n
k_s	1.000		
α	-0.997	1.000	
n	-0.996	0.967	1.000
k_s=2.0, α=2.0, n=1.8			
	k_s	α	n
k_s	1.000		
α	-0.928	1.000	
n	-0.998	0.806	1.000
k_s=3.0, α=2.0, n=1.8			
	k_s	α	n
k_s	1.000		
α	-0.961	1.000	
n	-0.999	0.953	1.000
k_s=3.0, α=2.0, n=1.3			
	k_s	α	n
k_s	1.000		
α	-0.997	1.000	
n	-1.000	-0.997	1.000

For the case of $\alpha - n$, r is very high ($r > 0.90$) for all points. Despite that r-values obtained with the HE and the GRM are similar, they are consistently higher in the former than in the latter. $\alpha - K_s$ correlation values are in general lower than in the former cases for both the HE and the GRM. However, they are still high ($r > 0.75$) in four of the five points.

The correlation values obtained from this analysis indicate that attempts to estimate all parameters may produce poor results as the uniqueness of the estimation would be questionable. A common way to deal with this problem would be to fix two parameters and calibrate the other one. Nevertheless, the analysis of *CSS* presented above indicated that all parameters have a considerable effect on the model outputs. Previous studies (e.g. Poeter and Hill, 1997) have indicated that measured values or independently obtained estimates of the parameters (i.e. prior information) can be very useful in order to attenuate parameter correlation effect.

Prior knowledge can be obtained either from independent measurements or from literature values. In order to use this additional information, Bayes theorem is applied. In this case, the conditional probability $p(\mathbf{p}|\mathbf{y})$ of the parameters given the measurements is:

$$p(\mathbf{p}|\mathbf{y}) = \frac{p(\mathbf{y}|\mathbf{p})p(\mathbf{p})}{p(\mathbf{y})} \tag{5.4}$$

where the conditional probability $p(\mathbf{y}|\mathbf{p})$ reflects the variability of the measurements $\mathbf{y}$ for a certain parameter set $\mathbf{p}$. The term $p(\mathbf{p})$ describes the distribution of the parameter vector without any information on the measurements $\mathbf{y}$, denoting the prior probability distribution function of the parameter vector. The marginal probability $p(\mathbf{y})$ is a scaling factor that does not depend on the parameters (Cirpka, 2010).

If we assume $p(\mathbf{y}|\mathbf{p})$ and $p(\mathbf{p})$ multi-Gaussians and neglect the marginal probability $p(\mathbf{y})$, we can express the posterior distribution of $\mathbf{p}$ considering the measurements $\mathbf{y}$ after Kitanidis (1997) as:

$$p(\mathbf{y}|\mathbf{p}) \propto exp\left(-\frac{1}{2}(\mathbf{y}-\mathbf{f(p)})^T \mathbf{C}_{\mathbf{yy}}^{-1}(\mathbf{y}-\mathbf{f(p)}) + (\mathbf{p}-\mu_p^*)^T (\mathbf{C}_{\mathbf{pp}}^*)^{-1}(\mathbf{p}-\mu_{\mathbf{p}}^*) \right) \tag{5.5}$$

where $\mu_{\mathbf{p}}^*$ is the prior mean and $\mathbf{C}_{\mathbf{pp}}^*$ the prior covariance matrix defined from the prior knowledge.

In order to find the best fit of the parameter set $\mathbf{p}$ both meeting the observations $\mathbf{y}$ and the prior information, we have to minimize the negative logarithm of $p(\mathbf{y}|\mathbf{p})$ (Kitanidis, 1997). The latter gives us a modified χ^2 criterion:

$$\chi^2(\mathbf{p}) = \mathbf{y}-\mathbf{f(p)})^T \mathbf{C}_{\mathbf{yy}}^{-1}(\mathbf{y}-\mathbf{f(p)} + (\mathbf{p}-\mu_{\mathbf{p}}^*)^T (\mathbf{C}_{\mathbf{pp}}^*)^{-1}(\mathbf{p}-\mu_{\mathbf{p}}^*) \tag{5.6}$$

As shown in Eq. 5.6, the prior information is included as a penalty term. The vector $\mu_{\mathbf{p}}^*$ of prior mean acts like a measurement of $\mathbf{p}$ with a related uncertainty expressed by $\mathbf{C}_{\mathbf{pp}}^*$. A deviation of $\mathbf{p}$ from its prior mean $\mu_{\mathbf{p}}^*$ is punished by an increase in the objective function χ^2 (Cirpka, 2010).

Prior values of saturated hydraulic conductivity k_s and van-Genuchten parameters α and n for the Borden-site experiment are available from Jones et al. (2006), i.e. μ_K=0.9 $[m/d]$, μ_α=1.9 $[m^{-1}]$ and μ_n=6.0 $[-]$. To define the covariance matrix $\mathbf{C}_{\mathbf{pp}}$ expressing the uncertainty related to the prior parameter values, we used the standard deviation values estimated by Carsel and Parrish (1988) for a sandy loam. The latter seems to be justified for the cases of k_s and α as the values are very similar. However, for the case of van-Genuchten n the value assumed in Jones et al. (2006) falls far from any of the values reported in Carsel and Parrish (1988). Hence, a higher covariance of n was assumed. Values used to account for prior information are presented in table 5.2.

The objective function is evaluated using Eq. 5.6 throughout the parameter space. For

Table 5.2: Information used to evaluate the objective function using prior knowledge for the Borden site test case. k_s: saturated hydraulic conductivity; α:inverse air-entry pressure; and n: pore-distribution factor

Parameter	μ	σ
$K_s[m/d]$	0.9	1.35
$\alpha[m^{-1}]$	1.9	3.7
$n[-]$	2.0	4.0*

comparison, the evaluation is done for both the hillslope equivalent and the geometrically realistic model. Scaled χ^2-values for the GRM and the HE are shown in Figure 5.7. Results obtained for different third parameter values were averaged.

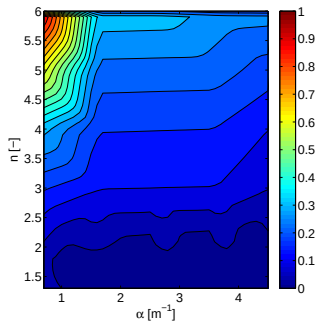

(a) GRM $\alpha - n$

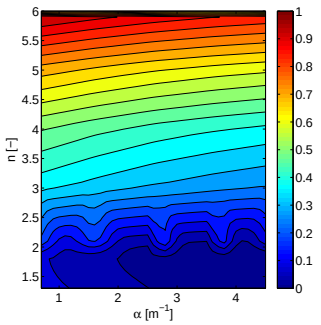

(b) HE $\alpha - n$

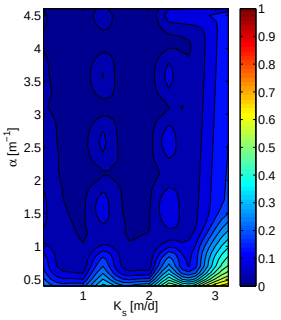

(c) GRM $K_s - \alpha$

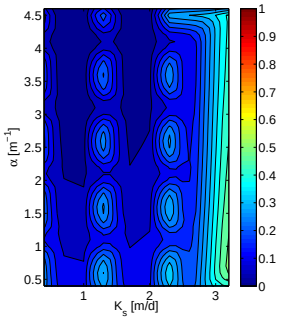

(d) HE $K_s - \alpha$

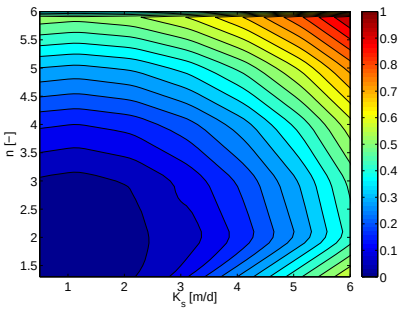

(e) GRM $K_s - n$

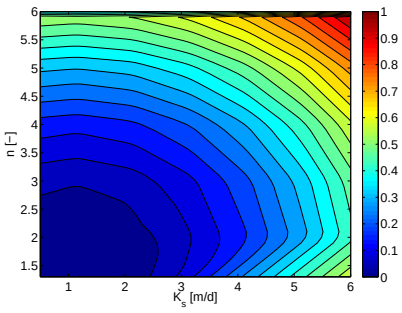

(f) HE $K_s - n$

Figure 5.7: Objective function χ^2 using prior information for the geometrically realistic model (GRM) and the hillslope equivalent (HE) of the Borden-site experiment

As it can be observed, the results for all cases are very similar. In figures 5.7a and 5.7b values of χ^2 for α and n are presented. Minimum values of the error are observed for $\chi^2 \in (1.2 < n < 2.0 \wedge 1.0 < \alpha < 4.0)$. There appears to be slight differences between the results obtained with the HE and the GRM as for the former smaller values of χ^2 are observed within a smaller region, i.e. $\chi^2 \in (1.2 < n < 2.0 \wedge 2.0 < \alpha < 4.0)$. Increases in n (i.e. $n > 2.5$) lead to increases in χ^2 for both the GRM and HE, however, the increase seems to be steeper in the latter compared to the former. Besides, the HE is unable to represent the anomaly observed when using the GRM at $\chi^2 \in (4.5 < n < 6.0 \wedge 0.5 < \alpha < 1.5)$.

In figures 5.7c and 5.7d values of χ^2 for k_s and α are presented. There are 8 peaks of χ^2 located at $K_s = 1.3$ and $K_s = 2.3$ for $\alpha = [1.5, 2.5, 3.5, 4.5]$ for both cases. Despite the similar pattern, differences appear to be highlighted for the case of the HE.

In figures 5.7e and 5.7f values of χ^2 for k_s and n are shown. The general pattern for both the GRM and the HE are almost identical. Smaller χ^2-values are observed in the region $\chi^2 \in (4.5 < n < 6.0 \wedge 0.5 < K_s < 2.2)$.

The set of optimal parameters obtained from the objective function evaluation is $K_s = 0.9[m/d]$, $\alpha = 1.3[m^{-1}]$ and $n = 1.9$. In Figure 5.8 measured and simulated hydrographs are presented. The root mean squared error (RMSE) and the Nash-Sutcliffe coefficient (N_r) calculated for the calibrated model are 0.03 $[l/min]$ and 0.68 $[-]$, respectively. These results indicates a relatively good performance of the model.

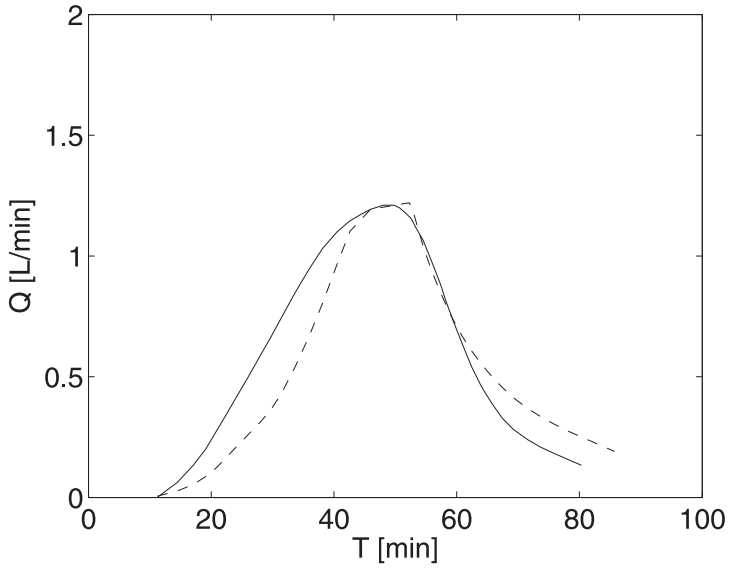

Figure 5.8: Simulated and Measured hydrograph at the Borden site experiment

In summary, results obtained at the Borden site show the ability of the hillslope equivalent to quantify the influence of the soil hydraulic parameters on the near-surface hydrological response, providing the modeler with enough information to design an adequate calibration problem.

The comparison with the realistic model indicates that findings obtained with the hillslope equivalent may be used directly in the parameterization of a model with the benefit of reducing computational times. The reduction in running times achieved by studying the parameter sensitivities with the hillslope equivalent rather than with the geometrically realistic model at the Borden site experiment is quite large. While a single run using a single PC with an Intel Core 2 Duo E6600 2.4 GHz with the GRM took between 15 to 30 minutes depending on the choice of the soil parameters, it took 2 - 3 min with the HE using the same PC.

From this perspective, the alternative modeling protocol which includes the use of the hillslope equivalent presented in Figure 5.1 represents a useful tool in the context of physics-based models. In the following, this protocol is used to develop the surface-subsurface physics-based flow model of the Lerma basin.

Chapter 6

Lerma Basin

6.1 Data Inventory

The Lerma basin ($\sim 7.5 km^2$) is located at the south-eastern part of the Arba catchment, see Fig. 6.1). It represents a semi-arid area, geologically characterized by quaternary deposits on the lower part of a pediment. In the following, I will refer to these deposits as ”glacis” in slight abuse of the geomorphologic term referring to the sediment covered part of a pediment.

The glacis consists of permeable, unconsolidated, clastic deposits that typically occur on pediments in arid or semi-arid climates and result from intense weathering and surface transport via episodic flow events. This glacis layer represents a shallow, phreatic aquifer that is seasonally fed by precipitation and irrigation return flows and discharges into the Lerma basin creeks. The glacis is overlying tertiary bedrock made up of lutites and marlstones. Locally this formation is called ”buro”, and I will adhere to this term hereafter. Causape (2002) indicated that the buro is relatively sensitive to weathering and fracturing processes and for this reason water seepage through the upper buro layers is likely to occur. Hence, it is assumed that water circulation through the top part of the buro does play a role for the subsurface part of the Lerma hydrosystem. Nevertheless, the buro unit as a whole represents an aquitard, so that we included only the top part of the buro unit into the model domain. The very thin soil cover at Lerma basin consists of inceptisols, which only exhibit moderate degrees of soil weathering and development. For this reason, the glacis sediments and the soil cover are considered as single model unit.

The climate of Lerma basin is classified by the Spanish Institute of Geomining Technology (SIGT) as Mediterranean warm climate (Garcia-Garizabal et al., 2009) characterized by moderate to low rainfall ($\bar{P}$=450 mm) and high potential evapotranspiration ($\bar{ET_p}$=1000mm). The driest months correspond to Winter (December-January) and Summer (July-September) seasons and the rainiest to Spring (April-May).

Beginning in October 2005, pre-defined plots (total area = 3.9 km^2) were year by year

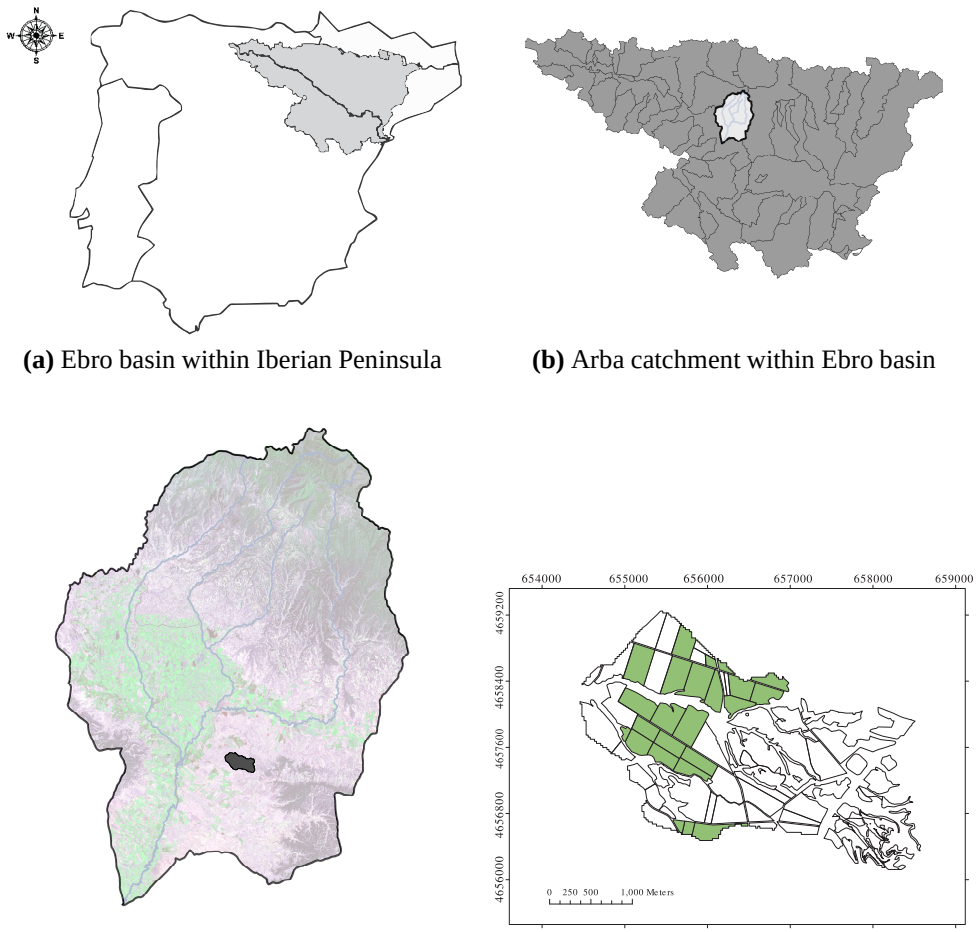

(a) Ebro basin within Iberian Peninsula

(b) Arba catchment within Ebro basin

(c) Lerma basin within Arba catchment

(d) Lerma Basin

Figure 6.1: Location of study area in the Arba basin: (a) the Ebro basin within the Iberian peninsula; (b) the Arba catchment within the Ebro basin; (c) the Lerma basin within the the Arba catchment and (d) the Lerma basin(the green areas represent irrigated plots for the hydrological year 2007)

transformed into irrigated crop land. In the hydrological year 2006 (ranging from October 2005 to September 2006), 32% of these pre-defined plots became subject to irrigation (i.e. an area of 1.25 km^2). In the hydrological years 2007, 2008 and 2009 the proportion of the irrigated plots increased up to 68% (2.65 km^2), 80% (3.12 km^2) and 90% (3.5 km^2), respectively. The amount of irrigated water is gauged at irrigation hydrants located at each plot and the logged data regularly checked for plausibility. The spatial pattern of this transition over time is depicted in Fig. 6.2.

Topographic information of the Lerma basin is given by a digital elevation model (DEM) with a horizontal resolution of 25 m. The land-use patterns are defined by 60 surface units outlining the pre-defined plots (55 units), the creeks (1 unit), the non-irrigated areas (3 units), and irrigation water reservoirs (1 unit). In Figure 6.3, the DEM is shown together with the surface unit polygons.

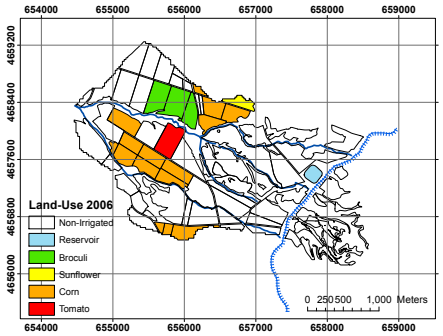

(a) Irrigated plots 2006

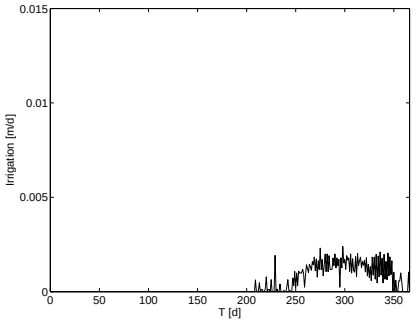

(b) Daily Irrigation 2006 for the whole basin

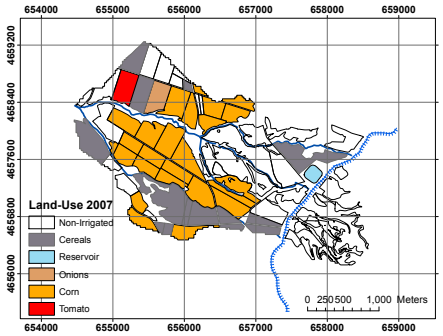

(c) Irrigated plots 2007

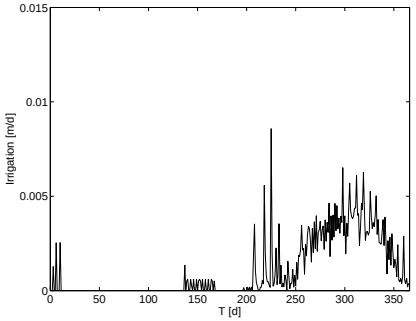

(d) Daily Irrigation 2007 for the whole basin

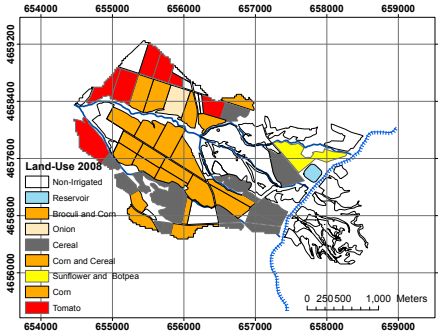

(e) Irrigated plots 2008

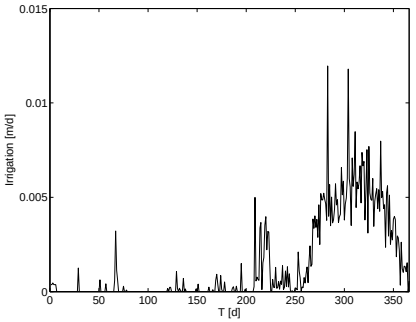

(f) Daily Irrigation 2008 for the whole basin

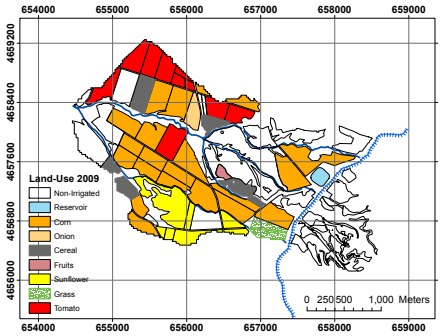

(g) Irrigated plots 2009

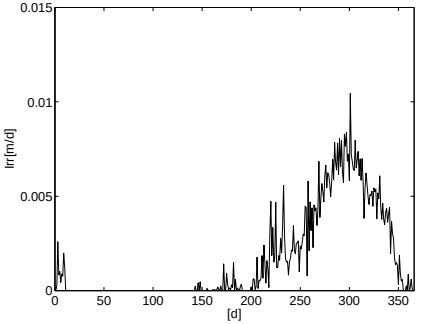

(h) Daily Irrigation 2009 for the whole basin

Figure 6.2: Irrigated plots for the simulated years 2006 - 2009 and the corresponding daily amounts of irrigation for the whole Lerma basin. The coloring scheme represents the land-used for each year which includes baresoil, tomatoes, corn, cereal, and a label for a local reservoir lake

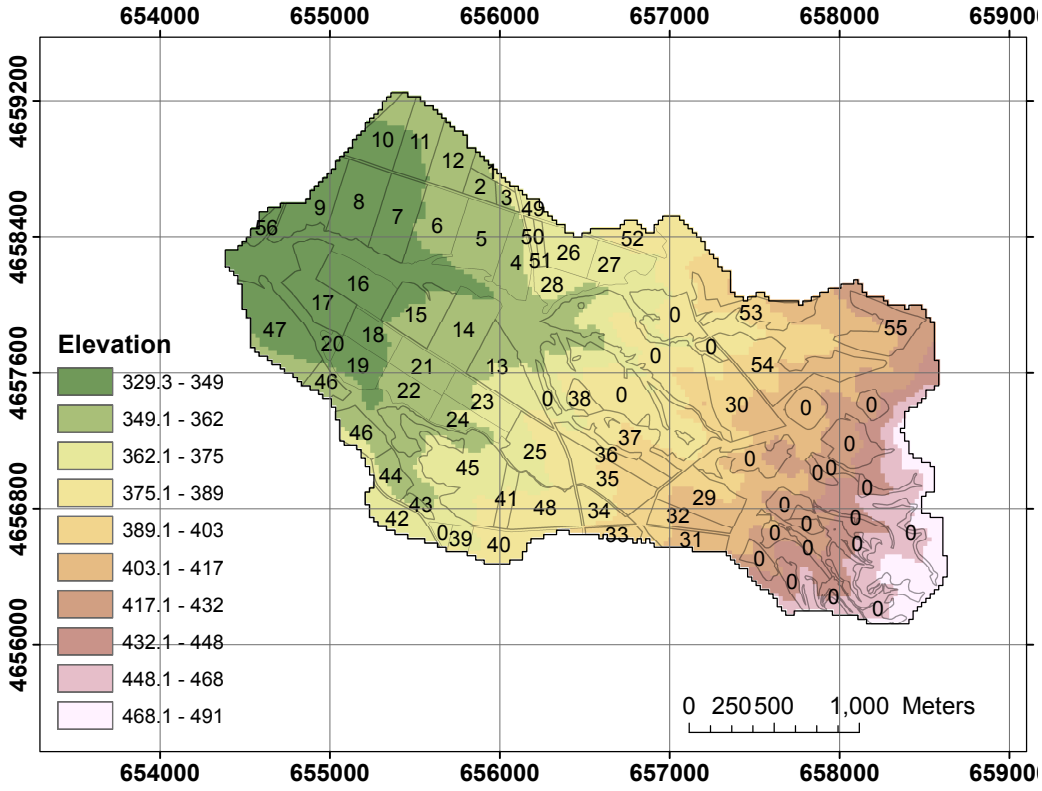

Figure 6.3: Digital elevation model with the established surface units. Coloring scheme shows the distribution of the terrain elevation. Plots with zeros indicate the non-irrigable areas; plots with numbers between 1 and 55 show the pre-defined irrigable plots; and areas with no numbers represent the known creeks

Daily rainfall, air temperature T_a, wind velocity at two meters height υ_2, relative humidity W_a and radiation R_n are obtained from the climatological station *Ejea de los Caballeros* (operated by the Government of Aragon (Gobierno de Aragón)) located within 5 km from the Lerma basin. In order to generate a reasonable hourly rainfall distribution (which is important for peak discharge simulation) for the Lerma basin for hydrological years 2006-2008 for which only daily rainfall is available, the hourly rainfall distribution from the roughly 22 km distant climatological station *Cola del Saso* (operated by Confederación Hidrográfica del Ebro (CHE)) was used to distribute the daily totals measured at *Ejea de los Caballeros* over each 24-hour period. As the 24-hour sums of both stations correlate very well this approach seemed to be justified. For the hydrological year 2009, hourly rainfall is available directly from the climatological station *Ejea de los Caballeros*.

Stream discharge Q is measured at the basin outlet in 15 minute intervals. Figure 6.4 shows daily precipitation P and daily discharge Q series for the simulated period, i.e. the hydrological years 2006-2009. Based on hydroclimatological data, potential evapotranspiration is calculated with the well-known Penman-Monteith method (Beven, 1979; Penman, 1948) using the FAO-Penman-Montieth approach (Allen et al., 1998). As discussed in section 2.1.2, the reference evapotranspiration ET_o is calculated using grass as the crop reference (Allen, 2005; Allen et al., 1998). By the correction crop factor k_c, the actual evapotranspiration ET_a is obtained. Luckily, for this particular catchment k_c values for each crop and each vegetative period are available from Garcia-Vera and Martinez-Cob (2004) who studied actual evapotranspiration throughout the cultivated areas of the region. k_c values for baresoil were taken from Allen et al. (1998). Values of k_c for typical land-use within the Lerma basin are presented in Table 6.1.

Considering the meteorological and agricultural patterns, three different seasons for the hydrological year (October to September) at Lerma basin can be defined: (i) *non-irrigated season*: the first 150 days -October to February- when comparatively small values of irrigation and precipitation are measured; (ii) *rainy season*: between March and mid-June when a high contribution of precipitation contrasts the much lower irrigation; (iii) *irrigation season*: mid-June to September, when predominantly irrigation takes place with scarce precipitation.

In terms of subsurface observation data, hydraulic heads are available for eight wells located within the basin for the hydrological years 2008 and 2009. (see Fig. 6.5). However, due to technical problems piezometers 2 and 6 located very close to the northwestern and southern boundaries, respectively, were disregarded for the calibration and the subsequent validation processes.

Porous media properties were obtained from a soil characterization campaign in the Bardenas district, which encompassed also 10 points (with a sampling depth of 1.0 m) within the Lerma Basin (see Fig. 6.5). The information consists of textures and bulk densities for the glacis unit. Porosities (ϕ) were indirectly calculated from bulk densities

Table 6.1: Monthly crop factors(k_c) for different common land-uses within the Lerma Basin

	Monthly variation of the crop factor (k_c)											
Crop	1	2	3	4	5	6	7	8	9	10	11	12
Baresoil	1.010	0.710	0.390	0.360	0.300	0.180	0.110	0.130	0.220	0.470	0.850	1.110
Alfalfa	1.010	0.710	0.370	0.920	1.010	0.950	0.920	0.920	1.160	0.470	0.850	1.110
Corn	1.011	0.707	0.392	0.308	0.309	0.647	1.173	1.222	0.781	0.394	0.849	1.110
WinterCereal	1.052	1.151	1.163	1.158	0.859	0.433	0.107	0.134	0.222	0.474	0.934	0.949
Rice	1.011	0.707	0.392	1.100	1.102	1.169	1.228	1.213	1.018	0.474	0.849	1.110
Grass	1.000	1.000	1.000	1.000	1.000	1.000	1.000	1.000	1.000	1.000	1.000	1.000
Sunflower	1.011	0.707	0.392	0.310	0.323	0.729	1.163	1.094	0.577	0.474	0.849	1.110
Pepper	1.011	0.707	0.392	0.306	0.336	0.676	1.033	1.071	0.969	0.474	0.849	1.110
Tomato	1.011	0.707	0.392	0.357	0.307	0.656	1.111	1.170	1.057	0.474	0.849	1.110
Onion	1.011	0.707	0.376	0.699	1.069	1.069	1.019	0.842	0.222	0.474	0.849	1.110
Broccoli	1.011	0.707	0.392	0.357	0.298	0.185	0.107	0.165	0.354	0.954	1.007	1.110
Peas	0.954	0.994	1.134	1.166	1.156	0.185	0.107	0.134	0.222	0.474	0.849	0.954
Trees	1.011	0.707	0.364	0.408	0.671	0.938	0.987	0.987	0.872	0.378	0.849	1.110
Barley	1.031	1.155	1.159	1.106	0.705	0.356	0.107	0.134	0.222	0.810	0.810	0.858
Oats	1.052	1.151	1.163	1.158	0.859	0.433	0.107	0.134	0.222	0.474	0.934	0.949
Cereal-Broccoli	1.052	1.151	1.163	1.158	0.859	0.433	0.107	0.165	0.354	0.954	1.007	1.110
Cereal-Sorghum	1.052	1.151	1.163	1.158	0.859	0.433	1.173	1.222	0.781	0.394	0.934	0.949
Cereal-Sunflower	1.052	1.151	1.163	1.158	0.859	0.433	1.163	1.094	0.577	0.474	0.934	0.949
Cereal-Corn	1.052	1.151	1.163	1.158	0.859	0.433	1.173	1.222	0.781	0.394	0.934	0.949
Broccoli-Corn	1.011	0.707	0.392	0.308	0.309	0.647	1.173	1.222	0.781	0.394	0.849	1.110
Peas-Sunflower	0.954	0.994	1.134	0.310	0.323	0.729	1.163	1.094	0.577	0.474	0.849	0.954
Peas-Corn	1.011	0.707	0.392	0.308	0.309	0.647	1.173	1.222	0.781	0.394	0.849	1.110
Pinetree	1.010	0.710	0.360	0.410	0.670	0.940	0.990	0.990	0.870	0.380	0.850	1.110

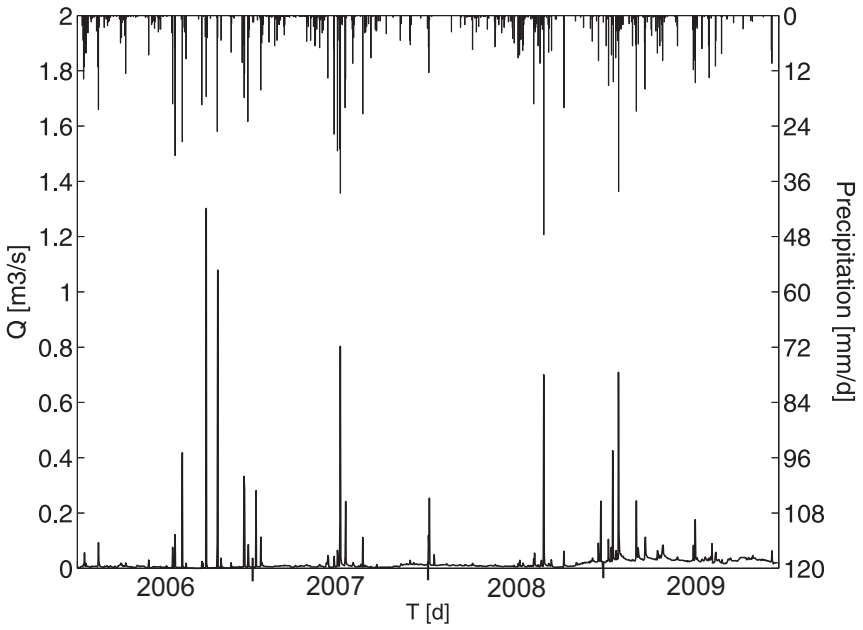

Figure 6.4: Daily precipitation(top) and daily discharges Q (bottom) at the basin outlet for the simulated years 2006-2009

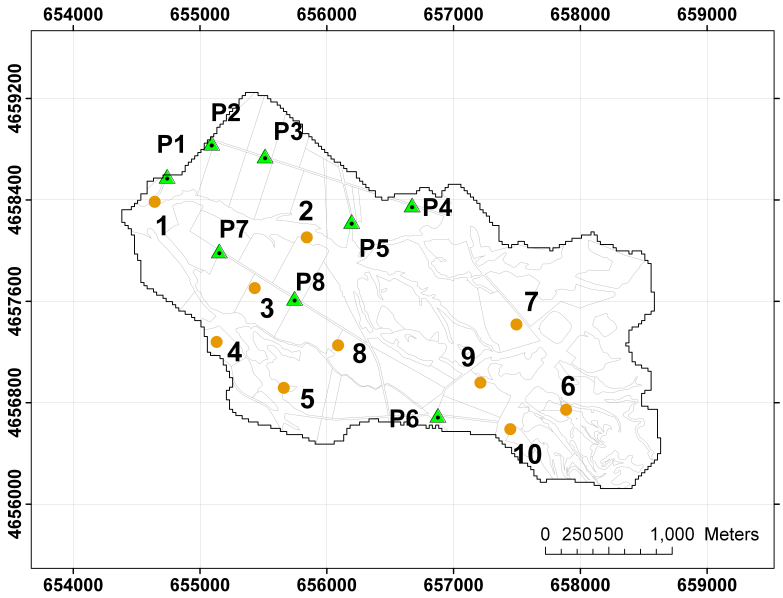

Figure 6.5: Location of piezometers and soil samples. Triangles represent the available piezometers. Circles represents the soil samples: samples 4, 7, 9 were associated during the soil campaign to *clay* texture. Samples 1, 2, 5, 10 were classified as *clay-loam*. Finally, samples 3, 6, 8 were labeled as *sandy-clay-loam*.

at saturated and dry conditions. Specific storage (S_s) and residual saturation (S_{w_r}) were defined from literature values (Freeze and Cherry, 1979). For the observed soil textures typical values of saturated hydraulic conductivity (k_s) found in the literature (Carsel and Parrish, 1988) range between 0.005 and 1.0 m/d. However, values of k_s measured in pumping tests in the north of the Arba basin within the same lithologic unit (i.e. the glacis) are larger (between 1 and 7.7 m/d).

Texture information and the corresponding ranges given in Carsel and Parrish (1988) are used to constrain the van-Genuchten parameters α and n for the glacis unit. Mean values ($\bar{x}$) and standard deviations (σ) from Carsel and Parrish (1988) for these textures are presented in Table 6.2.

Table 6.2: Soil hydraulic properties given in Carsel and Parrish (1988): saturated hydraulic conductivity (k_s), inverse air-entry pressure and pore-size factor (n)

Soil Texture	$k_s[m/d]$		$\alpha[m^{-1}]$		$n(-)$		Samples No.
	$\bar{x}$	σ	$\bar{x}$	σ	$\bar{x}$	σ	
Clayey	0.05	0.10	0.8	1.2	1.09	0.09	4, 7, 9
Clayey-loam	0.06	0.17	1.9	1.5	1.31	0.09	1, 2, 5, 10
Sandy-Clayey-Loam	0.31	0.66	5.9	3.8	1.48	0.13	3, 6, 8

6.2 Purpose of the Model

One of the main purposes of the model is to study the impact of the transformation of the semi-arid rainfed Lerma basin towards irrigation agriculture on the hydrological functioning of the basin. The ongoing land-use transformation during the simulated period and the strong influence of irrigation on the whole hydrosystem indicates that it is absolutely necessary to account for temporal changes of climate forcing and irrigation in order to reproduce the transient surface-subsurface water flow dynamics. In particular, field observations comparing the hydrological year 2006 with subsequent years show that the intermittent main creek in Lerma basin has become a perennial stream due to irrigation. Considerable groundwater exfiltration is therefore evident. This indicates a shift in runoff generation processes during the monitoring period due to the land-use evolution. I strongly believe that this situation can be best modeled by a coupled physics-based approach.

The ultimate goal of the study at the Lerma basin is to ensure the sustainability of current agricultural practices. In this context, the fate and transport of nitrate is of primary importance. The determination of surface-subsurface velocity fields and/or transient travel-time distributions are a prerequisite for transport simulations. Also the explicit consideration of the spatial distribution of transport parameters along different transport paths becomes important. In this respect, a fully-integrated physics-based model represents the

best choice.

In order to evaluate the degree of confidence and the predictive ability of the model of the Lerma basin. The validation protocol presented in Figure 5.1 is completed. It includes construction of the conceptual model, selection of the code, parameterization (using the hillslope equivalent), calibration and validation.

Following, the validated model is used to study spatially and temporally resolved flow variables as well as to investigate the impact of the transformation on the hydrological variables and on the surface-subsurface interaction. Finally, the flow model is integrated to a conservative physics-based nitrate transport model of the Lerma basin. The main purpose of the nitrate study is to show the huge potential of this type of models on the definition of water management strategies intended to guarantee the sustainability of the agriculture practices.

6.3 Conceptual Model and Model Design

6.3.1 Discretization

The 3-D flow model of the Lerma basin is given by a finite element mesh of 141,943 nodes and uses a triangulation of the DEM as its top boundary, including mesh refinements along the known creeks. For the surface domain, 15,718 elements were assigned to 60 surface units representing the pre-defined plots. The maximum plan-view length scale of the elements is 40 m and the smallest elements located at the known creeks extend over 2 m.

For the subsurface, a two-layered geometry consisting of 235,770 prism elements is defined. The top layer represents the glacis whose thickness varies in the irrigated area between 1.0 and 10.0 m; the bottom one represents the buro whose thickness varies between 1.0 and 4.0 m. Both layers are further divided into sub-layers. The uppermost layer was subdivided into 0.1 m thick sub-layers in the top half and 2.0 m thick ones in the second half. The lower layer was subdivided into 5 sub-layers of varying thickness from 2.0 m to 10.0m. Spatial variability of soil parameters within the glacis layer based on soil textures is introduced. To account for the spatial variability a further zonation is considered: *a*) Zone 1: the western region of the basin characterized by clay texture; *b*) Zone 2: eastern portion characterized by clay-loam texture ; and *c*) Zone 3: the middle of the basin characterized by sand-clay-loam texture . The buro layer was assumed to be uniform and labeled as Zone 4. Within each element hydraulic conductivity was assumed to be uniform and isotropic. The catchment model domain and zonation are shown in Fig. 6.6.

In the surface domain, 60 different sub-domains corresponding to the land-use units were defined. Actual evapotranspiration and irrigation amounts are set for each of these sub-domains separately. Manning's coefficients (n_m) are defined for each element accord-

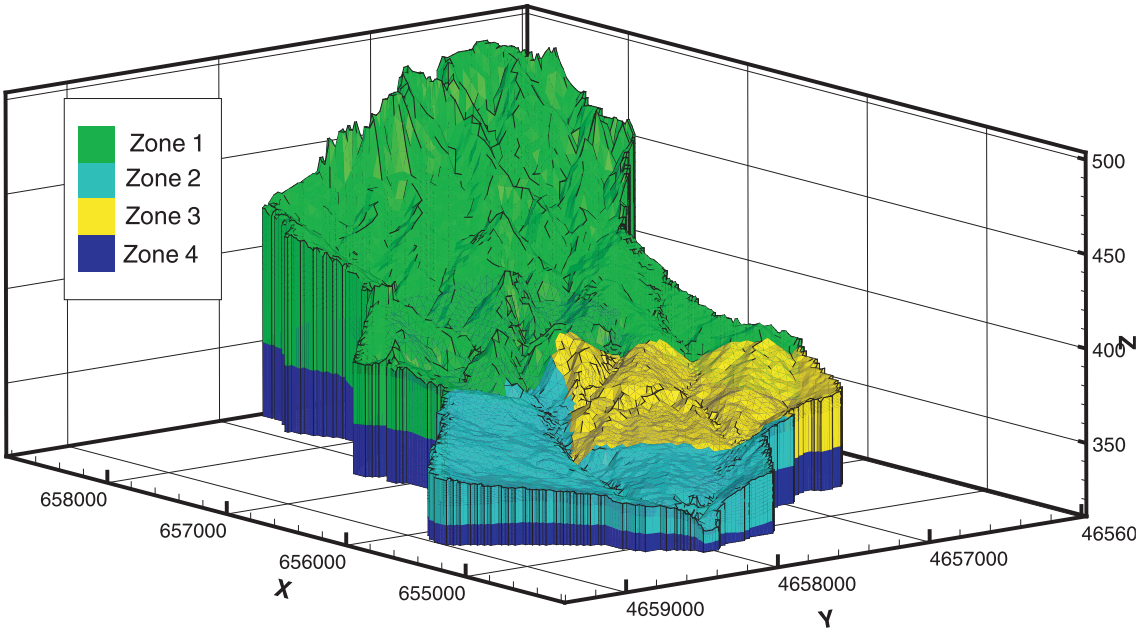

Figure 6.6: Three dimensional representation of the hydro-stratigraphic units defined in Lerma basin. Zone 1: Clay texture; Zone 2: clay-loam texture; Zone 3: sandy-clay-loam texture and Zone 4: buro

ing to the predominant land-use (see Table 6.3). Obstruction (h_{od}) and rill (h_{sd}) heights are both set to 0.002 m for the cultivated areas and to 0.0005 m for the non-cultivated areas. The coupling length required for the surface-subsurface exchange flow was assumed to be uniform for the whole domain and set to $l_e = 10^{-2}$ m based on the work of Ebel et al. (2009).

6.3.2 Boundary Conditions

For the surface domain, the following boundary conditions were defined: *a*) time-varying boundary condition of the second-kind (Neumann) for the forcing fluxes (i.e. rainfall, evapotranspiration, irrigation); *b*) boundary condition of the third kind (critical depth) at the lateral domain boundaries . The latter enforces a unique discharge flow-depth relationship, where the flow depth H is equal to the critical depth ($H = H_c$) and the relationship to the discharge per unit width at the boundary, Q_{eb}, can be expressed as:

$$Q_{eb} = \sqrt{gH_c^3} \tag{6.1}$$

The choice of the critical flow depth is supported by the fact that the gauging station at the basin outlet represents a weir, where critical flow is ensured. The upper boundary condition for the subsurface flow is given by the exchange fluxes through the interface layer to the surface as expressed in Eq. 3.8. We assume no-flow (q_g=0) for the bottom and lateral subsurface domain boundaries due to the headwater characteristics of Lerma

Table 6.3: Parameters for the predominant land-use within the Lerma Basin: n_m: Manning coefficient; h_{ds}: the height of depression storage; h_{os}: the height of storage within the obstructions and l_e: coupling length

Land-Use	$n_m[s/m^{1/3}]$	$h_{od}[m]$	$h_{sd}[m]$	$l_e[m]$
Baresoil	0.03	2.0e-03	2.0e-03	0.01
Alfalfa	0.04	2.0e-03	2.0e-03	0.01
Corn	0.04	2.0e-03	2.0e-03	0.01
WinterCereal	0.04	2.0e-03	2.0e-03	0.01
Grass	0.04	2.0e-03	2.0e-03	0.01
Sunflower	0.04	2.0e-03	2.0e-03	0.01
Tomato	0.05	2.0e-03	2.0e-03	0.01
Onion	0.035	2.0e-03	2.0e-03	0.01
Broccoli	0.035	2.0e-03	2.0e-03	0.01
Peas	0.04	2.0e-03	2.0e-03	0.01
Trees	0.04	2.0e-03	2.0e-03	0.01
Barley	0.04	2.0e-03	2.0e-03	0.01
Oats	0.04	2.0e-03	2.0e-03	0.01
Roads	0.03	2.0e-03	2.0e-03	0.01
Major creeks	0.025	5.0e-04	5.0e-04	0.01
Secondary Creeks	0.03	5.0e-04	5.0e-04	0.01
Pinetree	0.04	2.0e-03	2.0e-03	0.01

basin.

6.3.3 Initial Condition

For the Lerma basin a distributed initial condition is not readily available, hence to generate a suitable initial condition, the dynamic water balance approach was used. The system is repeatedly forced using meteorologic input data (one-year time-series of rainfall and evapotranspiration) measured for the hydrological year previous to the hydrological year 2006, until the head distribution in the entire catchment does not change anymore when comparing a certain day of the current year with the same day of the previous year. The initial water table for this procedure was set coincident with the ground surface. For the hydraulic properties of surface and subsurface domains uniform parameter values for hydraulic conductivity and van-Genuchten parameters are used. A dynamic-steady state was reached after 20 years of forcing with the same one-year series. The discharge (0.030 m^3/s) for the 30th of September 2005 resulting from this procedure was comparatively close to the average stream flow measured at the outlet of the Lerma basin over the first 40 days of the hydrologic year 2006 (0.038 m^3/s). Figure 6.7 depicts the total 3-D hydraulic head field for the initial condition.

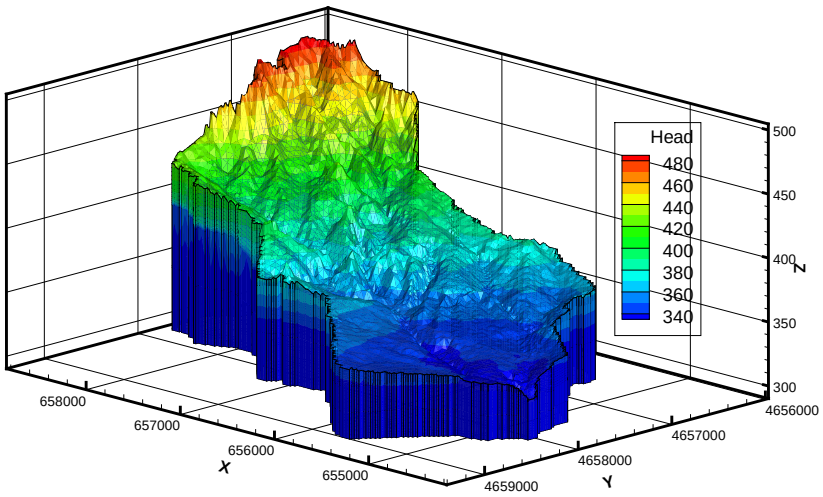

Figure 6.7: Initial condition used for the model simulations (at the beginning of the hydrological year 2006: October 1, 2005). Coloring scheme represents the total hydraulic heads obtained with the spin-up process

6.4 Parameterization

Due to the satisfactory results obtained with the Borden site experiment, the hillslope equivalent was used to design the calibration problem of the Lerma basin fully-coupled physics-based model which is deemed to be very complex due to the significant influence of the unsaturated zone on the aggregated hydrological response.

To evaluate the influence of catchment controlling parameters on the hydrological response of the Lerma basin, a parameter sensitivity analysis is performed. Instead of using the realistic model of the basin, the hillslope equivalent was used. The hypsometric curve calculated for the Lerma basin is shown in Fig. 6.8.

Unfortunately, the hillslope equivalent is unable to reproduce the spatial variability of soil parameters within the glacis. Therefore, a weighted-average uniform glacis is assumed as the aquifer unit. Thus, the hypsometric representation of this uniform aquifer (top and bottom surface) is reproduced. This results in a simplified two-layered subsurface structure with a shallow aquifer overlying an aquitard. The simplified geometrically realistic 3-D model of the Lerma basin used for the parameterization together with its 2-D hillslope equivalent are shown in Fig. 6.9.

The available climatological data (e.g. rainfall and evapotranspiration) and irrigation for hydrological year 2006 were applied to the hillslope equivalent. Considerations of the realistic model were transfered to the hillslope equivalent: boundary conditions were set to no-flow except for the outlet, which is defined as critical depth; the subsurface

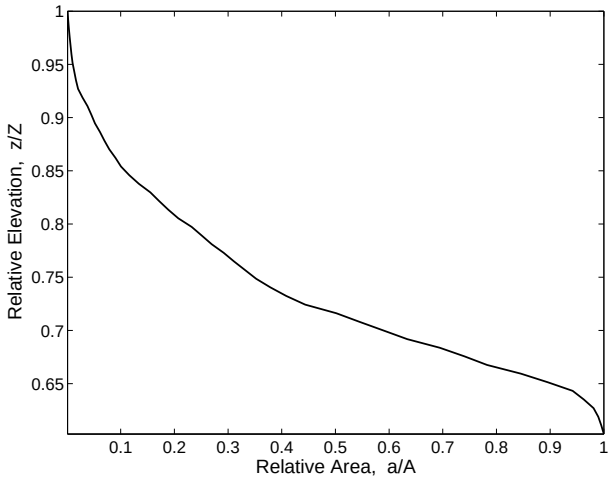

Figure 6.8: Percentage hypsometric curve of the Lerma Basin. *a* is the area associated to each elevation *z*. *A* is the total surface area (7.5 km^2) and *Z* the maximum elevation of the basin (527.9 m)

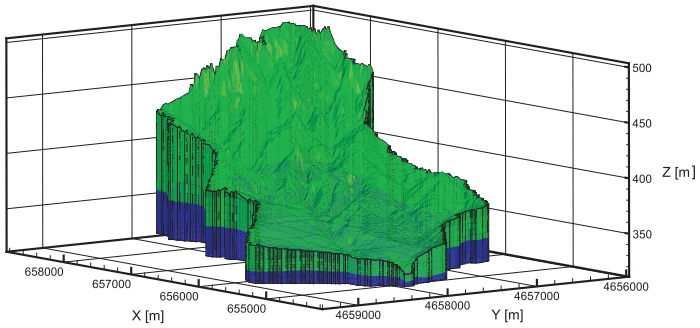

(a) GRM

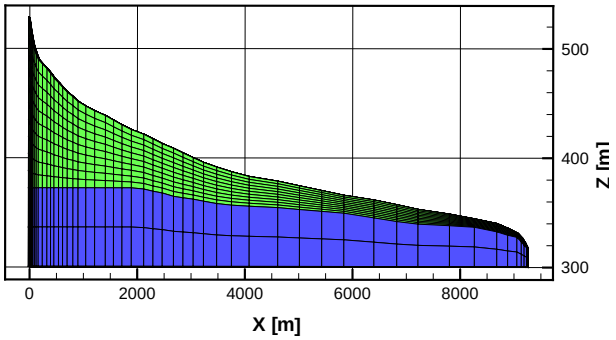

(b) HE

Figure 6.9: Geometrically Realistic Model (GRM) and Hillslope Equivalent (HE) for the Lerma basin (green: glacis(aquifer) and blue: tertiary materials (aquitard))

was assumed isotropic; and the initial condition was generated by forcing repeatedly the system with one year transient climatological data (rainfall and evapotranspiration) until a dynamic steady state was reached.

The saturated hydraulic conductivity k_s, the van-Genuchten parameters inverse air-entry pressure α and pore distribution factor n, and the Manning's roughness coefficient n_m are subject to investigation. Table 6.4 presents the range of model parameter values and the perturbation Δp used for each parameter p.

Table 6.4: Information used to calculate sensitivities for saturated hydraulic conductivity, k_s; inverse air-entry pressure, α; pore-distribution factor, n; and Manning's roughness coefficient $n-manning$ for the Lerma basin test case

Parameter	Min. Value	Max. Value	dp_i
$K_s[m/d]$	0.04	8.64	0.01 [m/d]
$\alpha[m^{-1}]$	0.01	6.0	0.005 $[m^{-1}]$
$n[-]$	1.0	3.0	0.05 [-]
$n-manning[s/m^{1/3}]$	0.03	0.05	0.001 $[s/m^{1/3}]$

From the sensitivity study a parameter ranking was performed. The parameter averaged-*CSS* values were used, the average is computed with the set of sensitivities calculated at the s_i values for each parameter p. Larger *CSS* values indicate more meaningful parameters or parameters for which the available observations provide more information.

To define the parameters which have a relevant effect on the hydrological response of the Lerma basin, a parameter ranking of catchment controlling parameters (i.e. k_s, α, n and n_m) was calculated using the HE. The ranking is presented in figure 6.10. From this figure, one may say that the Manning's roughness coefficient (n_m) has a negligible sensitivity compared to k_s, α and n. Hence, in the following our investigation is focused on k_s and the van-Genuchten parameters α and n.

In order to narrow down the dimensions of the parameter space and by this reduce the computation time during the calibration, ranges in which relevant parameters are sensitive are defined. Multiple simulations at different parameter value combinations are performed for k_s, α, and n. Figure 6.11 shows different one-year model transient outputs obtained by changing soil hydraulic properties. It can be observed that there is a significant variation on the stream discharges generated using different parameter values of k_s, α and n.

The quantitative evaluation of the sensitivities was performed using composite scaled sensitivities (*CSS*). The weighting factor ω is assumed as the inverse of the measurement errors matrix $\mathbf{C_{yy}^{-1}}$. The measurement errors are assumed uncorrelated, so that $\mathbf{C_{yy}}$ simplifies to a diagonal matrix containing the variance of the measurement error for each observation on the diagonal. The latter is set to 12% relative error.

From the *CSS*s, a curve for each single parameter is built, that represents the variation of the sensitivity throughout the parameter space (see Fig. 6.12). Calculated *CSS*-curves

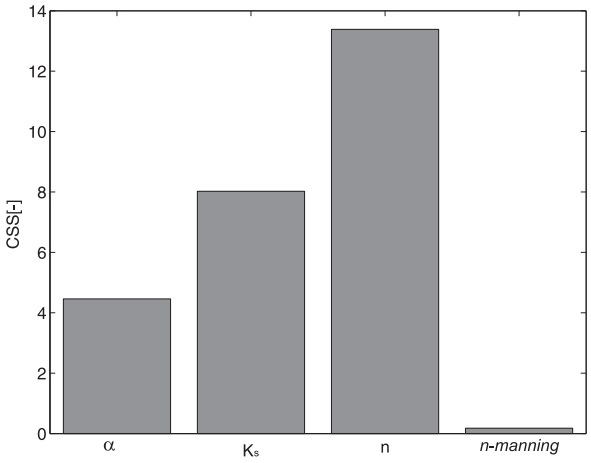

Figure 6.10: Composite scaled sensitivities (*CSS*) calculated from the hillslope equivalent simulations. α and n are the van-Genuchten inverse of the air-entry and pore-distribution factor respectively; k_s is the saturated hydraulic conductivity; and $n-manning$ is the Manning's roughness coefficient

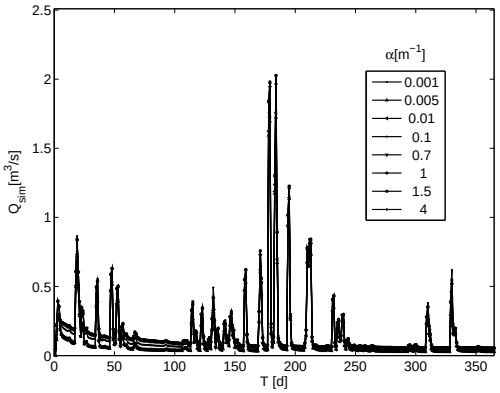

(a) Model outputs with different α values

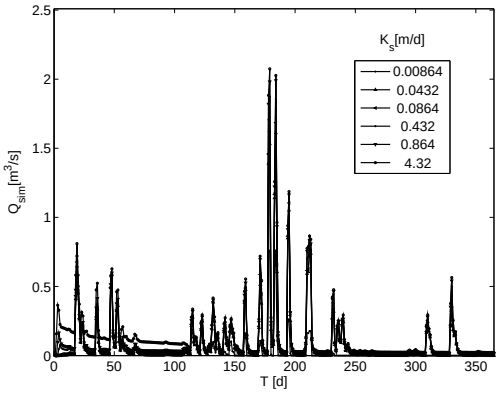

(b) Model outputs with different k_s values

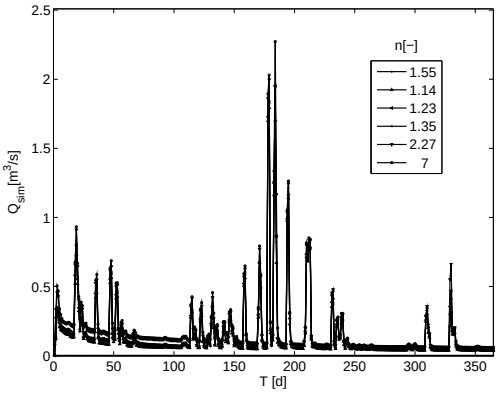

(c) Model outputs with different n values

Figure 6.11: Stream discharges simulated using the hillslope equivalent of the Lerma basin for different values of saturated hydraulic conductivity, k_s; inverse air-entry pressure, α; and pore-distribution factor, n.

for each parameter show areas where the parameter values variation have a much higher sensitivity on the model outputs and others where this sensitivity is negligible.

*CSS*s obtained from the information provided by the 8760 measurements (hourly data for 1 year) were classified into three categories: high $CSS > 10$; moderate $1 < CSS < 10$; and small $CSS <= 1$. This classification was used to define at which values (or ranges of values) the parameters are *important* or *inconsequential*(Foglia et al., 2009). High and moderate *CSS* were assumed important while small was assumed inconsequential. This process allows narrowing the calibration ranges for each parameter. In the figure 6.12, the original parameter space obtained from the texture classes observed within the Lerma basin (hollow boxes) and the narrowed parameters space(filled boxes) defined from the *CSS*-analysis are shown. As it can be observed in this graph, the sensitivity analysis helps reducing the parameter range to be explored during the calibration process, and in this way also saving valuable computation time.

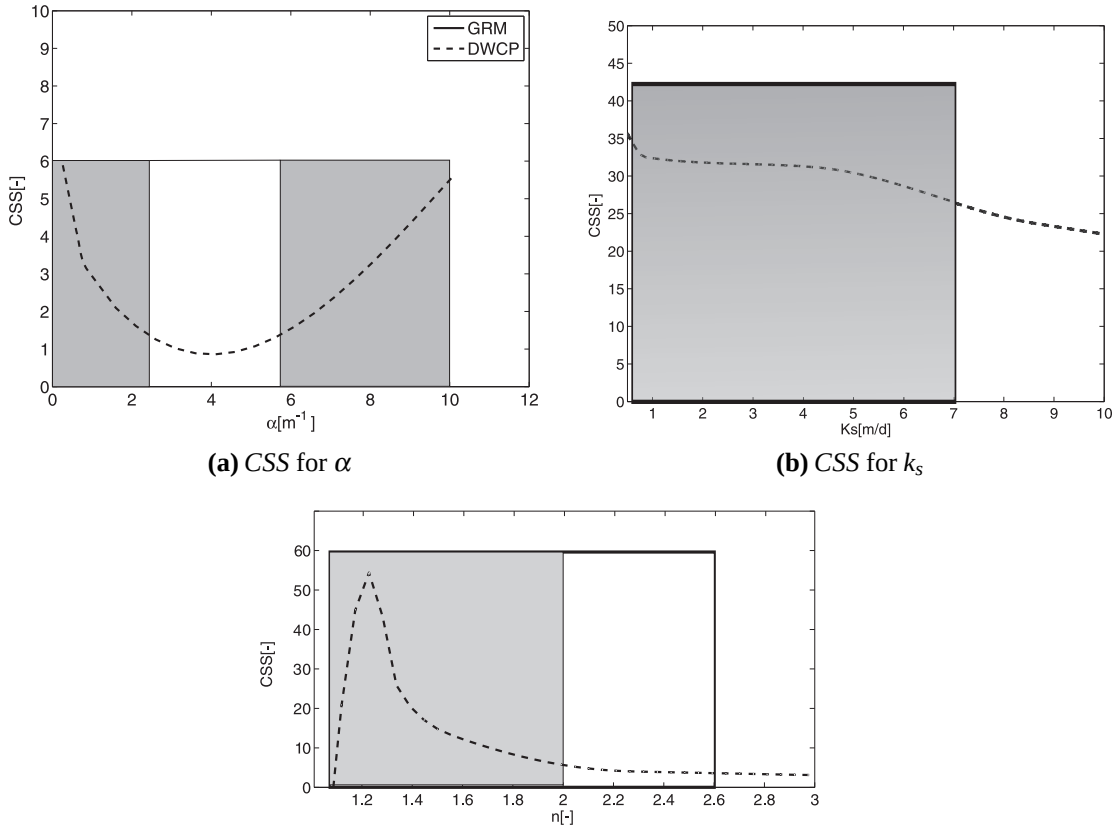

(a) *CSS* for α

(b) *CSS* for k_s

(c) *CSS* for n

Figure 6.12: Sensitivity Analysis using the Hillslope Equivalent. Shaded areas correspond to the narrowed parameter ranges

In the following, the hillslope equivalent was used to evaluate parameter correlations by exploring a random set of points within the parameter space; and to generate an appropriate set of parameter values to be used as initial guess in the calibration process of the Lerma basin model.

The matrix of sensitivities **J** obtained previously with the hillslope equivalent are used to compute correlation coefficients *r*, relative standard deviations of estimation σ_r, and composite scale sensitivities (*CSS*) at a random set of points (vector of parameter values) within the narrowed parameter space. The different set of parameters together with the correspondent values of *r*-and *CSS*s are shown in the table 6.5. σ_r-values for each parameter are shown on the main diagonal of this table.

Table 6.5: Initial saturated hydraulic conductivity (k_s), inverse air-entry pressure (α) and pore-size factor (n) values for the Lerma basin. $\mathbf{C_{pp}}$ using the GRM and the hillslope equivalent HE. $\sigma_r[-]$ is presented on the main diagonal of the matrix

	$K_s(m/d)$	$\alpha(m^{-1})$	$n(-)$
Estimated value	4.0	0.72	1.56
CSS and correlation coefficients *r* obtained using the HE			
CSS	31.5	8.0	34.7
k_s	1.7e-5		
α	-0.4569	0.375	
n	-0.5194	-0.9347	0.147
CSS and correlation coefficients *r* obtained using the GRM			
CSS	27.0	5.8	31.2
k_s	1.696e-5		
α	-0.4569	0.363	
n	-0.5194	-0.9019	0.142

Calculated values of σ_r are very high for α and n indicating a very high uncertainty associated to the determination of the parameters. Furthermore, *r*-value calculated between α and n is very high (> 0.90) indicating a high correlation of these parameters.

To find an appropriate initial set of values (initial guess) for the calibration of the Lerma basin model, the objective function was evaluated for each of the simulations used in the sensitivity study with the hillslope equivalent, that fall within the narrowed calibration space. The minimum value within this set of objective function values was defined as the initial guess. The set of initial values obtained for the glacis was $k_s = 0.9\ [m/d]$; $\alpha = 0.7\ [m^{-1}]$; and $n = 1.56\ [-]$; and for the buro $k_s = 0.01\ [m/d]$; $\alpha = 1.0\ [m^{-1}]$; and $n = 1.39\ [-]$.

Comparison with the Geometrically Realistic Model

To show the applicability of the hillslope equivalent to a more complex geometry, *CSS*s are also calculated using the geometrically realistic model of the Lerma basin. In order to make the results comparable a weighted-averaged uniform glacis is again assumed. The *CSS*s are calculated at the same combination of parameter values and applying the same conditions in terms of precipitation, evapotranspiration and irrigation used with the hillslope equivalent.

Calculated *CSS*-values for the HE and the GRM are very similar (see Figure 6.13). Both show a lower sensitivity for α compared to n and k_s. *CSS*s for n show a pronounced peak around $n = 1.28[-]$. The peak-width (measured at the height of 60% of the peak) is 0.25. Around the peak, i.e. $n \in [1.1 - 1.35][-]$, *CSS* change drastically. For $n > 2.1[-]$, *CSS*s become much smaller and for further increase in n its *CSS* remains constant.

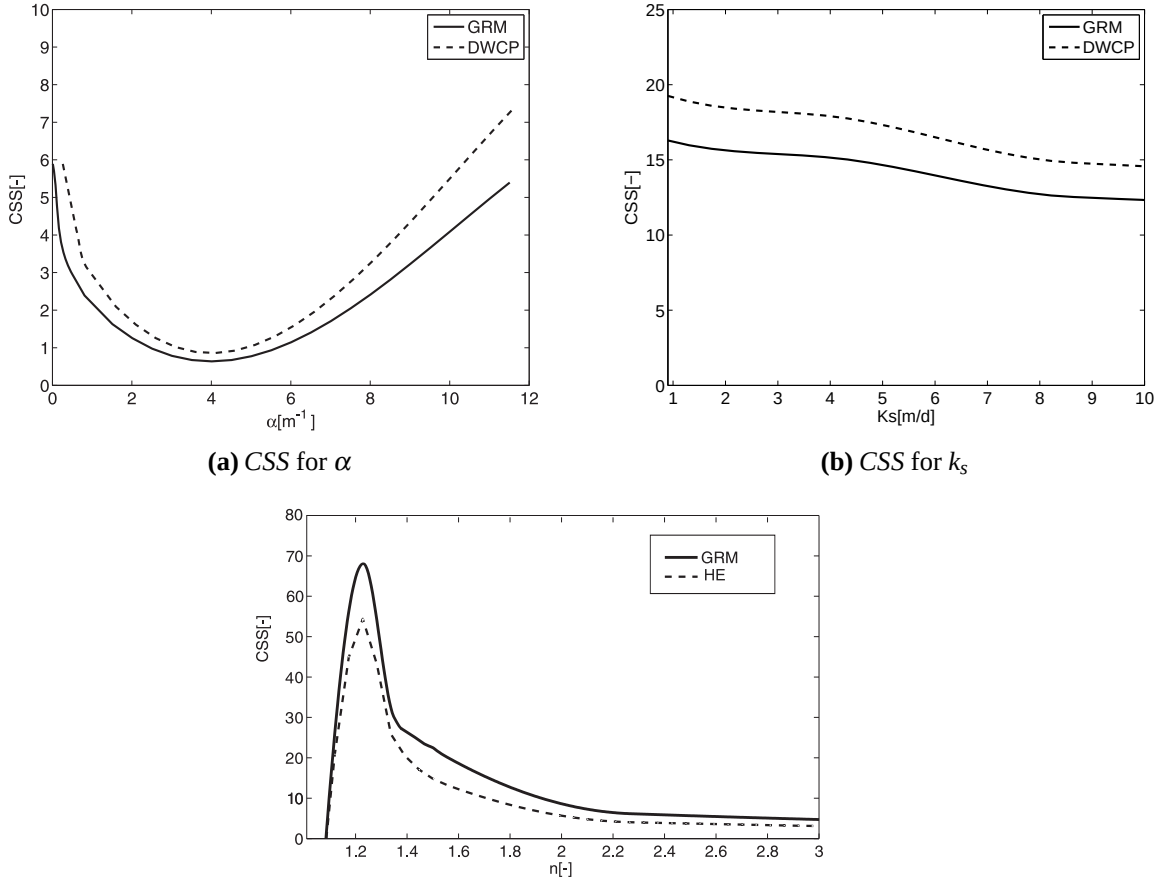

(a) *CSS* for α

(b) *CSS* for k_s

(c) *CSS* for n

Figure 6.13: Composite scaled sensitivities for the geometrically realistic model (GRM) and for the Hillslope Equivalent(HE) of the Lerma basin

*CSS*s of k_s are higher than those calculated for α for the whole simulated range. The trend for *CSS* of k_s is a slight decrease with increasing values of k_s. Overall the HE and GRM show a very similar behavior in terms of their *CSS*s.

The change in *CSS* observed at different values of α follows the same pattern for the GRM and HE. Clayey and sandy textures associated to very small and very high values, respectively, have in general a higher sensitivity than those calculated for sandy-clay and sandy-clay-loam, i.e. $\alpha = 2.0 - 5.0[m^{-1}]$.

The parameter sensitivities and correlations are also evaluated at the same initial set of parameters used with the hillslope equivalent but with the geometrically realistic model. The parameter sensitivities and the correlation matrix obtained using the GRM at the

optimal values are also shown in the table 6.5. *CSS*s and σ_r values obtained at optimal values for the GRM correlate very well with those obtained with the HE.

The reduction in running times achieved by studying parameter sensitivities with the hillslope equivalent rather than with the geometrically realistic model is quite large. While a single run with the geometrically realistic model took between 9 to 12 hours depending on the choice of the soil parameters, it took 5 - 15 min with the hillslope equivalent. The latter means that a sensitivity study for our fully-coupled model for a one-year transient simulation (which implies at least 500 runnings) using a single PC with an Intel Core 2 Duo E6600 2.4 GHz would take 200 days with the GRM. In contrast, with the hillslope equivalent it only took around 3.5 days using the same PC.

In summary, all the soil hydraulic parameters evaluated appear to be sensitive which may indicate that they are identifiable. However, there is a high uncertainty associated to the determination of the parameters α and n, as σ_r-values calculated for these parameters are higher than 10%. This suggests that there may be problems to estimate those parameters given only stream discharge for the hydrological year 2006. Therefore, measured discharge for the hydrological year 2007; and measured discharge and hydraulic heads for the hydrological year 2008 were included in the calibration dataset. Additionally, the parameter space is narrowed down to physical and sensitive ranges for all calibration parameters according to the results obtained for the sensitivity analysis with the hillslope equivalent.

An uniform glacis, and the set of values obtained with the HE (i.e. glacis: $k_s = 0.9$ $[m/d]$; $\alpha = 0.7$ $[m^{-1}]$; and $n = 1.5$ $[-]$; duro:$k_s = 0.01$ $[m/d]$; $\alpha = 1.0$ $[m^{-1}]$; and $n = 1.39$ $[-]$) are used as initial guess for the calibration of the Lerma basin.

6.5 Calibration and Prediction

To match simulated and observed signals (i.e. calibration after Anderson and Woessner, 1992) for 2006, 2007 and 2008, k_s, α and n for the different zones were manually calibrated. The root mean squared error (RMSE) and the Nash-Sutcliffe coefficient (N_r) are considered as criteria for the goodness-of-fit. Automated calibration was not an option due to the long computation times of 9 -12 hrs on a PC with an Intel Core 2 Duo E6600 2.4 GHz for a one-year simulation. The choice of the calibration parameters was based on the following: (i) no measured soil-retention curves were available, so that van-Genuchten parameters α and n could be only constrained by the texture information in combination with pedotransfer functions (Carsel and Parrish, 1988; Schaap and Leij, 1998; Schaap et al., 2001). (ii) no measurements of saturated hydraulic conductivity were available from inside the Lerma basin, but k_s measured outside the Lerma basin in the glacis unit were higher than the ranges obtained from the pedotransfer functions of Carsel and Par-

rish (1988); (iii) significant texture changes were observed within the glacis unit; (iv) results of the parameterization presented in section 6.4 showed a high impact of n, α and k_s on the simulated discharge dynamics. Calibrated values of n, α and k_s for the four zones defined within the Lerma basin are shown in Figure 6.6.

Table 6.6: Calibrated saturated hydraulic conductivity (k_s), inverse air-entry pressure (α) and pore-size factor (n) values for the different zones within the Lerma basin

Zone Label	$k_s(m/d)$	$\alpha(m^{-1})$	$)n(-)$
Zone 1	0.9	0.01	1.09
Zone 2	4.5	0.5	1.31
Zone 3	6.5	5.9	1.72
Zone 4	0.9	2.0	1.39

The model performance for both, surface and subsurface domains, was evaluated by visual comparison of time series of observed and simulated stream-discharge and subsurface hydraulic heads, as well as quantitatively by goodness-of-fit measures. Based on hourly discharge measurements at the outlet and the set of hydraulic heads measurements for the subsurface, we calculated the maximum error (ME), the root mean squared error (RMSE), the coefficient of residual mass (CRM) and the Nash-Sutcliffe coefficient(N_r).

Simulated and observed discharge values for 2006, 2007 and 2008 are presented in Fig. 6.14. In general, they show good agreement. Peak flows are reproduced relatively well for the whole simulation period. For the non-irrigated season, the model is able to reproduce the measured flows adequately; however, for the year 2008 a minor tendency to overestimation is noticeable. For the rainy season, in particular for years 2007 and 2008, the highest peaks are slightly delayed. For the irrigation season, the simulated hydrograph captures the timing and the peak values relatively well. However, the most pronounced peaks are still underestimated.

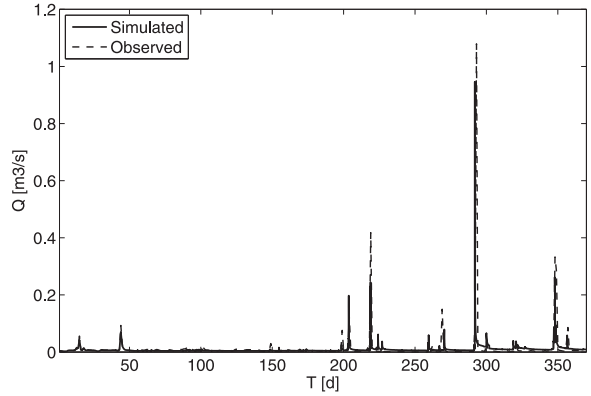

(a) Hydrological year 2006

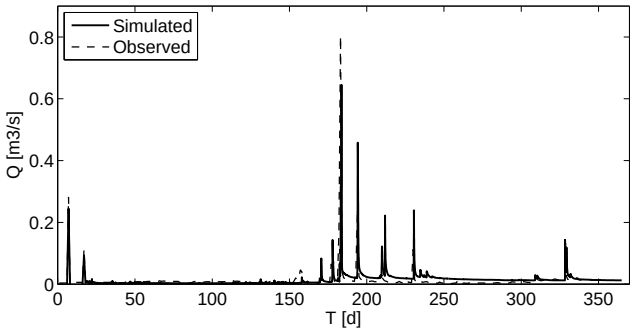

(b) Hydrological year 2007

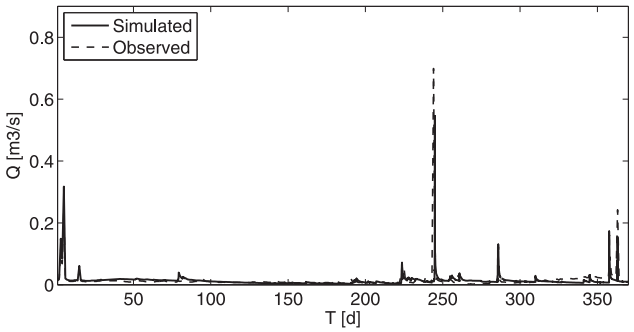

(c) Hydrological year 2008

Figure 6.14: Simulated (solid) and measured (dashed) discharge for hydrological years 2006, 2007 and 2008. Note: The graphs are presented using different scales

As shown in Figure 6.15, simulated water tables for 2008 match the measured hydraulic heads considerably well. Sharp increases of the water level at piezometers 3, 4 and 5 reflect the intensification of the irrigation during the second half of the year 2008. Hence, it could be stated that the model is able to reproduce adequately the seasonal

variation in the subsurface response.

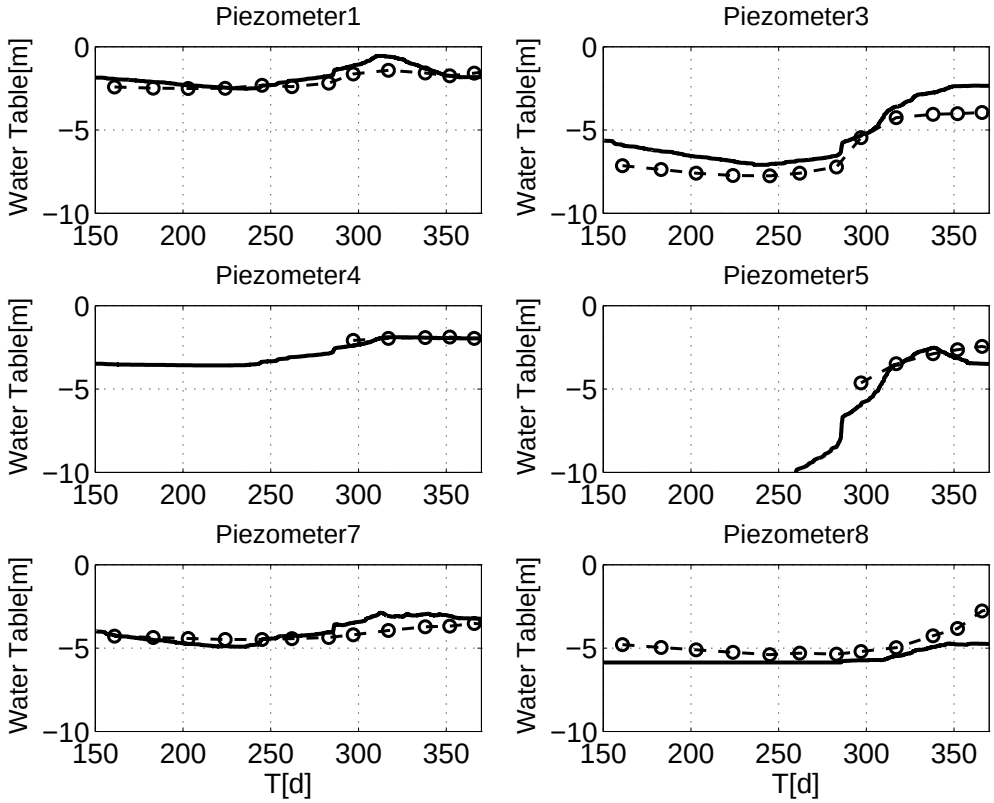

Figure 6.15: Simulated (solid) and measured (dashed) groundwater tables for the hydrological year 2008. Piezometers 4 and 5 were dry during the first 7 measurements

The model performance statistics for the calibration period (years 2006, 2007 and 2008) are shown in Table 6.7.

Table 6.7: Model performance statistics for the calibration period (hydrological years 2006, 2007, 2008) and the validation period (hydrological year 2009). ME: maximum error, RMSE: root mean square error; CRM: coefficient of residual mass; and N_r: the Nash-Sutcliffe coefficient

Year	ME$[m^3/s]$	RMSE$[m^3/s]$	CRM$[-]$	$N_r[-]$
Calibration				
Surface				
2006	0.160	0.0136	0.60	0.639
2007	0.139	0.0417	-0.59	0.869
2008	0.066	0.0487	-0.18	0.857
Subsurface				
2008	1.50	0.68	0.0217	0.9322
Validation				
Surface	0.0737	0.0230	-0.09	0.901
Subsurface	1.35	0.75	0.0330	0.868

To validate the model, the data set for 2009 is used. Hourly rainfall was available for

this period directly from the station Ejea de los caballeros (within 5 km distance from Lerma basin) and used as the model input. No additional model parameter changes were applied. The integrated model was used for the prediction of discharge and groundwater heads for the entire Lerma basin. As can be seen in Fig.6.16, the model is able to reproduce the hydrological response of the surface domain: peak and base flows are both represented very well, aside from a slight overprediction of stream discharge during the intensive irrigation phase. Simulated water tables match the measured hydraulic heads considerably well (Fig.6.17). Only during the intensive irrigation phase the water tables are slightly overestimated.

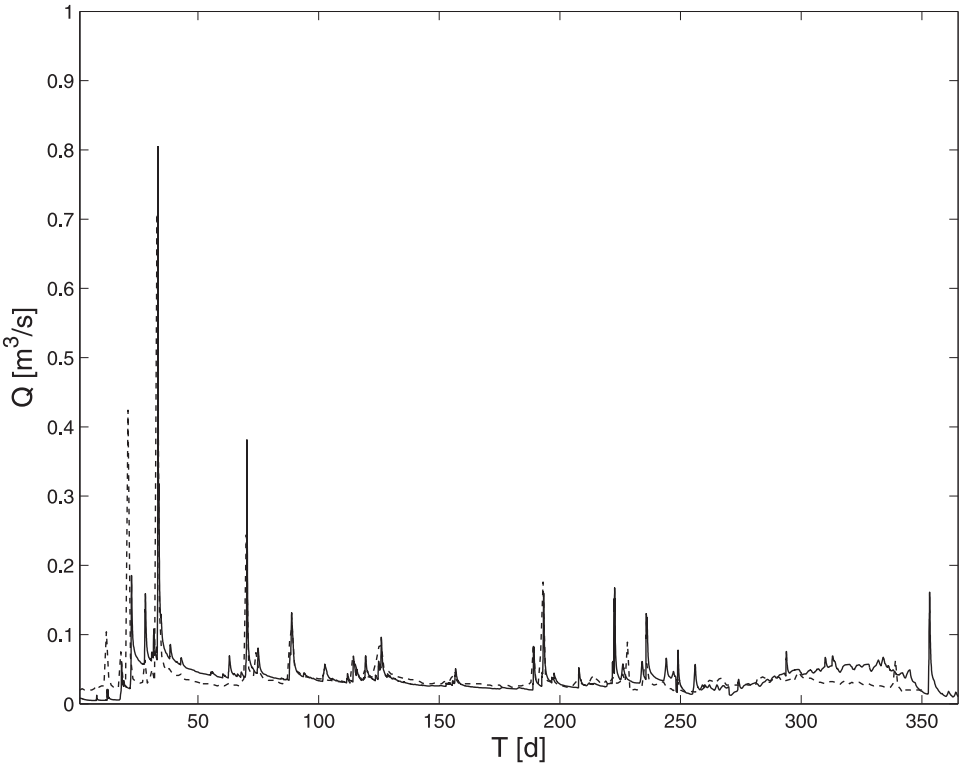

Figure 6.16: Predicted (solid) and measured (dashed) stream discharge at the basin outlet for the hydrological year 2009

The performance statistics for the validation period (i.e. hydrological year 2009) are integrated in Table 6.7.

6.6 Performance measures

Considering the performance results obtained from the calibration and validation, the following can be stated: The Nash-Sutcliffe coefficients, N_r, calculated for the calibration

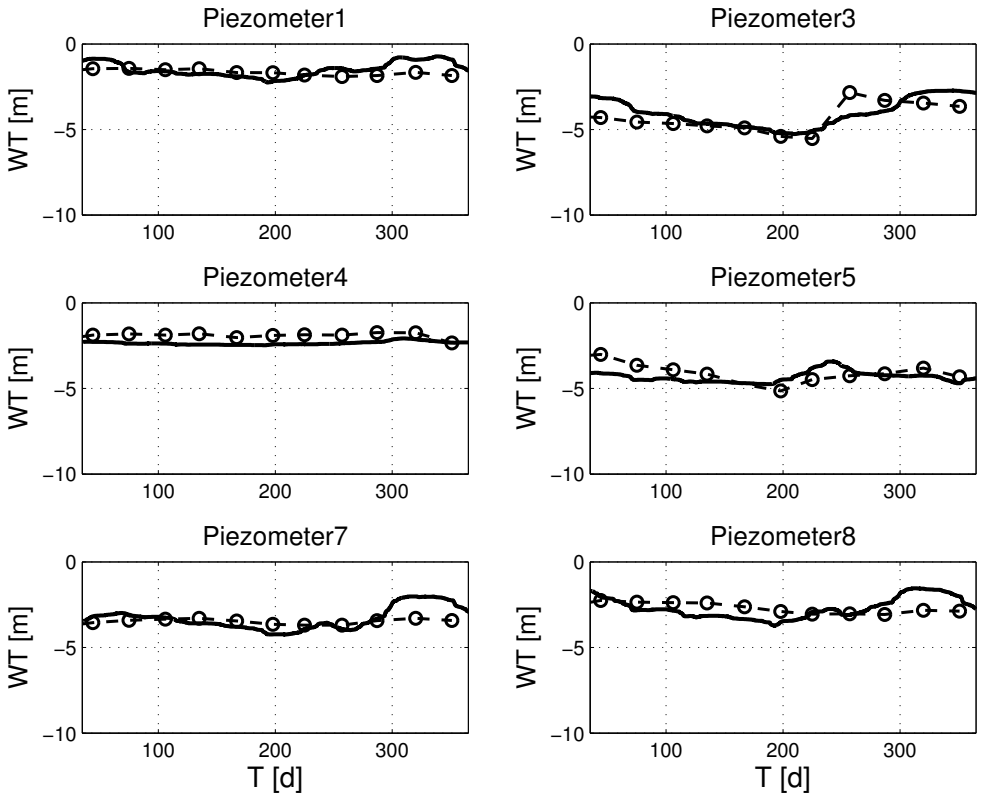

Figure 6.17: Predicted (solid) and measured (dashed) water tables for the hydrological year 2009

years 2007 and 2008, and for the validation year 2009 are very good (0.87, 0.86 and 0.90, respectively) which expresses the suitability of the model to simulate the hydrological response of the basin to the land-use transformation with respect to high and low flow timing.

For 2006, the model efficiency is worse (0.64). This comparatively low value arises from the underestimation of the peaks during the rainy season. A source for this underestimation could be the high uncertainty of the actual short-term rainfall distribution within the Lerma basin. As discussed by Bronstert and Bardossy (2003) the exact temporal variation of precipitation intensity and duration plays an important role for runoff generation, in particular for high-intensity rainfall events. These were very common during 2006 -which was the rainiest year in the analyzed time period. Support for this hypothesis comes from the observation of the better performance obtained for 2009, when discharge was predicted using hourly rainfall available directly from the closer climatological station.

Small negative values of CRM for the years 2007, 2008 and 2009 reflect the tendency of the model to slightly overestimate discharge. Overestimation of both, the simulated stream discharge and subsurface heads may be caused by the assumption that the subsurface water divide coincides with the surface water divide, i.e. no lateral subsurface

flow exists. There may also be a seasonal regional groundwater flow not considered in the model simulations, as the no-flow conditions assigned to the lateral subsurface boundaries force all water to leave the system at the surficial outlet, neglecting any kind of regional groundwater flow. This problem could be approached by the introduction of transient flux boundaries. However, additional field data would be required to quantify these boundary fluxes. Subsurface head mismatches may also be related to the uncertainty in the definition of the spatial variability of the hydraulic properties of the porous media, but, the information available to characterize the internal heterogeneity of the hydrostratigraphic units is limited.

In order to test whether the model is good in the sense that the deviations between the measured and simulated values are within the measurement error prescribed by matrix $\mathbf{C_{yy}}$, a χ^2-test of the objective function normalized by $\mathbf{C_{yy}}$, expressed as Eq.4.5, is performed. Uncorrelated errors are assumed, so that $\mathbf{C_{yy}}$ simplifies to a diagonal matrix containing the variance of the error for each observation on the diagonal. The error expressed by matrix $\mathbf{C_{yy}}$ contains both, the aleatoric and the epistemic error or measurement and model error, respectively. More precisely, the error represents the relative measurement error for stream discharge in the surface domain and the head measurement error, as well as the epistemic error due to the uncertainty in model structure and in boundary conditions for the subsurface. This kind of a decomposition is consistent with the difference in available information regarding the surface and subsurface domain. To evaluate the performance of the model the maximum error that would allow us to accept our model in a χ^2-test is calculated. The analysis shows that a 12% relative error for the stream discharge and an error of 0.4 m (including head measurement error, uncertainty in model structure and boundary conditions) for the subsurface domain would be sufficient to pass the χ^2-test as the ratio $\varepsilon^T \mathbf{C}_{\mathbf{yy}}^{-1} \varepsilon / (n_{obs} - n_{par})$ equated to $0.98 \approx 1.0$. These error values can be called very satisfactory for both domains, given that the 0.4 m for the subsurface also include the error in model structure and boundary conditions.

In general, the model performance statistics obtained for both, surface and subsurface domains, reflect the ability of the model to reproduce the flow dynamics during the land-use transformation.

Sensitivity analysis

As it has been widely discussed in the literature (e.g. Beven, 1989; Ebel and Loague, 2006), non-uniqueness and identifiability may cause problems in the parameterization of physics-based models. In this study, the definition of Ebel and Loague (2006) is followed and a distinction between uniqueness and identifiability is made. A set of parameter values is called identifiable, if each individual parameter has an influence on the model output, i.e. the model output is sensitive to changes in each parameter evaluated about the

set of calibrated parameter values. A set of parameter values is called unique, if the same optimal model performance can not be achieved with another set of (different) parameter values. Uniqueness and identifiability can but do not need to be related.

By the following sensitivity analysis, identifiability and parameter correlation are explored, which can also evaluate non-uniqueness about the set of calibrated parameter values. However, the question of uniqueness or non-uniqueness in the sense defined above can not be resolved by such an analysis, since there could always exist points somewhere in parameter space associated with the same or a better model performance. The decision about the existence or non-existence of such points for non-convex performance functions could only be made by exhaustive sampling of the parameter space which is almost always infeasible in practice and certainly in this case.

Van-Genuchten parameters are calibrated, as very complex unsaturated flow dynamics are expected due to the large contrast in soil water contents given the transition from semi-arid land to irrigated crop fields. Hence, van-Genuchten parameters are expected to have a considerable relevance for the ability of the model to reproduce the flow patterns. Restricting the calibration to the physical ranges associated to texture classes identified for the Lerma basin, a set of values for α, n and k_s for zones 1 to 4 deemed to be optimal was found (Table 6.6).

The covariance matrix of the parameters $\mathbf{C_{pp}}$ and the relative standard deviation of estimation σ_r [%] about the calibrated set of optimal values are shown in table 6.8.

σ_r-values for each parameter are shown in the main diagonal in table 6.8. Most of the calculated values of σ_r are relatively small ($< 10.0\%$) indicating a low uncertainty associated to the determination of the parameters. Only α_2 has a value higher than 10% (11.18%). In this sense, the set of calibrated parameter values may be called identifiable.

In Table 6.8, it can be observed that none of the 66 values of r is higher than 0.75. The highest correlation coefficient (r=0.719) was calculated between parameters α_1 and n_1.

The sensitivity analysis shows that the calibration resulted in a set of parameter values which are identifiable and unique in a small neighborhood of this set of parameters. Given the results of the validation it can be also stated that the model has good predictive capabilities. In the following, the physics-based model of the Lerma basin is used to investigate spatio-temporal patterns of change in hydrological processes induced by the land-use transition and the intensification of irrigation.

6.7 Impact of the Land-Use Changes and Irrigation

Basin-scale water balances are the starting point of our analysis of the overall flow dynamics in the Lerma basin. The inputs are defined as measured precipitation and irrigation amounts, and the output as estimated evapotranspiration and measured stream discharge,

Table 6.8: Correlation coefficient r matrix calculated at the optimal values. On the main diagonal of the matrix we present the relative standard deviation of estimation $\sigma_r[\%]$. $K_{s_i}[m/d]$: saturated hydraulic conductivity for the zone i; $\alpha_i[m^{-1}]$: van-Genuchten inverse of air-entry pressure for the zone i; and $n_i[-]$: van-Genuchten pore-size factor for the zone i

	K_{s_1}	α_1	n_1	K_{s_2}	α_2	n_2	K_{s_3}	α_3	n_3	K_{s_4}	α_4	n_4
Estimated value	0.9	0.01	1.09	4.5	0.5	1.31	6.5	5.9	1.72	0.9	2.0	1.39
Correlation calculated at optimal values												
K_{s_1}	7.94											
α_1	-0.033	11.19										
n_1	-0.415	0.719	1.21									
K_{s_2}	-0.223	-0.548	-0.193	1.52								
α_2	0.169	-0.023	-0.061	0.017	2.32			Symmetric				
n_2	0.280	-0.019	-0.139	-0.010	0.327	1.40						
K_{s_3}	-0.380	0.185	0.290	-0.109	-0.225	-0.162	1.17					
α_3	-0.249	-0.714	-0.469	0.332	-0.219	-0.133	0.031	1.25				
n_3	-0.073	-0.098	0.105	0.331	0.010	-0.067	-0.413	-0.280	3.98			
K_{s_4}	0.120	0.075	0.118	-0.036	-0.260	-0.262	0.175	-0.221	0.079	8.77		
α_4	-0.375	-0.166	-0.067	-0.068	0.102	-0.120	-0.259	0.311	-0.079	-0.658	3.44	
n_4	0.045	0.010	0.030	-0.079	0.327	0.300	-0.360	-0.125	0.079	-0.504	0.291	4.00

thereby neglecting possible measurement errors or limited representativeness of measurements. The contributions of precipitation and irrigation varied considerably within the simulation period: during 2006, irrigation represents 24.1% of the total amount of water input (the rest is precipitation). 2007 was drier in terms of precipitation (12.4% less than in 2006), while the total irrigation amount increased considerably (125.8% more relative to 2006). 2008 was drier than 2007 (21.3% less precipitation compared to 2007), but more irrigation took place (22.2% more than in the previous year). In 2009, irrigation increased by another 12.3% compared to 2008 (precipitation decreased by 17.4% compared to 2008).

For the yearly water balance, the change in water storage over the hydrological year is assumed close to zero ($\Delta w_s + \Delta w_g \approx 0$). Furthermore, no water entering or leaving the basin via lateral groundwater flow and no water losses occur through the buro are assumed. Adhering to these assumptions, the left hand side of the water balance equation (Eq.3.1) needs to equate to zero in order to close the water balance. If this is not the case, and lateral groundwater flow as well as water loss through the buro can still be ruled out, a negative value means that more water has left the basin than was introduced via precipitation and irrigation (which is equivalent to a release of water from storage), and a positive value means that the amount of water stored inside the basin must have increased by this value. The input and output terms as well as the water balances calculated for the years 2006-2009 are presented in Table 6.9. For 2006, the balance is slightly negative (-9.5 *mm*). In the following two years, during which irrigation increased considerably, the yearly water balances do not close either: compared to 2006 one order of magnitude of more water is stored inside Lerma basin (water balance values: +80.1 *mm*, +25.0 *mm* for 2007, 2008, respectively). In 2009, the balance is again slightly negative (-8.4 *mm*)

Table 6.9: Water balances for hydrological years 2006, 2007, 2008, and 2009

Hydrological year	P (*mm*)	ET (*mm*)	Irrig. (*mm*)	Discharge (*mm*)	Water balance (*mm*)
2006	457.0	491.6	145.2	120.1	-9.5
2007	400.5	545.3	327.8	102.9	80.1
2008	315.1	582.9	400.6	107.8	25.0
2009	370.0	645.0	450.0	183.4	-8.4

The water balance results indicate that subsurface storage can not be neglected over a hydrologic year for the period in which irrigation agriculture in the Lerma basin has intensified. Moreover, neither the discharge nor the pattern of the change in storage observed for the four years under observation does simply follow the monotonically increasing irrigation load. Hence, in the following the physics-based model is used to investigate more spatially and temporally resolved variables.

The total length of streams within a catchment is a quantity of high ecological importance that is deemed to be affected by the intensification of agricultural activities due to the

increase of irrigation return flows. It is also seen as a prominent spatial feature of the hydrological system groundwater–surface water exchange. From this perspective, the ability to compute such a quantity naturally, i.e. the spring of a creek is where the groundwater table reaches the land surface, represents a huge advantage of fully-coupled physics-based models. Similarly, runoff generation processes depend on soil moisture content and/or the distance of the water table to the surface. Hence, a shift in runoff generation processes may also be a relevant implication of the transition to irrigation agriculture.

In the following, both total length of streams, and the shift in runoff generation processes for the whole transition of the Lerma basin into irrigation agriculture are investigated.

6.7.1 Total length of streams within the Lerma basin

The first parameter analyzed with the physics-based model aims at changes of the drainage network. The evolution of the total length of streams, $\sum L$, in the Lerma basin is calculated. For this the topographical setting of individual surface nodes (i.e. whether they are located in a valley) is considered. A cut-off value of at least 10 cm water depth for a node to become a stream node is also defined.

The evolution of the total stream length (see Figure 6.18) shows that the additional input of irrigation waters over four consecutive years has led to an increase of the length of the drainage network within the Lerma basin. Clearly observable are periods of increasing and decreasing total stream length over the hydrological year. For the first two years, irrigation did not result in a significant increasing trend of the total river length. Figure 6.18 shows that for the years 2006 and 2007 the curve returns to essentially the same minimum level. In 2008, however, the pattern changes and the total river length does not return to the same level as in 2006 and 2007 instead it returns to a minimum level which is raised by roughly 600 m. This increasing trend continues for the year 2009 where the highest peak in total stream length is reached. Also the total river length never falls below the end level of year 2008, but rather returns to a minimum level which is again raised compared to 2008.

As observed in Figure 6.18 the total stream length within Lerma basin has generally increased progressing transformation from rainfed to irrigation agriculture. The curve contains a seasonal trend induced by the rainy and irrigation seasons and some high-frequency fluctuations which could be identified via the physics-based model, as the appearance of new intermittent creeks, that are mainly fed by quick irrigation return flow.

It is interesting to notice that the input of irrigation waters in the first two years did not result in a significant increase of the total stream length over the whole year. As the total stream length curve returns to essentially the same base level of 1 km, it seems reasonable to interpret this as the proportion of the drainage network that represents perennial streams

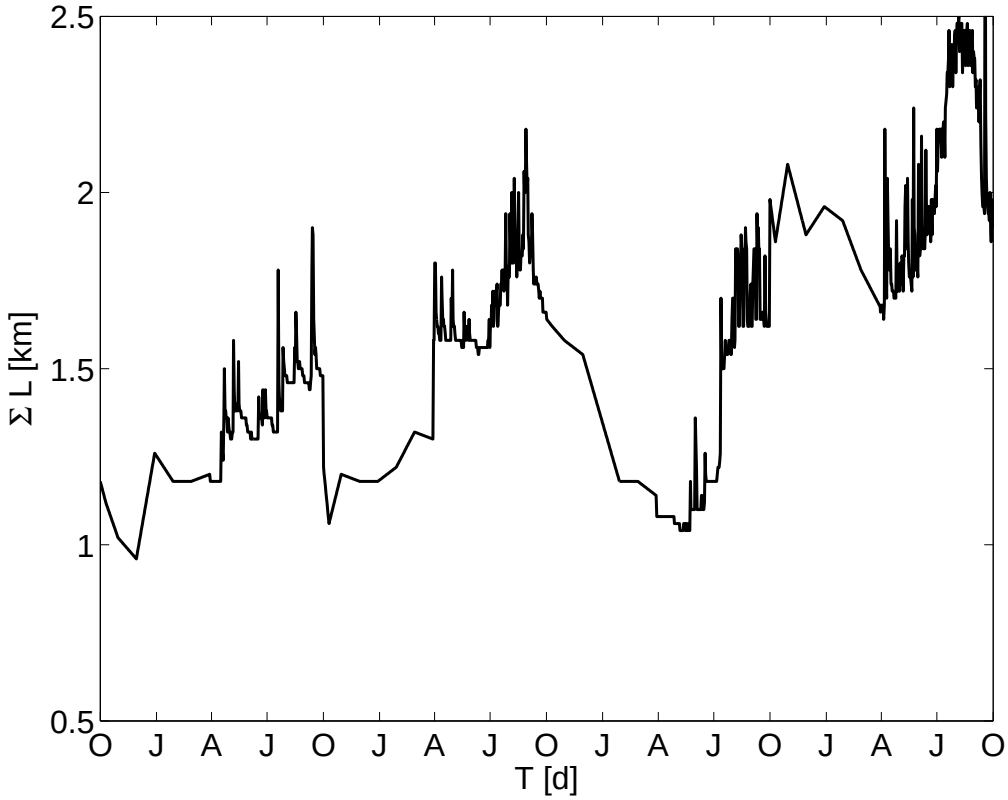

Figure 6.18: Evolution of the total length of the streams within Lerma basin

during 2006 and 2007. In 2008, apparently a threshold was reached as the total stream length does not return to the former base level at the end of 2008, and a new proportion of the drainage network becomes perennial.

Looking at the basin-scale water balance, the high storage of water in 2007 and 2008 and the continued input in 2009 also seems to suggest that the Lerma system may now be able to sustain spring areas at a higher topographic level - at least in some parts of the basin. Model inspection indicates that the additional stream length may result from the creek south of the main stream of Lerma basin becoming perennial. Field observations give support to this hypothesis as this stream is not longer falling dry during summer.

6.7.2 Surface-runoff generation processes

The second parameter analyzed with the physics-based model aims at the shift in surface-runoff generation processes from Horton (infiltration excess, Horton, 1933) to Dunne (saturation excess, Dunne and Black, 1970) flow. Considering the complete spatial differentiation of soil moisture over time, the temporal evolution of an average *approximate* infiltration capacity, $\bar{Q}_{cap}$ and the total water input rates, Q_{ri}, (i.e. rainfall + irrigation) are calculated. $\bar{Q}_{cap}$ was obtained by integrating the unsaturated hydraulic conductivity of the top subsurface nodes over the whole surface area of the Lerma basin model taking spatial differences in saturation, van-Genuchten parameters and saturated conductivity into account and normalizing by the surface area (Eq. 6.2). Since the conditions for Hortonian runoff are given when the rainfall intensity exceeds the infiltration capacity of the soil (e.g Dingman, 2002; Loague et al., 2010), it is expected that the approximate infiltration capacity $\bar{Q}_{cap}$ is indicative for whether or not a certain rainfall event will generate Hortonian runoff at a particular model element:

$$\bar{Q}_{cap} = \frac{1}{A_{total}} \int_A k_{rw}(x, y, z_{surf}) k_s \mathrm{d}A \tag{6.2}$$

The actual infiltration capacity, however, changes during a rainfall event, such that this definition (at an hourly time step) can only represent an approximation of the actual infiltration capacity. Therefore, $\bar{Q}_{cap}$ is called an (average) *approximate* infiltration capacity. $\bar{Q}_{cap}$ should also not be confused with the empirically defined infiltration capacity for a catchment in "steady-state" at field-saturation (Betson, 1964).

The integration given in equation 6.2 was repeated using 1-hour time-step for the whole simulated period. The resulting curve is presented in Figure 6.19.

Considering the general trend of the curve, the following can be stated: Values of $\bar{Q}_{cap}$ are relatively low for 2006 before irrigation starts. During this period Q_{ri} is often higher than the average approximate infiltration capacity. 2007 was drier in terms of total precipitation. Nevertheless, there are two distinct maxima of $\bar{Q}_{cap}$ observable, which are not

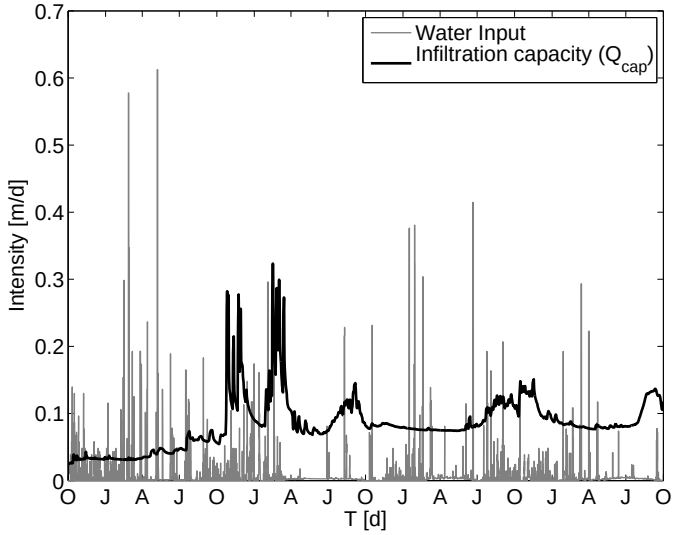

(a) Infiltration capacity, Q_{cap}

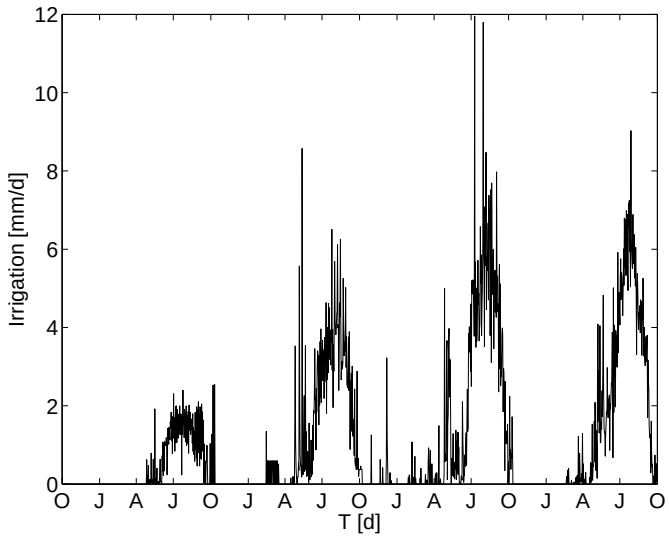

(b) Irrigation

Figure 6.19: Evolution of the infiltration capacity, Q_{cap}, of the Lerma basin

time-related to the major irrigation phase. These two distinct maxima do not re-occur in the following years. Only within the rainy season and during a few events that the rainfall intensity Q_{ri} exceeds $\overline{Q}_{cap}$. Despite the increase of Q_{ri} during the irrigation season, Q_{ri} is never larger than $\overline{Q}_{cap}$. During 2008 the base level of $\overline{Q}_{cap}$ increased considerably, so that $\overline{Q}_{cap}$ is again exceeded only during a few extreme rainfall events. In the hydrological year 2009 the base level of $\overline{Q}_{cap}$ is larger than in all other years. Still for a few events in the second half of the year Q_{ri} exceeds $\overline{Q}_{cap}$. Additionally, one can observe that the major irrigation phases coincide with prolonged (local) maxima of $\overline{Q}_{cap}$ in 2007 and 2009.

The comparison of the evolution of $\overline{Q}_{cap}$ vs. Q_{ri} shows that in 2006 the conditions for Hortonian runoff, i.e. $Q_{ri} > \overline{Q}_{cap}$, are reached in about 24 events. During the next three

years, conditions for Hortonian runoff are only reached in about 17 events in total. While this is partly due to differences in the rainfall distribution, it is also obvious that the higher base level of the average infiltration capacity curve requires stronger rainfall intensities for Hortonian runoff generation. This suggests a shift in the runoff generation processes in the Lerma basin: from relatively regularly occurring Hortonian runoff in 2006, characterized by high discharge during rainfall events and followed by longer periods of zero overland flow, to a more Dunne flow dominated runoff generation process in the later years.

Particularly interesting is the year 2007, where the infiltration capacity curve has two distinct maxima from November 2006 to March 2007. During these two time periods water input by irrigation does not play a major role. However, the base level of the infiltration capacity curve is already raised due to the irrigation phase in late 2006. The frequent precipitation events occurring during the two time periods in question (in 2007) are not too intense, but would have led to Hortonian runoff generation in early 2006. In 2007, however, the infiltration capacity is just high enough to accommodate the rainfall at these rates and most of the rainfall contributes to soil wetting. This may be the reason for the two distinct maxima of $\bar{Q}_{cap}$ in 2007, which are not related to intensive irrigation. This conclusion is also supported by the characteristics of these maxima: they are only of short duration and fluctuating quite intensively, whereas $\bar{Q}_{cap}$ maxima induced by irrigation during later times show a comparatively smooth variability. The reason that the 2007 maxima type does not re-occur in later years is believed to be chiefly the non-recurrence of longer duration low intensity rainfall events.

As the approximate infiltration capacity $\bar{Q}_{cap}$ represents only an average value for the total Lerma basin area, it does not account for local differences in runoff generation. In order to also include these in our analysis, the total area with Hortonian runoff generation (i.e. $Q_{ri} > Q_{cap}$) based on the individual contributions from each model element is estimated. The latter is achieved by computing the relative area of Hortonian runoff generation A_H as:

$$\bar{A}_H = \frac{1}{A_{total}} \int_A I(Q_{ri} > Q_{cap}) \mathrm{d}A \tag{6.3}$$

where I is a function which is set to 1 when the property $Q_{ri} > Q_{cap}$ holds and 0 otherwise.

As this analysis only makes sense for time periods with an actual rainfall event, A_H is computed for all n^e rainfall events in each hydrological year. More specifically, four A_H distributions are established with $n^e_{2006} = 156$, $n^e_{2007} = 192$, $n^e_{2008} = 205$, $n^e_{2009} = 219$ using a fixed number of 9 histogram classes determined after Sturges (1926).

The calculated histograms for 2006-2009 are shown in Figure 6.20. A clearly observable feature is that in 2006 the number of events with more than 30% of the basin contributing to Hortonian runoff is much higher than in any other year. Beginning in 2007 the mode of the A_H distributions stabilizes at 30%, which is about the areal propor-

tion of the Lerma basin that remains un-irrigated. For 2007-2009, one can hardly observe events in which Q_{cap} is exceeded in more than 70% of the total basin area, which occurred relatively frequently in 2006. Overall the distribution of 2006 seems to have lost its right tail and to concentrate frequency mass in the three lowermost classes.

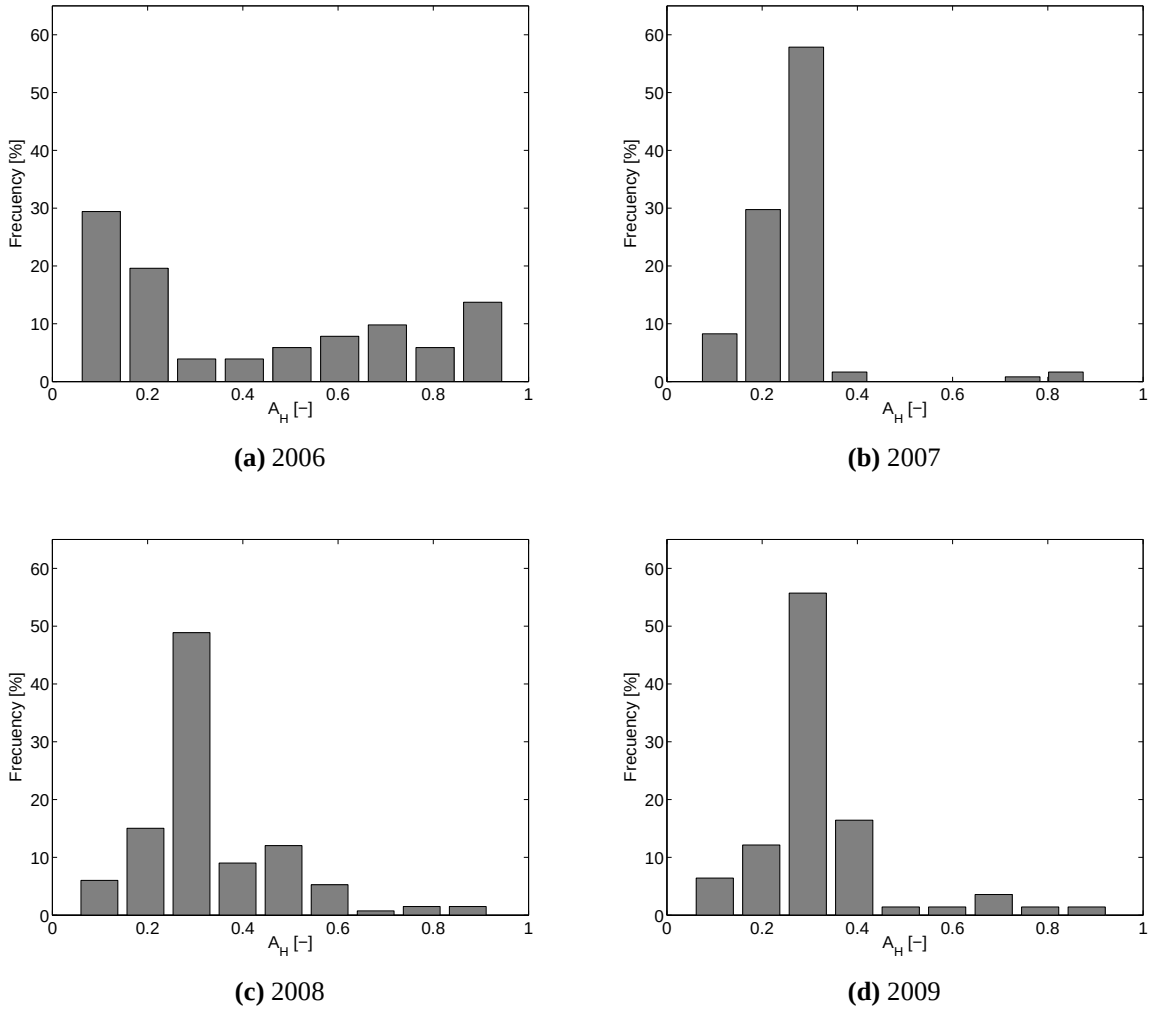

(a) 2006 **(b)** 2007

(c) 2008 **(d)** 2009

Figure 6.20: Histograms of the proportion of areas associated to Hortonian runoff A_H generation (relative to total catchment area) for hydrological years 2006-2009

While these distributions are still also a function of the actual rainfall distribution within the respective years, the similarity between 2007 - 2009 and their dissimilarity with 2006 further supports our conclusion that the Hortonian runoff generation process becomes less important for the Lerma basin. Furthermore, these statistics seem to indicate that Hortonian runoff generation remains mainly active in the non-irrigated part.

In order to highlight the spatial differences between 2006 and 2009, the catchment response to two rainfall events of similar intensity (i.e. 13.5 and 12.4 mm/hr respectively) are showed. To minimize the influence of antecedent moisture conditions, the events were selected from a subset of events with 3 preceding dry days. For the two selected events,

the ratio between Q_{ri} and Q_{cap} at each node is calculated. In Figure 6.21 the spatial distribution of the logarithm of this ratio $\log_{10}(Q_{ri}/Q_{cap})$ is presented, so that areas with Hortonian runoff are associated with positive values.

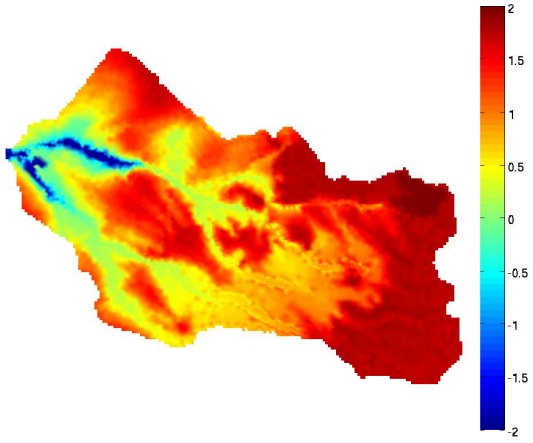

(a) $\log_{10}(Q_{ri}/Q_{cap})$ for year 2006

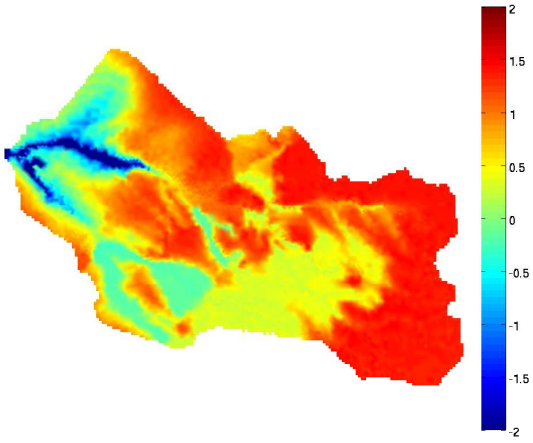

(b) $\log_{10}(Q_{ri}/Q_{cap})$ for year 2009

Figure 6.21: Spatial distribution of the ratio of the input flow rate Q_{ri} and the infiltration capacity (Q_{cap}) for a typical rainfall event during the hydrological year (a) 2006 and (b) 2009

Despite the similarity of the rainfall events the response for both hydrological years can be well distinguished: In 2006 as Q_{cap} is exceeded in 91% of the total area. In 2009, Q_{ri} only exceeds Q_{cap} in 54% of the total area and event water can infiltrate at low elevations and within intensively irrigated areas. The percentage of areas with Hortonian runoff generation is almost as high as the percentage of the total non-irrigated area in 2009 ($\sim$47%). The remaining $\sim$7% of the former are either regions close to the discharging streams or associated with a portion of the pinetree field located in the middle of the basin. That part is not irrigated, but likely receives water from adjacent irrigated plots.

In order to support the applicability of the average approximate infiltration capacity defined in Eq. 6.2, the spatial distribution of fluxes exfiltrating from the subsurface domain were extracted directly from the physics-based model for the same rainfall events referred to above. Areas with exfiltrating fluxes represent areas of Dunne-runoff by definition. The results are shown in Fig. 6.22, where positive values represent exfiltration and negatives values represent infiltration. It can be observed that the areas associated to exfiltration correlate very well with those areas considered as Dunne-runoff areas in Fig. 6.21. This indicates that the proposed approximate infiltration capacity Q_{cap} represents indeed a good measure to discriminate between areas of Hortonian and Dunne-runoff generation processes.

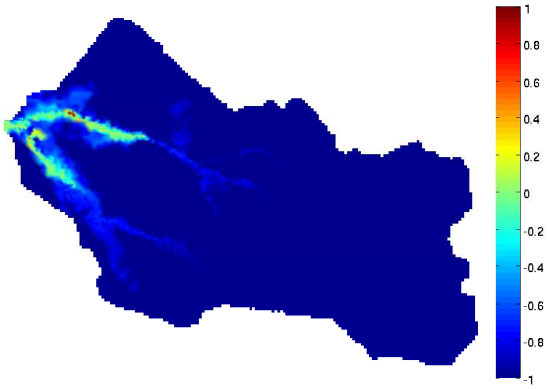

(a) Exfiltration for year 2006

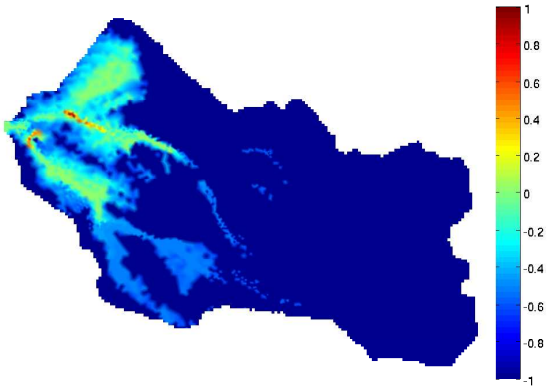

(b) Exfiltration for year 2009

Figure 6.22: Exfiltration values $[m/s]$ for a typical rainfall event during the hydrological years (a) 2006 and (b) 2009

Additionally, the sum of exfiltrating fluxes (i.e. the Dunne flow contribution) were

compared to the stream discharge at the Lerma basin outlet. This total exfiltration was obtained by integrating the exfiltration over the whole surface area of the Lerma basin model taking spatial differences into account and normalizing by the total precipitation:

$$\mathrm{Exf} = \frac{\int_A \frac{k_r k_{33}}{l_e}(\psi - H)\mathrm{d}A}{P} \tag{6.4}$$

The integration given in equation 6.4 was repeated using a 1-hour time-step for the whole simulated period. Considering the size of the Lerma basin and the velocity of surface runoff it can be assumed that the error introduced by differing arrival times of exfiltrating water is small. The effect of run-on (i.e. infiltration of overland flow running over pervious downstream areas) is also neglected. Although, it may introduce an error for a particular event, it becomes insignificant when considering the time evolution of stream discharge and its Dunne flow contribution. The resulting curve is presented in Figure 6.23. It can be observed that the contribution of Dunne flow has increased along with the intensification of the irrigation in the Lerma basin. This behavior is in agreement with the rise of dry-weather baseflow measured at the outlet of the Lerma basin and with the increase of the total length of perennial streams discussed in section 6.7.1 .

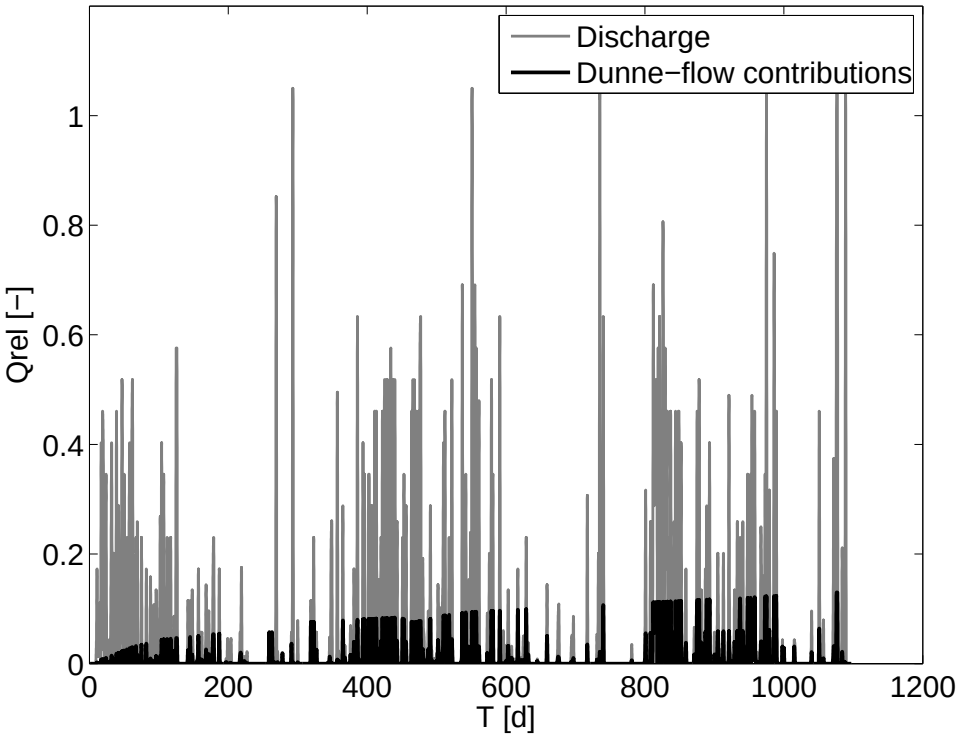

Figure 6.23: Relative contributions from exfiltration (Dunne runoff) on stream discharge for hydrological years 2006-2009

To further highlight the change in Dunne overland flow contribution, a close-up view

of the hydrological response at the outlet of the Lerma basin for the two events used above (i.e. for hydrological years 2006 and 2009) is presented. In Fig. 6.24, discharge and Dunne flow contribution for these particular events can be observed. Despite the similarity of the events (i.e. duration and intensity), Dunne flow represents a considerably larger portion of the measured discharge for the event in 2009 (28%) than for the event in 2006 (10%).

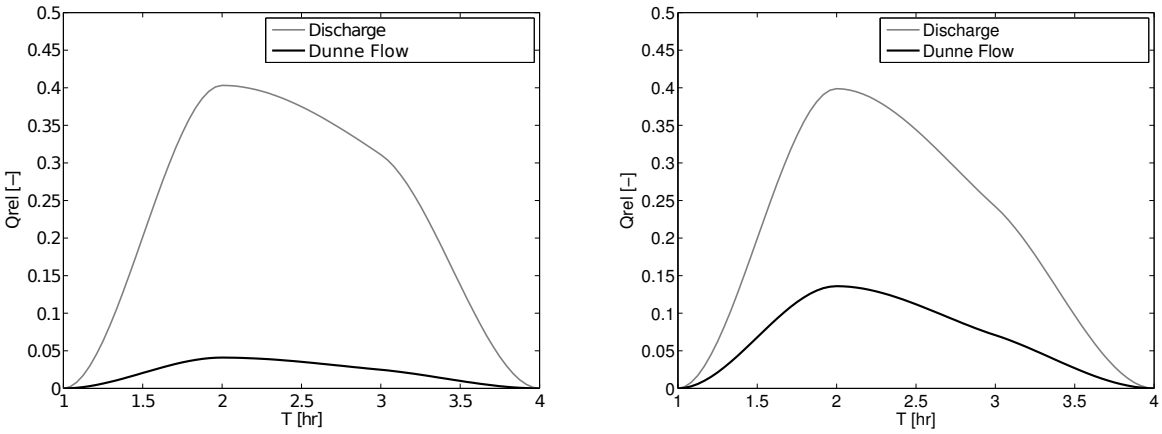

(a) 2006 **(b)** 2009

Figure 6.24: Dunne overland flow and measured stream discharge for two typical rainfall events with similar intensity and duration in hydrological years (a)2006 and (b)2009

In summary, the validation results of the flow model of the Lerma basin demonstrated that it is possible to simulate land-use change with physics-based models using physically meaningful and identifiable parameter sets at catchment scale. Additionally, the model is able to simulate spatial features which were indeed observed in the field, e.g. the increase of total length of the creeks. The spatially resolved analysis used to investigate the evolution of the Lerma basin into irrigation agriculture indicated a shift in the occurrence of Hortonian runoff generation. In particular, while in 2006 most of the basin is associated to Hortonian-runoff generation, in 2009 only non-irrigated areas are associated to this mechanism. This analysis also show a considerable increase of the contribution of Dunne flow in the stream flow induced by the intensification of irrigation.

In the following, a nitrate transport model will be integrated into the flow model in order to study the impact of fertilization on water quality at the Lerma basin.

6.8 Nitrate Transport Model

In order to guarantee the sustainability of agricultural practices, it is of primary importance to investigate the impact of fertilizers on water quality. Hence, the study of the evolution of nitrate concentrations in both surface and subsurface compartments has be-

come a priority objective in agriculture catchments worldwide. The ultimate goal of these studies is to forecast nitrate concentrations under different crop pattern distribution and future climate scenarios as it would allow the design of strategies to maintain nitrate concentrations below drinking water limits or to reverse the effect of fertilization. From this perspective, a model able to describe nitrate fate and transport at the Lerma basin represents a valuable contribution.

In this chapter, the construction of the nitrate fate and transport model of the Lerma basin is presented. As discussed in section 3.2, the solute transport equation requires the transient velocity field which is obtained from the calibrated and validated flow model discussed in the previous chapter. The transport model is integrated into the flow model, so that both the flow and transport systems of equations are solved at every time-step.

The transport model is validated using nitrate concentrations measured at the outlet of the basin during the transition of the Lerma basin into irrigation agriculture, i.e. in the hydrological years 2006 to 2008. No calibration is performed in this case. Instead, values obtained from previous studies, namely other calibrated models, are used to estimate the model parameter values. After the model is validated, water management alternatives at the Lerma basin are studied. In particular, the model is used to predict nitrate concentrations under two hypothetic cropping pattern scenarios, and an ideal irrigation agriculture scenario without nitrogen fertilization.

In the first part of this section, the available data used to build the transport conceptual model is presented. In the second, a local-mass balance which represents the starting point of the nitrate study is discussed. In the third section, assumptions and simplifications of the physics-based model used to simulate transport in the Lerma basin are discussed. Finally, results of the model are presented and discussed.

6.8.1 Data Inventory

At the Lerma basin, the use of fertilizer increased along with the increase of irrigated areas. Fertilizer application on a daily basis was recorded by farmers and collected by Spanish researchers for the hydrological years 2006-2008. During the hydrological year 2006, the total amount of fertilizer applied to the Lerma basin was 35.457 Kg. It increased to 80.817 Kg and 90.597 Kg in 2007 and 2008, respectively. The daily amounts of fertilizer applied within the Lerma basin for the hydrological years 2006-2008 are shown in Fig. 6.25.

Two methodologies of fertilizer application were observed within the Lerma basin. In some areas, the fertilizer is dissolved in water and applied through a sprinkler system. The nitrogenous solution mostly used was *N-32* whose mass fraction of accumulated nitrogen is 32%. This type of fertilizer is deemed to be very efficient as the losses for volatilization are negligible and the plant response is very fast.

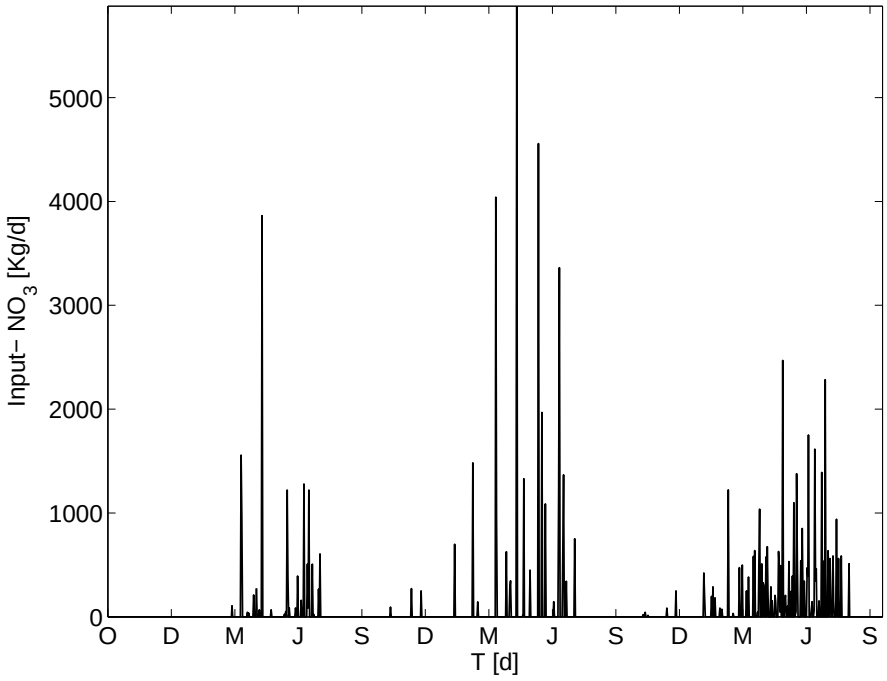

Figure 6.25: Total fertilizer applied during hydrological years 2006-2008 within Lerma basin

In other areas, solid fertilizer (powder or manure) was directly applied to the soil. This methodology of application is not very common within the Lerma basin but introduces a very high uncertainty into the model. In particular, it is quite difficult to determine how much nitrate is advected into the subsurface because the solid fertilizer is not applied together with the irrigation water, instead, it is commonly applied at the beginning of the plant growing period.

To estimate the nitrogen wet deposition, three rain water samples were taken during different seasons of the year (i.e. winter, summer and spring). Concentrations of ammonium, nitrate and nitrites were measured. For the three seasons, measured nitrites and ammonium concentrations were consistently very small (< 0.01 mg/L). In the case of nitrate, concentrations were higher but still considerably small 0.17, 0.82 and 0.12 mg/L, respectively. In this respect, nitrate wet deposition at the Lerma basin appears to be negligible.

The nitrate concentrations measured on a daily basis at the outlet of the Lerma basin during the hydrological years 2006-2008 are shown in Fig. 6.26. In general, the nitrate concentration signal shows an increasing trend, that appears to be in agreement with the intensification of the fertilization. However, a correlation between fertilizer application and nitrate concentrations can hardly be defined without further analysis. In that respect, a physics-based model able to account for spatially distributed patterns would help to understand better the impact of fertilization on stream nitrate concentrations and predict

future impacts under different agriculture management scenarios.

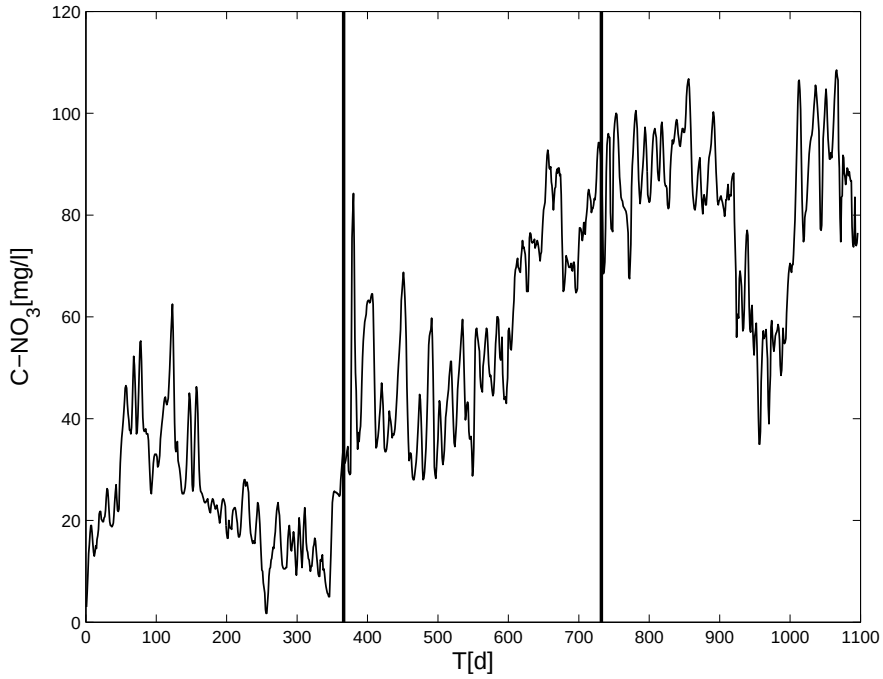

Figure 6.26: Measured concentrations at the outlet of the Lerma basin for hydrological years 2006-2008

Additionally, groundwater nitrate concentrations were measured at 8 piezometers during the hydrological year 2008 (Fig 6.27). For this dataset, it results very difficult to distinguish a trend induced by the intensification of the fertilizer. In piezometers 1 and 3, an increase in nitrate concentration during the irrigation period is observed. In piezometers 2, 3 and 8, on the other hand, a steep decrease in concentration is observed during the same period. Piezometer 4 and 5 seems to have a delayed response to the aggregated application of fertilizer but in opposite direction: while the concentrations in piezometer 5 shows a noticeable increase, they decrease in piezometer 4.

As can be observed from the visual inspection of the measured data, the subsurface and surface concentrations do not simply follow the monotonic increase in fertilization. Hence, in the following a more comprehensive study of nitrate fate and transport at the Lerma basin is presented that accounts for spatially and temporally inputs.

6.8.2 Mass balances

A mass balance represents the starting point of the nitrate study of the Lerma basin. The mass balance equation as used in this investigation can be expressed as:

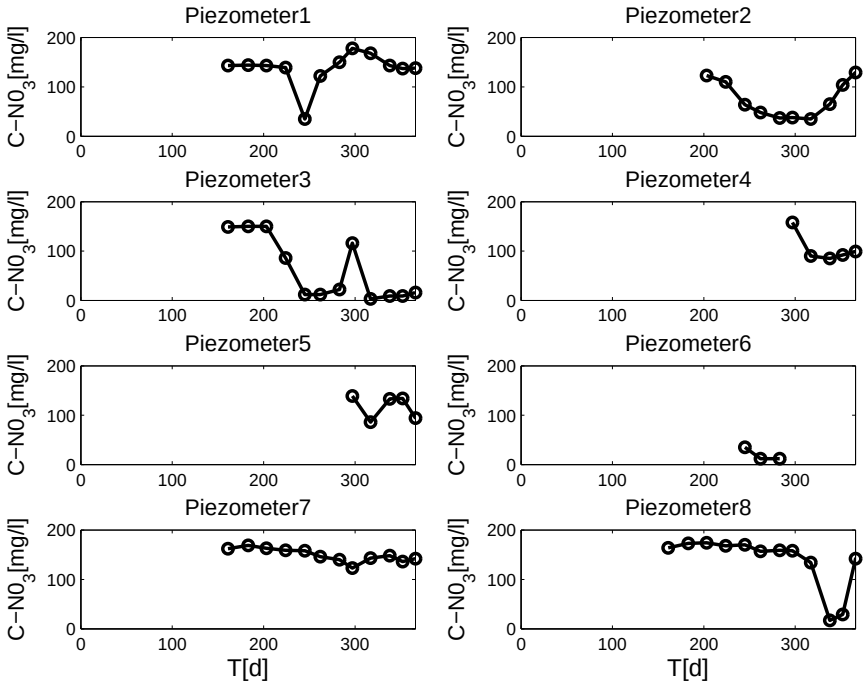

Figure 6.27: Measured concentrations at eight piezometers of the Lerma basin for hydrological year 2008

$$\left[\left(\sum_{j=1}^{N} F_j A_j\right) - \left(\sum_{j=1}^{N} U_j A_j\right) \pm q_r - q_m^o\right] = (\Delta M^s + \Delta M^g) \tag{6.5}$$

where N is the number of surface units(one for each land-use category); F_j is the nitrate application rate via fertilization $[ML^{-2}T^{-1}]$ for each plot j with area A_j $[L^2]$, U_j is the nitrate plant uptake rate associated to each plot j $[ML^{-2}T^{-1}]$. ΔM^s and ΔM^g are the changes in surface and groundwater nitrate storage $[MT^{-1}]$. q_r is a term that accounts for chemical reactions $[MT^{-1}]$. q_m^o is the rate of nitrate leaving the system through the outlet $[MT^{-1}]$ defined as $Q_s C_o$ with Q_s being the discharge $[L^3T^{-1}]$ and C_o the nitrate concentration $[ML^{-3}]$, measured both at the basin outlet.

Accumulated values of imported nitrate by fertilization and nitrate exported through the outlet measured at the Lerma basin for the hydrological years 2006-208 are presented in Figure 6.28.

If change in mass storage and chemical reactions are neglected for a given period of time (i.e. $\Delta M^s + \Delta M^g = 0$ and $q_r = 0$), the difference between the mass introduced to the system by fertilization and the mass exported through the basin outlet would give us an *approximate* nitrate plant uptake:

$$\sum_{j=1}^{N} U_j A_j = \sum_{j=1}^{N} F_j A_j - Q_s C_o \tag{6.6}$$

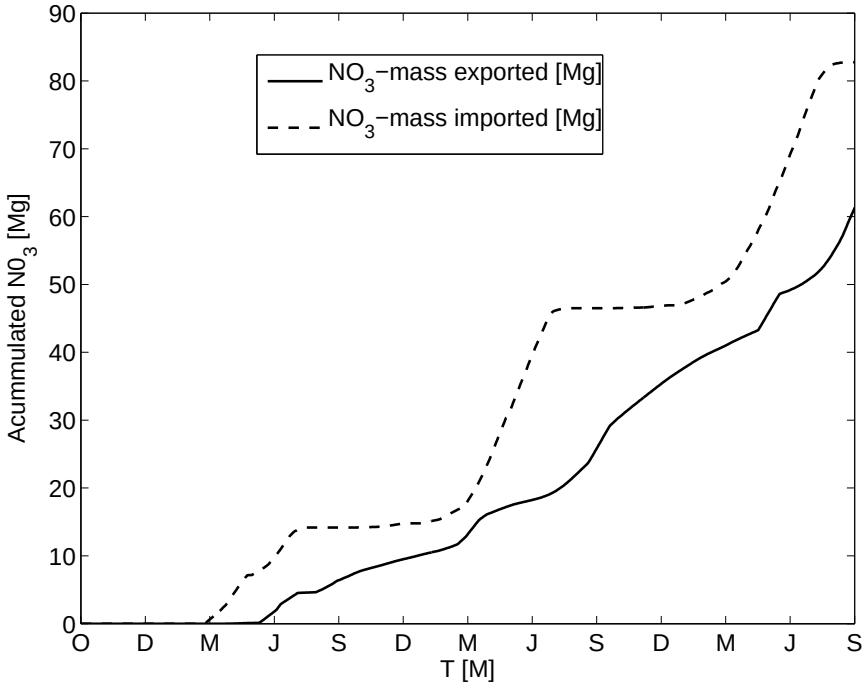

Figure 6.28: Accumulated Imported and Exported Nitrates at the Lerma Basin

To test to what extent this assumption would affect the transient concentrations at the Lerma basin, spatial and temporal distribution of both fertilization amounts and plant nitrate uptake are studied. For the estimation of plant nitrate uptake, actual cropping patterns observed during the simulation period are considered.

At the Lerma basin, during the simulated period, i.e. the hydrological years 2006-2008, corn was the most extended crop. Its planting and harvest was done in April and October, respectively. The average yield of corn for this period was 12 Mg/ha. Although during the hydrological year 2006 winter cereal within the Lerma basin was not present, it was the second most extended crop for the hydrological years 2007 and 2008 (mainly wheat and barley). The length of the growing season ranged between from 8-10 months depending on the type of cereal. Planting of the winter cereal was done between November and December, and the harvest between June and August. Winter cereal yield for the hydrological years 2007 and 2008 were 5.8 Mg/ha and 3.4 Mg/ha, respectively. The considerable decrease of yield may be caused by the smaller amount of irrigation water during hydrological year 2008 (Abrahao, 2010).

Broccoli during the hydrological year 2006, and tomato in the hydrological years 2007 and 2008 were the most extended vegetables during the period under study. Broccoli was typically grown between August and November, and tomato between May and October. Broccoli and tomato yields were 9 Mg/ha and 80 Mg/ha, respectively (Abrahao, 2010).

Other cropping patterns observed within the Lerma basin were sunflower, botpeas,

onions and sorghum. These crop types were mainly grown using double cropping patterns with two different crops per year. This practice became more common when the irrigated areas increased, i.e., in the hydrological years 2007 and 2008. Typical double cropping patterns within the area were botpea or broccoli with corn; and winter cereal with sorghum or sunflower. The appearance of double cropping patterns has increased water and fertilizer needs. Nonetheless, in average nitrogen fertilization per area (Kg/ha) remains constant for the whole simulated period (Abrahao, 2010). Increase in total amount of fertilizer was exclusively related to the increase in irrigated areas.

The theoretical yearly nitrate plant uptake (Kg/Mg of crop-yield) can be estimated from typical literature values. As plant uptake rates depend on the amount of fertilizer applied (e.g. Stapleton et al., 1983), actual fertilizer amounts applied for each cropping pattern within the Lerma basin are used to constrain the uptake values obtained from literature. More precisely, only literature studies for agricultural fields with fertilizer treatments similar to one observed within the Lerma basin were considered to define the plant nitrate uptake rates in this investigation.

In Table 6.10, average yearly nitrate application $Fert$ $[Kg/ha]$, average yearly crop yield Yi $[Mg/ha]$ and theoretical nitrate uptake (per Mg of crop yield) u_t $[Kg/Mg]$ values for the main cropping patterns observed within the Lerma basin are presented. For the case of double-cropping, the values were estimated based on weighted averages taking into account areas associated to each combination of crops. Literature ranges were checked for consistency using a study that includes some typical crops within the Ebro basin developed by Andreu et al. (2006).

For the cropping patterns observed within the Lerma basin, information on daily (or monthly) plant nitrate uptake based on growing seasonality is neither available from local studies nor from literature. Therefore, monthly values of relative nitrate uptake u_{rel} $[-]$ for each crop pattern were directly estimated from plant transpiration cycles presented by Garcia-Vera and Martinez-Cob (2004) (Fig. 6.29). This methodology is supported by the fact that nitrate plant uptake cycles are deemed to be related to transpiration cycles (Arkley, 1963; Stapleton et al., 1983).

In the following, maximum and minimum (theoretical) monthly nitrate uptake u^{max} and u^{min} $[ML^{-2}]$ for each cropping pattern were calculated by multiplying the monthly relative nitrate uptake with the associated yearly (theoretical) maximum and minimum nitrate uptake rate presented in column 7 of the table 6.10, and by the total yield associated to the cropping pattern:

$$u^{max} = u^{rel} u_t^{max} Yi \qquad\qquad u^{min} = u^{rel} u_t^{min} Yi \tag{6.7}$$

Monthly accumulated values of u^{max} $[Kg/ha]$ and u^{min} $[Kg/ha]$ for different cropping

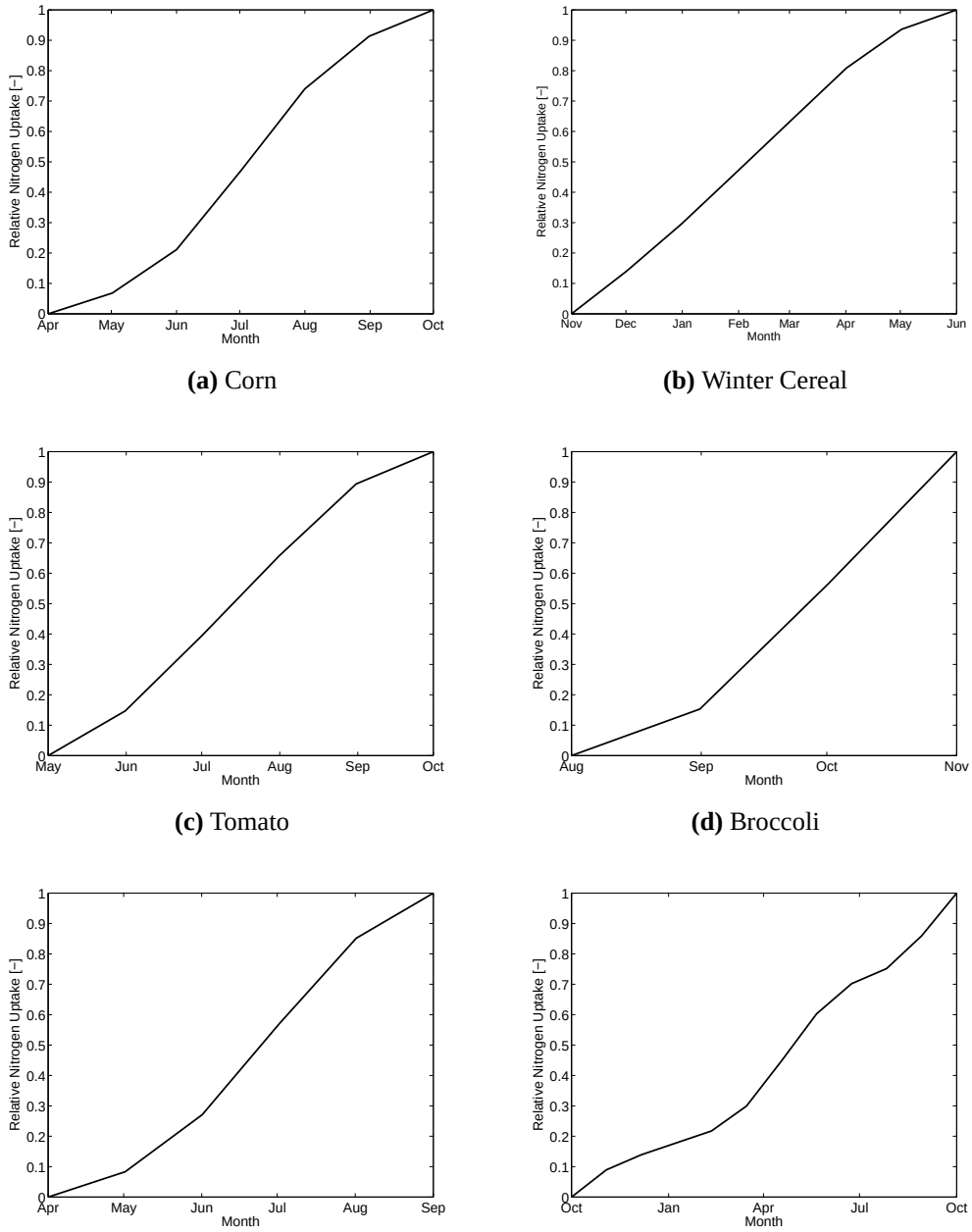

(a) Corn **(b)** Winter Cereal

(c) Tomato **(d)** Broccoli

(e) Sunflower **(f)** Double cropping

Figure 6.29: Relative nitrate uptake for the different cropping patterns within Lerma basin: (a) Corn; (b) Winter Cereal; (c) Tomato ;(d) Broccoli; (e) Sunflower; and (f) Double Croppings

patterns observed within the Lerma basin are presented in Fig. 6.30.

Individual u^{max} and u^{min} obtained for each crop are summed up in order to compute a *theoretical* range of monthly nitrate plant uptake $[U^{max}, U^{min}]$ $[Kg/month]$:

$$U^*_{max} = \sum_{k=1}^{n_{crops}} u_k^{max} A_j \qquad\qquad U^*_{min} = \sum_{k=1}^{n_{crops}} u_k^{min} A_j \tag{6.8}$$

The *approximate* nitrate plant uptake calculated after equation 6.6 is compared to the

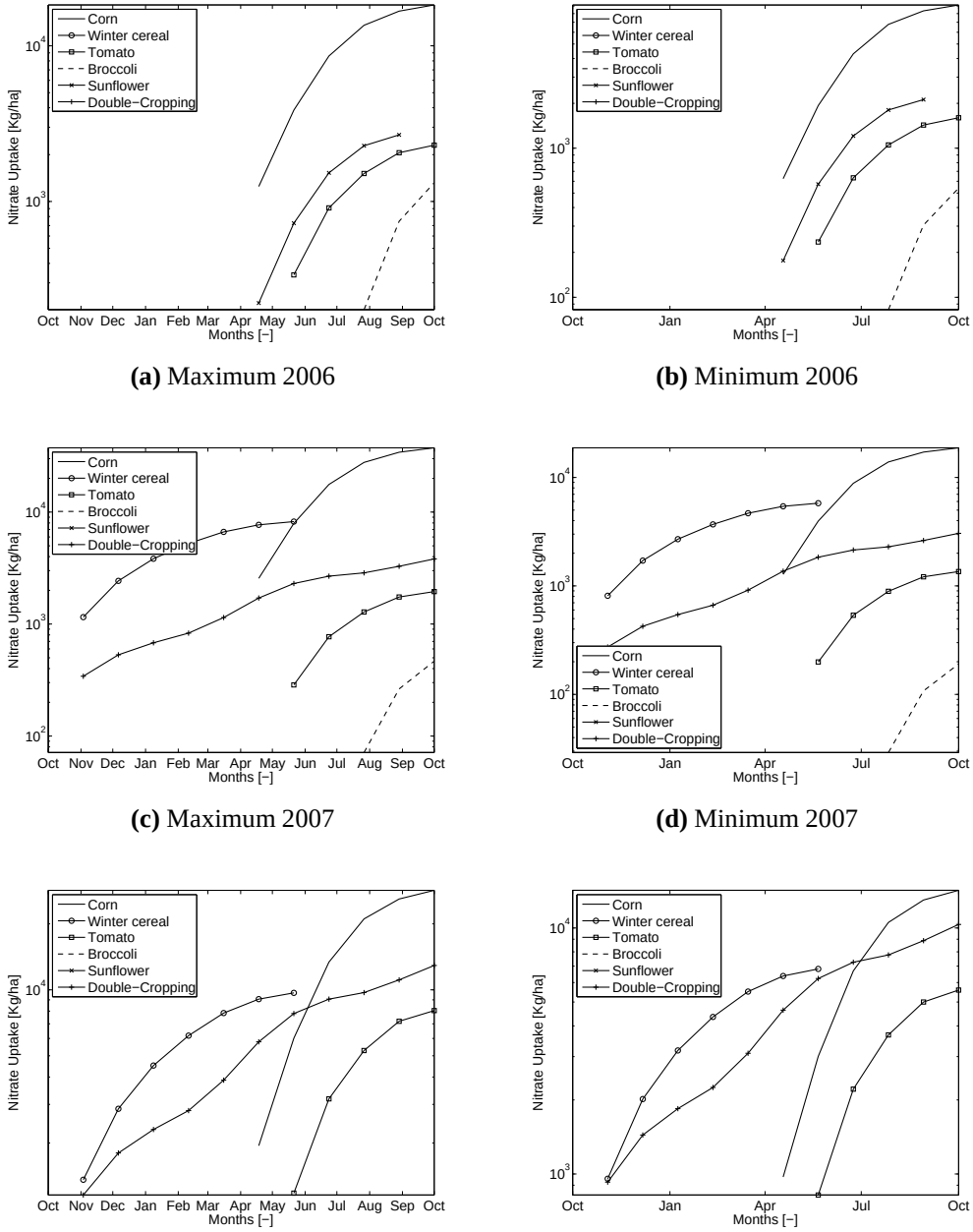

(a) Maximum 2006 **(b)** Minimum 2006

(c) Maximum 2007 **(d)** Minimum 2007

(e) Maximum 2008 **(f)** Minimum 2006

Figure 6.30: Maximum and Minimum theoretical monthly nitrate uptake (u^{max} and u^{min}) for the different cropping patterns within Lerma basin for hydrological years 2006, 2007 and 2008

theoretical nitrate uptake calculated by combining the actual cropping patterns observed within the Lerma basin, and plant nitrate uptake values taken from agricultural fields with similar fertilization treatments. Accumulated values of approximate and theoretical plant nitrate uptake for the simulated period are shown in the Fig.6.31. As shown in Fig. 6.31, the approximate accumulated nitrate uptake curve falls within the theoretical accumulated curves during the whole simulation period. This may suggest that disregarding chemical reactions and storage only have a relatively small effect on the overall response

of the Lerma basin. However, this hypothesis can only be investigated by the validation of a conservative transport model at the Lerma basin, i.e. by comparison of simulated and measured concentrations. Hence, in the following, a conservative transport model integrated to the validated flow model will be used to simulate the increase of nitrate concentrations induced by the intensification of fertilization in the Lerma basin.

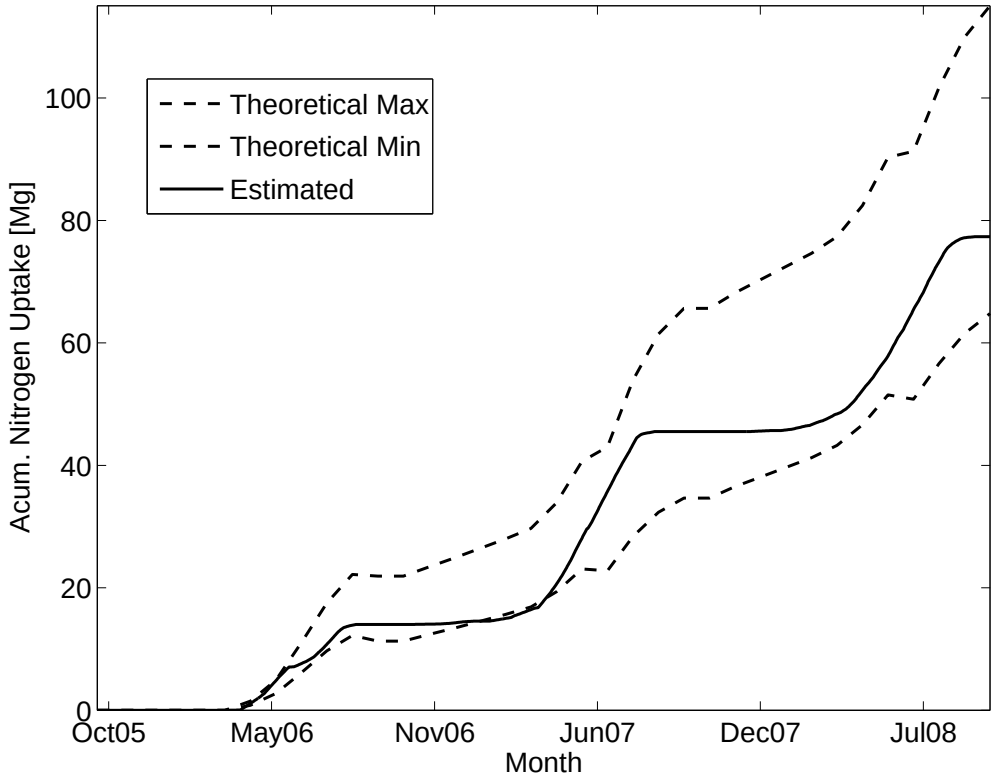

Figure 6.31: Comparison between theoretical accumulated nitrate uptake and approximate accumulated nitrate uptake within the Lerma basin

6.8.3 Physics-based model

In order to gain a better understanding of the system under study, a conservative nitrate transport model integrated into the previously validated flow model is used. As discussed in section 2.2.3, some authors (e.g Birkinshaw and Ewen, 2000a; Crawford and Glass, 1998) indicated that nitrate appear to be the most abundant nitrogen form in agricultural catchment. Hence, in this investigation other forms of nitrogen are disregarded, and I will focus exclusively on the nitrate fate and transport model of the Lerma basin.

Neglecting wet and dry depositions and nitrate losses by evaporation or volatilization, the nitrate source term for the surface domain q_m^s $[ML^{-3}T^{-1}]$ (in Eq. 3.9) can be expressed as the difference between the mass rate of nitrate imported to the system in form

of fertilizer at a point, and the actual plant uptake rate at the same point. For the subsurface, a simplified model is assumed, that neglect chemical reactions, i.e. immobilization-mineralization, nitrification and denitrification, in both the unsaturated and saturated zone, i.e. $r = 0$. The simplified conceptual model assumed in this investigation is summarized in Figure 6.32.

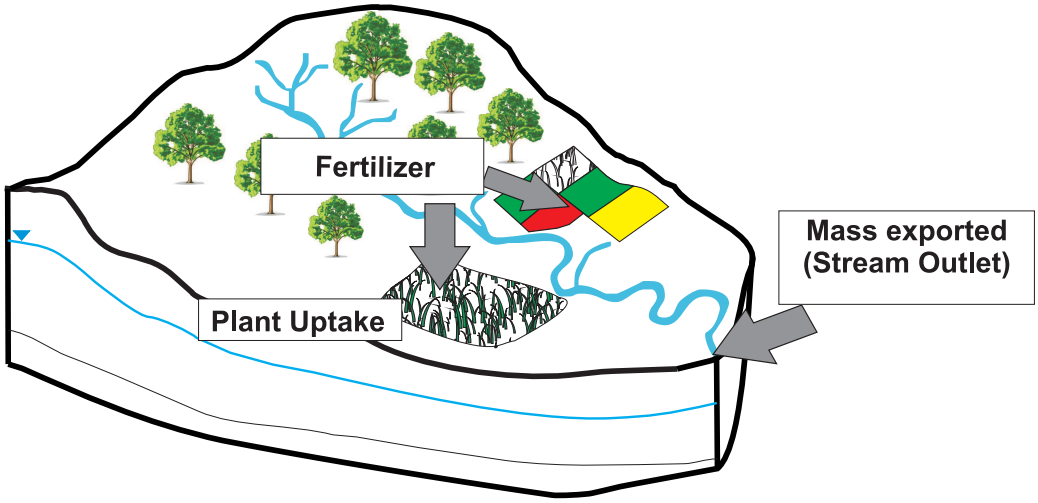

Figure 6.32: Simplified conceptual model of the nitrate processes at an agricultural catchment

The 3-D transport model grid is defined by the same finite element mesh and the same sub-layering scheme used in the flow model (section 6.3.1). The zonation defined for the surface domain of the flow model, i.e. 60 different sub-domains corresponding to the land-use units, was kept and used to account for the spatial (and temporally) distributed fertilization and plant uptake.

To calculate the source term q_m^s $[ML^{-3}T^{-1}]$, cropping patterns observed within the Lerma basin (i.e. Corn, Winter Cereal, Tomato, Broccoli, Sunflower and Double-Cropping) are considered. Monthly q_m^s for each node of the grid are calculated by dividing the difference between the total fertilizer ft_{ij} $[MT^{-1}]$ and the plant uptake u_{ij} $[MT^{-1}]$, by the total amount of water associated to the correspondent node W_{ij} $[L^3]$.

$$q_m^s = \frac{ft_{ij} - u_{ij}}{W_{ij}} \tag{6.9}$$

Monthly ft_{ij} are taken directly from the fertilizer application dataset. Monthly u_{ij} values are calculated using a simple relation that takes into account theoretical (maximum) and approximate total plant nitrate uptake:

$$u_{ij} = \frac{(\sum_{j=1}^{N} F_j A_j - Q_s C_o) u^{max}}{U_{max}^*} \tag{6.10}$$

The monthly values of fertilizer applied and the source term per m^3 of water are presented in Figure 6.33.

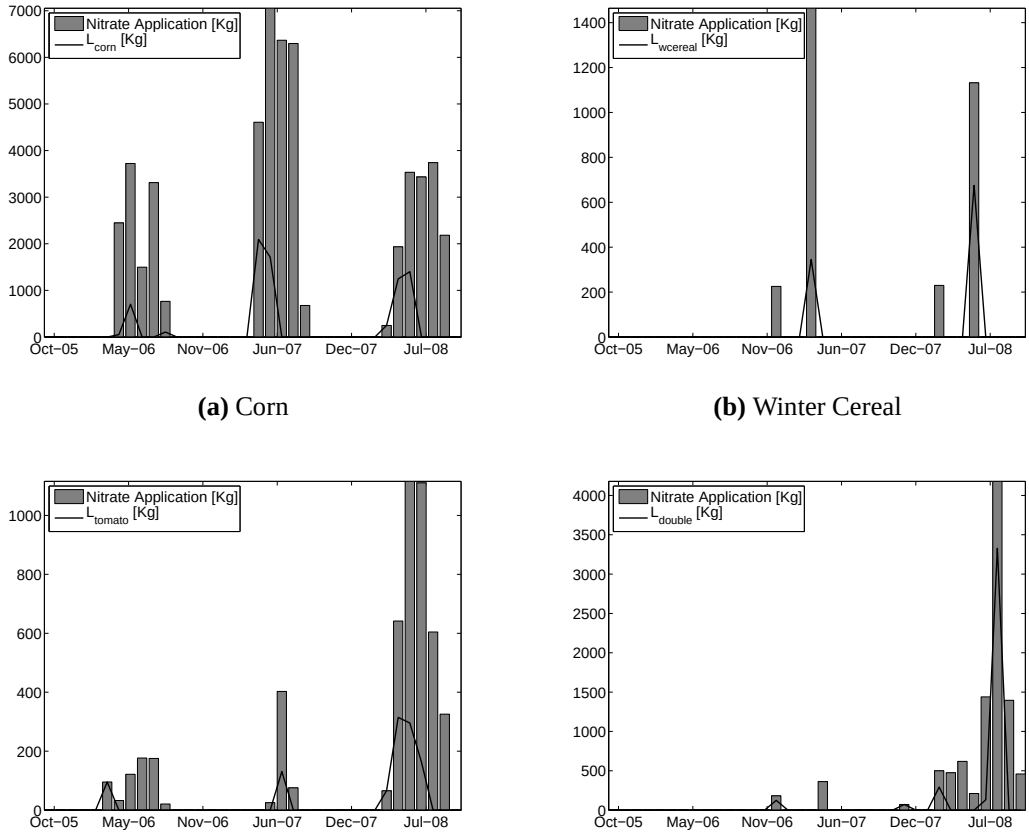

(a) Corn

(b) Winter Cereal

(c) Tomato

(d) Broccoli

Figure 6.33: Monthly total fertilization $[Kg]$ and surface source term after plant uptake $[Kg]$ for the most commonly observed cropping patterns within the Lerma basin the simulated period

In the case of liquid fertilizer, this approach seems to be justified as the fertilizer is dissolved in the irrigation water. In the case of solid fertilizer when fertilization and irrigation are concurrent, it may be also justified as the fertilizer would be dissolved by the irrigation water once it is applied. Conversely, in the case that fertilizer is applied long before the irrigation takes place, it remains difficult to estimate when the nitrate is advected and in what proportion. As discussed in section 2.2.3, when the fertilizer is applied to the soil it may undergo immobilization which ultimately transforms fertilizer into a part of soil organic matter. This may reduce the availability of the nitrate added in form of fertilizer because this form of nitrogen is not readily available to plants. Recalling the mass balance results presented in section 6.8.2, the net storage of nitrate appears to be negligible over a year. Hence, in this investigation an admittedly strong simplification will be made, that nitrate applied in early stages of the growing season will be available to be advected into the subsurface whenever the irrigation takes place. An alternative approach would be to introduce the (solid) nitrate as an injection of solute mass to the system and let q_m^s be calculated by the computational model(dividing the mass by the water content at each grid node for each time step). Unfortunately, this approach leads to unrealistic concentrations during dry periods, i.e. huge concentrations as a result of very small water contents.

Additionally, the occurrence of high-intensity rainfall may wash the fertilizer out of the basin before the plant is able to take it up reducing in this way the availability of nitrate. To minimize the effect of high-intensity rainfall events, only fertilizer application that are not affected by these kind of events were considered in the calculation of q_m^s. For this purpose, a subset of rainfall events with intensities higher that 15 mm/hr is defined. Fertilization events that take place before one of these events without the previous occurrence of an irrigation event (or a lower intensity rainfall event) were disregarded.

At the beginning of the simulation period (October 1st, 2005), the initial concentration measured at the outlet of the Lerma basin (5 mg/L) is considered as the initial concentration for the whole catchment. In order to validate the integrated model, nitrate concentrations measured at the outlet of the Lerma basin for the hydrological years 2006-2008 were used. The performance of the validation was evaluated by visual comparison of time series of observed and simulated nitrate concentrations, as well as by performance statistics.

The choice of (longitudinal and transverse) dispersivity values at field scale have been widely discussed in the literature (e.g Gelhar et al., 1992; Neuman, 1990; Xu and Eckstein, 1995). Theoretical and experimental investigations have found that field-scale dispersiveness are several order of magnitude greater than lab scales. Hence, laboratory values of dispersivity can not be used to define catchment-scale values of dispersivity. Ideally, field-scale dispersivities would be established from a tracer test at our particular case study. Unfortunately, such a test is not available for the Lerma basin. In this inves-

tigation, the longitudinal dispersivity α_L and the transverse dispersivity α_T are set to 1.0 and 0.1 m, respectively. These values are in agreement to the range of values reported by Gelhar et al. (1992) for an observation scale between 100 m to 1000 m.

After the model is validated, it is used to predict nitrate concentrations under three hypothetic scenarios: two mono-culture scenarios assuming (a) corn and (b) tomatoes; and an additional scenario (c)without fertilization. Climatological forcing measured during the hydrological years under study was used. Irrigation, fertilization and plant uptake cycles were also taken from typically observed practices during these years.

6.9 Results and Discussion

The goal of the conservative nitrate model of the Lerma basin was to reproduce the overall trend observed during the transition into irrigation agriculture. As only monthly values of plant nitrate uptake were available, the performance of the model was evaluated using weekly concentration values.

Simulated and observed concentration values at the outlet of the Lerma basin for the hydrological years 2006, 2007 and 2008 are presented in Fig. 6.34. In general, simulated and observed concentration values for the whole period under study show a good agreement. For the hydrological year 2006, the seasonality is reproduced relatively well. For the non-irrigated season, the model is able to reproduce the measured concentrations adequately, in particular two peaks of concentrations observed during this season are reproduced very well; however, the second one appears to be slightly delayed. For the rainy season, the model is able to reproduce very well the effect of dilution on the system (due to high water inputs and low fertilizer application). For the irrigation season, a drop in concentrations induced by the intensification of irrigation is simulated relative well for the model. However, after this drop the model slightly underestimates concentrations values.

For the hydrological year 2007, during the irrigation season, the first peak of concentrations measured at the outlet is well reproduced for the model. However, the model is unable to reproduce the second one. For the rainy season, despite of the good performance of the model, it has a minor tendency to underestimate concentration values. For the irrigation season, the model is able to reproduce the increase in nitrate concentration induced by the intensification of fertilization at the beginning of the season; and the drop of concentrations during the peak of irrigation induced by dilution. After the drop, a minor tendency of the model to overestimation is noticeable.

For the hydrological year 2008 the model is able to reproduce very well the measured concentrations including the gentle increase in concentrations at the beginning of the hydrological year, and the steep drop measured during the rainy season. During the irrigation season, the simulated values also show a relatively good agreement with the

measured signal.

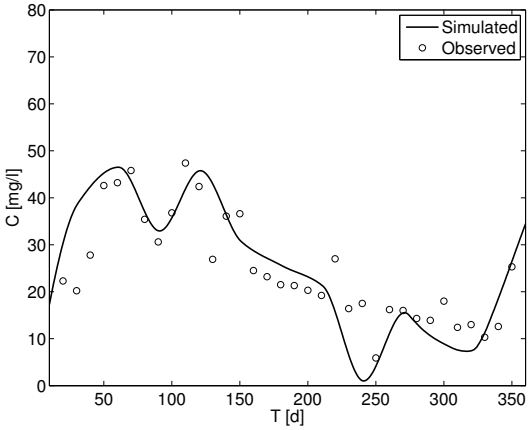

(a) Simulated vs. Observed Concentrations 2006

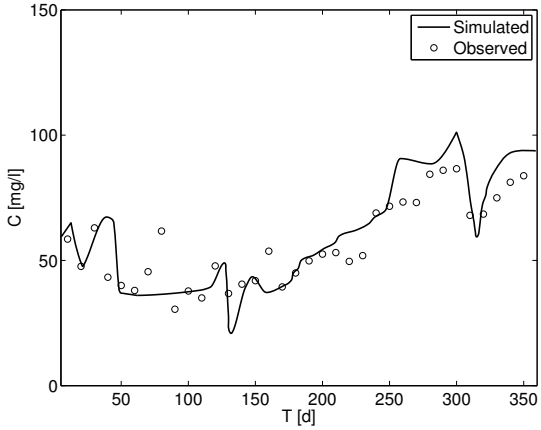

(b) Simulated vs. Observed Concentrations 2007

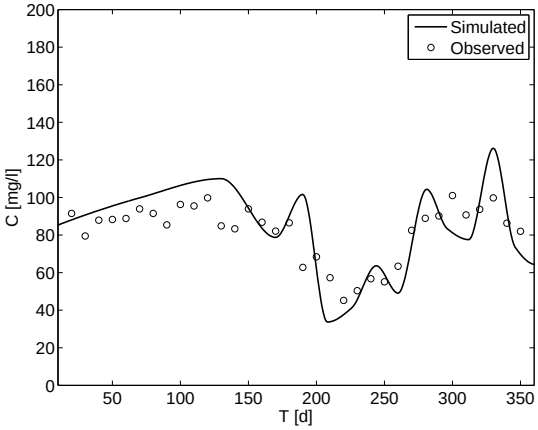

(c) Simulated vs. Observed Concentrations 2008

Figure 6.34: Observed and simulated nitrate concentrations at outlet of the Lerma basin

The model performance for the hydrological years 2006-2008 was also evaluated quantitatively by goodness-of-fit measures. The root mean squared error (RMSE) and the maximum error (ME) were calculated (table 6.11). Calculated errors are admittedly higher than expected. Nevertheless, considering the large uncertainties caused by both the simplifying model assumptions and the fertilization dataset, the range of errors obtained should certainly be satisfactory. The latter may be justified if the errors are compared to the absolute range of variation in nitrate concentrations during the whole simulated period which is 110 mg/l. This implies an error of 4.5-15.4% of the observed range. Fully-coupled physics-based application studies in the scientific literature trying to match nitrate concentrations are rather scarce. As one of the few, Birkinshaw and Ewen (2000a) presented monthly simulated and observed nitrate concentration values at the Slapton Wood catchment. Concentrations were simulated using a much more complex model than the one presented in this investigation, that accounts for a large number of nitrogen

transformation processes both in the surface and the subsurface. However, estimation of the RMSE equals 2.1 mg/l, that compared to the absolute range of variation which is 8.5 mg/l gives an error of 24.3% of the observed range, that is higher than the errors calculated for the conservative transport model of the Lerma basin.

Table 6.11: Model performance statistics for the validation period (hydrological years 2006-2008) of the nitrate transport model. ME: maximum error and RMSE: root mean square error

Year	ME$[mg/l]$	RMSE$[mg/l]$
2006	10.879	5.111
2007	27.761	17.347
2008	20.242	12.541

Following, the model is used to predict nitrate concentrations for one hydrological year under two hypothetical mono-culture scenarios: (1) corn, and (2) tomato. These cropping patterns are very commonly observed within the Lerma basin, and they are grown using very different fertilization treatments. Corn is the most extended cropping pattern during the simulated period, i.e. 51, 69 and 38%, and it is also the one with the highest nitrogen application (380 Kg/ha). Tomato is the cropping pattern with the highest crop yield (80 Mg/ha) but with a considerably smaller amount of nitrogen applied (182 Kg/ha). Averaged climatological conditions from the three gauged years, i.e. the hydrological years 2006-2008, were used in the simulation of the scenarios. This seems to be justified as the three years represents an average climatological behavior (Abrahao, 2010). Amounts of irrigation and fertilization for both cases (i.e. corn and tomato) were extrapolated for the whole basin from typical values observed during the hydrological years 2006-2008. As initial condition for the scenarios simulations, the concentration distribution obtained for the last day of the hydrological year 2008 (30th September/2008) was used. For comparison, a third scenario that considers no fertilization is simulated. Despite being unrealistic in practical terms, this scenario represents a base case to which the previously discussed mono-culture scenarios were compared.

Results of the simulations for the hypothetical scenarios are presented in Figure 6.35. Concentration signals for different scenarios show a very different behavior, but in all of the cases concentrations remain above the drinking water EU standard which is 50 mg/l.

For the case that corn is grown in all of the pre-defined plots, higher peaks of concentrations (up to 180 mg/l) than in the other cases are observed. Also, a higher variation in concentrations values can be observed during the irrigation season. This situation seems to be induced by larger concentrations of nitrate in the return flows as a result of a less efficient fertilization. Support for this hypothesis comes from figure 6.33 where fertilizer applied to corn is much higher than the plant nitrogen needs. Also, nitrogen applied for the case of corn (380 Kg/ha) within the Lerma basin is very high compared to common values reported in the literature (200-300 Kg/ha) (e.g Freeman et al., 2007; Stapleton

et al., 1983). Concentration values at the end of one simulated year for this case (130-135 mg/L) shows a considerable increase (50%) compared to the values at the beginning of the year (90 mg/l). In that respect, the obtained results indicate that a corn mono-culture scenario would boost the negative impact of fertilizer on surface water quality at the Lerma basin.

For the case that only tomato is grown, in general lower values of nitrate concentration are observed. The latter may be associated to better agricultural practice that results in smaller nitrate concentrations in the irrigation return flows. In fact, there is a good correlation between literature values of nitrogen applied (90-220 kg/ha) (e.g. Sainju et al., 2001) and the nitrogen actually applied within the Lerma basin (180 kg/ha). Furthermore, the first concentration peak associated to runoff with high nitrate contents during the early rainy season observed for the corn scenario is not simulated for the case of tomato. Concentration values at the end of the simulated year for this case (85-90 mg/L) are very similar to the values at the beginning of the year (90 mg/l). This may indicate that the tomato mono-culture scenario would represent a sustainable long-term scenario at the Lerma basin. Of course, in order to confirm this hypothesis simulations for longer periods would be required.

For the case that no fertilization is assumed, a steep decrease is observed during the non-irrigated season. After a relatively small peak towards the end of the non-irrigated season, a minimum value of concentrations (58 mg/l) is reached, this value remain constant until the end of the simulated hydrological year. Despite being much smaller than the typical values observed for the other scenarios, this value represents a much higher value than the observed at the beginning of the transformation (5 mg/l). The latter appears to indicate that in order to reverse the effect of fertilization on water quality in the Lerma basin a much longer period would be required. Indeed, the minimum level reached for this hypothetical case is still above the EU drinking water limit (50 mg/l).

In summary, the validation results of the transport model showed that it is possible to simulate general concentration trends and important features of the transformation of the Lerma basin into irrigation agriculture using a conservative transport model of nitrate that uses parameter values obtained from previous cases studies. In particular, the simplified model is able to simulate the large variation of concentration values induced by the climatological, irrigation and fertilization seasonality. The analysis of hypothetical scenarios indicated that in both mono-culture scenarios corn and tomato, the concentrations would remain above recommended levels. In the case without any fertilization, despite the noticeable decrease, concentration values do not reach values below the EU drinking water limit either.

In order to improve the prediction capabilities of the transport model, a nitrogen transformation component that accounts for chemical reactions, i.e. immobilization, mineralization, nitrification, denitrification, could be coupled to the transport model. However,

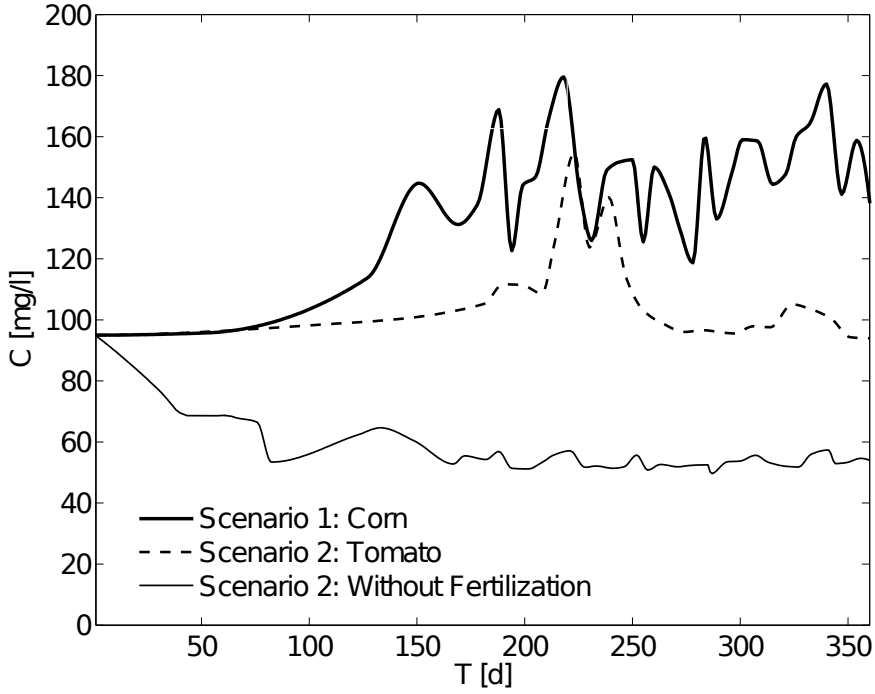

Figure 6.35: Transport simulations of different cropping patterns scenarios (Corn, Tomato, and no fertilization) at the Lerma basin

this would require the definition of additional parameters and, hence, it would introduce a larger parameter uncertainty given our fixed amount of data.

Table 6.10: Typical and estimated nitrate uptake rates for each cropping pattern within the Lerma basin

	Area Percentage			*Fert*	*Yi*	u_t	Reference
	2006	2007	2008	Kg/ha	Mg/ha	Kg/Mg	
Total Area(ha)	125	265	312				
Corn	61%	59%	38%	380	12.0	10-28	Andreu et al. (2006); Stapleton et al. (1983)
Winter Cereal	0%	25%	25%	184	4.6	19-27	Delogu et al. (1998)
Tomato	10%	4%	14%	182	80.0	1.6-2.3	Sainju et al. (2001)
Broccoli	24%	4%	0%	150	9.0	9-22	Thompson et al. (2002)
Sunflower	5%	0%	0%	130	2.0	38-48	Zubillaga et al. (2002)
Double Cropping	0%	8%	23%	290	18.0	14-20	Andreu et al. (2006)

Chapter 7

Summary and Conclusions

This dissertation addressed five fundamental questions on how the transformation of semi-arid rainfed basins towards irrigation agriculture and its impact on its hydrological functioning can be studied by fully-integrated surface-subsurface, physics-based models.

How can we develop a surface-subsurface physics-based flow model at catchment scale? How can we validate such a model?

In this investigation, a protocol to build a surface-subsurface physics-based model was presented. The protocol proposes a series of steps that starts by establishing the purpose of the model, followed by the development of a conceptual idea that best represents the natural system that is modeled. The conceptual idea should encompass the definition of the area of interest by the identification of its boundaries; also the surface and subsurface units describing the spatial variability should be defined. In most of the cases, it would also required to characterize the flow system. A computer code able to numerically solve the system of partial equations describing the relevant processes in the modeled system should be selected. In case that a suitable model is not available, the computer code must be developed. The selection (or development) of the computer code completes the first stage of the modeling process.

In order to verify that the mathematical formulation holds for a particular case study, we need to compare the numerical model simulations to field observations. For this purpose, a number of steps are proposed that start with the identification of parameters that can be defined from available field data and the parameters which need to be estimated by calibration. Additionally, ranges of sensitive, physically-acceptable values of the calibration parameters should be estimated. After the calibration problem is fully defined, we need to identify parameter values based on stream discharges and hydraulic heads (and soil moisture measurements if available) in the case of flow models; transport model also requires measurement of surface and subsurface concentrations. Parameter estima-

tion is achieved by systematically modifying the parameter values until the agreement between measured and simulated values is maximal. To establish a greater confidence in the model, we use the set of calibrated parameters to reproduce a second set of field data. A record of climatological (and anthropogenic) forcing with different historical conditions may be used to show the ability of the model to reproduce field observations under different conditions, e.g. land-use change or wetter scenarios.

Using this protocol, a surface-subsurface physics-based model was set-up, intended to simulate the transformation of the Lerma basin (Spain) from a non-cultivated dry land into an irrigated crop land. A comparison of measured and simulated flow dynamics -despite the large variation in forcing induced by the transition- revealed that our model is able to reproduce detailed temporal and spatial features of the flow dynamics. In that respect, the results presented in this thesis indicate that the guideline proposed to build fully-coupled physics-based model represents a valuable tool in order to investigate flow dynamics and surface-subsurface interactions in complex hydrosystems.

How can we determine the influence of catchment controlling factors from typically available observations? To what extent can a geometrical simplification be used to parameterize a physics-based model? What are the factors that control the surface-subsurface hydrological response at catchment scale?

The identification of parameters that have an important effect on the model simulation results, commonly called catchment controlling factors, is referred to in this thesis as parameterization. In the parameterization, we should be able to define a set of calibration parameters for which there should be enough information contained in the observations, so that their values can be estimated. We may also define the calibration parameter space, that should comprise only physically acceptable and sensitive ranges of values.

An adequate parameterization process must combine a sensitivity study and a parameter correlation analysis. Although, it helps speeding-up the model verification, this process is commonly avoided in complex physics-based hydrosystems due to large running-time requirements. Thus, the set of relevant parameters are left to be decided by the modeler based on subjective criteria. To overcome this problem, I introduced a geometrical simplification, the so-called *hillslope equivalent*.

The hillslope equivalent is used to perform an adequate parameterization process. The main goal of the hillslope equivalent is to speedup the parameter estimation of physics-based fully-coupled models. The novel methodology is tested first at the Borden site experiment, and is subsequently used in the calibration of the Lerma basin flow model. The comparison with the geometrically realistic model shows in both test cases that sensi-

tivities and parameter correlation values correlate very well with the values obtained with the hillslope equivalent. Thus, during the parameterization of a model one may not need to calculate sensitivities using the realistic model, instead one could rely on the hillslope equivalent analysis. In this respect, the hillslope equivalent represents a very useful tool to investigate the physical system, identify catchment controlling factors, and recognize potential problems during the calibration at the benefit of reduced computing times.

The results from the analysis of sensitivities for the van-Genuchten parameters indicate that due to the high non-linearities associated with these parameters, global sensitivity studies are required in order to obtain a more comprehensive understanding of the modeled system, and in that way achieve a better parameter estimation. A local sensitivity study would only provide incomplete information regarding the effect of these parameters on the overall hydrological response. In particular, there are regions of the parameter space with a relatively high sensitivity of the inverse air-entry pressure α and the pore-size factor n, while there are other regions where the sensitivity is negligible. Unlike results presented in previous studies, we found that the inverse air-entry pressure α and the pore-size factor n have a considerable effect on the catchment hydrological response. From this perspective, they should be part of the set of calibration parameters when a high influence of the unsaturated zone is expected.

Sensitivities for the saturated hydraulic conductivity k_s show consistent high values throughout the parameter space, i.e. a significant effect of k_s on the catchment hydrological response. This suggests that for k_s a local sensitivity analysis would provide enough information to be used in the design of the calibration problem.

To what extent can surface-subsurface spatial and temporal flow dynamics be explained by a physics-based model? What are field data and spatial resolution requirements to reproduce adequately those dynamics at catchment scale?

A physics-based model is used in this investigation as a model of coupled partial differential equations derived from the principles of conserving mass and momentum of water. In particular, these are the shallow-water equations for flow at the land-surface and in streams and the Richards equation for flow in the subsurface. The model is considered physics-based because parameters appearing in the equations have a physical meaning at a particular scale and may be measured at this scale. However, in the transition to larger scales, parameters attributed to more coarsely defined units become effective values which can not directly be measured, but must be obtained by model calibration where details of the unresolved variability needed for rigorous upscaling are missing. Still, the principles of conserving mass and momentum hold and the relevant flow processes are

directly represented in a spatially distributed way.

In this investigation, a physics-based model of the Lerma basin was developed. The purpose of the model was to evaluate the impact of the transformation of the semi-arid rainfed Lerma basin towards irrigation agriculture on the hydrological functioning of the basin. An important reason for the use of a physics-based model lies in the nature of the hydrosystem under consideration. The Lerma basin is a semi-arid, formerly fallow land, whose transformation into an irrigation agriculture catchment has been closely monitored. Another reason for the use of a physics-based model to simulate the Lerma basin is related to data availability. Available data includes stream discharge, hydraulic heads and soil samples for the whole transition process of the basin into irrigation agriculture, i.e. the hydrological years 2006-2009. Precipitation and irrigation were also gauged during this period. Evapotranspiration can be estimated using the FAO-Penman-Monteith equation from climatological measurements and locally-estimated crop factors k_c. In this respect, the Lerma basin represents a better equipped catchment than most of the catchments in the hydrological literature. Hence, in this investigation, a parameter hungry physics-based model, is proposed rather than a (traditional) conceptual hydrological model (i.e. a network of inter-connected storages) as used in most catchment-hydrological studies.

Despite concerns on the validity of Richards' equation and its spatial resolution requirements, the good model performance on the validation data set implies that it is possible to simulate catchment systems under land-use change with physics-based models assuming Richards' equation as an effective law leading to appropriate system behavior and using physically meaningful, identifiable parameter sets.

Apart from the considerably good validation results, simulated distributed variables show the ability of the model to reproduce detailed spatial features observed in the field. In spite of the non-uniqueness problems reported in the literature in the estimation of unsaturated van-Genuchten parameters, these parameters were found to be identifiable when the parameter estimation problem is constrained by a geology-guided zonation approach and a restriction to physical parameter value ranges based on texture.

In catchment scale models, parameters and state variables at the grid nodes often do not correspond with the field-measurements (i.e.the incommensurability problem Beven, 1989, 1993, 2002). Parameters cannot realistically be obtained from every point within the spatial domain without excavating the entire catchment. Another reason for the discrepancy of the resolution of the computational grid and the resolution of the available data is related to the resolution demanded by the numerical scheme to remain stable or accurate enough. In this case, the resolution becomes a mathematical requirement for the adequate numerical solution of the partial differential equations. From this perspective, the assumption of effective parameter values, a condition of distributed models, is inherent to physics-based models.

The fairly high data requirements to describe the spatial variability of model param-

eters and boundary conditions in physics-based models may represent a limitation in ungauged catchments. In complex hydrosystem, as the one presented in this investigation, the computational demand may be fairly high, as the large non-linearities when solving the subsurface variably-saturated flow equations during dry months, and the small time-steps enforced during the high-intensity rainfall events may slow down the simulations. However, the accelerated development of high-perfomance computing will certainly help to overcome such limitations.

How can spatially and temporal resolved variables obtained from a physics-based model be used to define the impact of the transformation from rainfed into irrigation agriculture at catchment scale? What are the benefits of using a fully-coupled physics-based model?

The water balance analysis at the Lerma basin indicates that subsurface storage can not be neglected over a hydrological year for the period in which irrigation agriculture in the Lerma basin has intensified. Moreover, neither the discharge nor the pattern of the change in storage observed for the four years under observation does simply follow the monotonically increasing irrigation.

Traditional hydrological models estimate a functional relationship between concurrent input and output time series based on statistical inference. However, this functional relationship becomes unreliable, if new input series are presented to the model that do not follow the statistics of those used to derive the functional relationship. Conversely, a physics-based model has a particularly estimated set of effective parameter values derived from the calibration and unlike a traditional hydrological model, its response to a new input series will not be unphysical, if these effective parameter values remain within physical ranges. In that respect, an important benefit of physics-based models is that direct measurements (or indirect estimations) can be used to narrow the range of the model parameter values.

A physics-based model was used to calculate spatially and temporally resolved variables. In order to indicate changes in the runoff generation process and catchment functioning, the evolution of the total stream length and the approximate infiltration capacity provided by the distributed results of the model are investigated. The total length of streams within the catchment represents a feature of high ecological relevance and a prominent feature of the hydrological system representative for groundwater – surface water exchange. A particular advantage of the physics-based model approach is that it is able to compute the length of the streams naturally: the spring of a creek is where the groundwater table reaches the land surface. A model that does not provide the spatial distribution of groundwater heads would be unable to simulate shifting springs induced

by changes on irrigation practice. Model results show that irrigation agriculture has raised the base level of the water table of the Lerma aquifer causing new portions of the drainage network to become perennial. The evolution of the total length of streams within Lerma basin show the ability of the model to reproduce detailed spatial features, in particular the change of the southern creek from intermittent to perennial, as well as the effect of quick irrigation return flows on the size of the drainage network.

Runoff generation processes depend on soil moisture content and the distance of the water table to the surface. Hence, a shift in runoff generation processes is expected as a result of the transition to irrigation agriculture. The concept of approximate infiltration capacity was introduced to investigate such shift in runoff generation processes. The evolution of the approximate infiltration capacity curve shows a raising base level due to irrigation agriculture that is indicative of a shift in the occurrence of Hortonian runoff generation from frequently in 2006 to episodic in 2009. Indeed, while in 2006 most of the basin is associated to Hortonian-runoff generation, in 2009 only non-irrigated areas (47% of the total area of the basin) are associated to this mechanism. Furthermore, the sum of exfiltrating fluxes obtained directly from the physics-based model considering spatial differences demonstrate that both, the approximate infiltration capacity curve, and the contribution of exfiltration to stream flow are consistent in indicating a shift from Hortonian towards Dunne flow runoff generating processes triggered by the land-use change. In that respect, the Lerma basin turned from a system of low interaction with the underlying aquifer into a system with a much higher groundwater-surface water interaction.

In the absent of independent field measurements a physics-based model could also be seen as a contribution in the pursuit of an improved dialogue between modelers and experimentalists for reducing parameter uncertainty, in the sense that results of a physics-based model, like the one presented in this investigation, provide useful guidelines to future field experiments and long-term observations in order to better capture the variables associated with the distributed hydrological response of a catchment.

To what extent can a conservative physics-based model reproduce the nitrate fate and transport at catchment scale? How can this model be used to predict local impacts of the ongoing change?

A conservative transport model is integrated into the flow model of the Lerma basin. The flow and transport fully-integrated model is then validated using the concentrations measured at the outlet for the hydrological years 2006-2008, without any parameter calibration and using plant-uptake related typical parameter values from similar agricultural fields.

Despite many simplifying assumptions, the model is able to reproduce the general

increasing concentrations trend induced by the evolution of the fertilization treatment during the transition of the Lerma basin into irrigation agriculture. The model is also able to reproduce adequately the concentrations' seasonality caused by the climatological forcing, and the variability caused by the evolution of irrigation.

The model was also used to investigate mono-culture scenarios for two representative cropping patterns that widely differ from each other in both irrigation and fertilization amounts. The results show that a corn mono-culture scenario would considerably raise nitrate concentration values, hence, negatively impacting water quality in the Lerma basin. Conversely, model simulations indicated that the tomato mono-culture scenario would be sustainable in terms of concentrations as the values appears to remain constant after the simulated period. In this respect, a longer simulation, i.e. until a dynamic steady-state is reached, would give support to this hypothesis. In the case without any fertilization, despite the noticeable decrease, concentration values do not reach values below the EU drinking water limit within a single year either. It may indicate that in order to reverse the effect of fertilization on water quality at the Lerma basin a much longer period would be required.

Our case study represented a modeling challenge due to the large complexity induced by the climatological conditions and the strong anthropogenic influence. However, the validation results shows that it is possible to simulate transport at catchment systems with a parsimonious physics-based model approach. The lack of data to describe the nitrogen transformation processes is a typical case at medium size (and large) catchments. In that respect, the conservative approach presented in this investigation represents an important contribution in the study of the sustainability of agricultural practices.

7.1 Concluding Remarks

The model protocol proposed worked well in the construction and validation of the physics-based model of the Lerma basin. The good model performance on the validation data set indicated that it is possible to simulate catchment systems under land-use change with physics-based models using physically meaningful parameter sets. The flow model of the Lerma basin developed in this investigation is also able to reproduce detailed spatial features of the transition into irrigation agriculture.

The *hillslope equivalent* proved to be a very computationally efficient and useful tool to identify catchment controlling factors in physics-based models. It allows defining a set of calibration parameters and the calibration parameter space based on a comprehensive sensitivity study.

Our analysis of the Lerma basin indicates a significant influence of the van-Genuchten parameters on the aggregated hydrological catchment response. Hence, they should be

included in the set of calibration parameters when a strong influence of the unsaturated zone is expected.

The transition into irrigation agriculture at the Lerma basin induced a higher contribution of Dunne flow to the stream flow and a much higher groundwater-surface water interaction.

The validation results for the transport model showed that it is possible to simulate transport at catchment scale with a conservative physics-based model approach.

7.2 Future Research

The following additional studies may be used in future research.

1. One of the purposes of the physics-based model developed in this investigation is to ensure the long-term sustainability of the agriculture practices in the Lerma basin. In this respect, a study that consider more water management scenarios for longer simulation periods would be very helpful. This could be done by using the conservative model to predict nitrate concentrations until a dynamic steady state is reached. Five hypothetic scenarios are proposed: two mono-culture scenarios with (1) corn and (2)tomato; (3) and (4) combinations of corn and tomato considering two different spatial distributions; and (5) an additional scenario without irrigation or fertilization.

2. The model proposed can be extended to incorporate nitrogen transformation and nitrate leaching in the root zone in order to represent more accurately the complexity of the nitrogen cycle. This could be achieved by coupling the model presented in this investigation to an existent nitrogen transformation model, e.g. Expert-N.

3. Additional scenarios can be considered to analyze the effect of climate change on irrigation agriculture. Climate changes scenarios generated by the School of Civil Engineering and Geosciences of the Newcastle University for the Ebro basin could be used for that purpose.

4. Combining the more sophisticated nitrogen transformation model and the climate change scenarios, water management alternatives can be investigated in order to ensure the sustainability of the irrigation agriculture in the Lerma basin. Cropping pattern scenarios, economical variables and climate could be integrated in the design of optimal agriculture practices that includes the optimization of cropping patterns, irrigation and fertilization scheduling.

Bibliography

Abbott, M., Refsgaard, J., 1996. Distributed hydrological modelling. Springer.

Abdul, A., 1985. Experimental and numerical studies of the effect of the capillary fringe on streamflow generation. Ph.D. thesis, University of Waterloo.

Abdul, A., Gillham, R., 1989. Field studies of the effects of the capillary fringe on streamflow generation. Journal of Hydrology, 112(1-2):1–18.

Abrahao, R., 2010. Impactos ambientales del riego: La transformación de la cuenca de Lerma (Zaragoza, España). Ph.D. thesis, Tesis Doctoral. Departamento de Ingeniería Química y Tecnologías del Medio Ambiente. Universidad de Zaragoza. 166 pp.

Abrahao, R., Perez, A., Causape, J., Cirpka, O., Buerger, C., In preparation. Simulating the Transition of a Semi-Arid Rainfed Catchment towards Irrigation Agriculture. Agricultural Water Management.

Allen, R., 2005. The ASCE standardized reference evapotranspiration equation. American Society of Civil Engineers.

Allen, R., Pereira, L., Raes, D., Smith, M., 1998. Crop evapotranspiration: guidelines for computing crop water requirements. FAO Irrigation and Drainage paper (56), 300 pp. FAO, Rome, Italy.

Anderman, E., Hill, M., Poeter, E., 1996. Two-dimensional advective transport in groundwater flow parameter estimation. Ground Water, 34(6):1001–1009.

Anderson, M., Woessner, W., 1992. Applied Groundwater Modeling: Simulation of Flow and Advective Transport. Academic Press.

Andreu, J., Aso, B., Enguita, D., Carbó, E., Luis, J., Martínez, G., López, G., Soteras, I., Climente, I., Pérez, M., et al., 2006. Fertilización nitrogenada: guía de actualización. Gobierno de Aragón. Centro de Transferencia Agroalimentaria.

Arkley, R., 1963. Relationships between plant growth and transpiration. University of California, Division of Agricultural Sciences.

Arnold, J., Srinivasan, R., Muttiah, R., Williams, J., 1998. LARGE AREA HYDROLOGIC MODELING AND ASSESSMENT PART I: MODEL DEVELOPMENT1. JAWRA Journal of the American Water Resources Association, 34(1):73–89.

Azam, F., Simmons, F., Mulvaney, R., 1993. Immobilization of ammonium and nitrate and their interaction with native N in three Illinois Mollisols. Biology and fertility of soils, 15(1):50–54.

Bear, J., 1979. Hydraulics of Groundwater. McGraw-Hill Companies.

Bear, J., 1988. Dynamics of Fluids in Porous Media. Courier Dover Publications.

Betson, R., 1964. What is watershed runoff. Journal of Geophysical research, 69(8):1541–1552.

Beven, K., 1979. A sensitivity analysis of the Penman-Monteith actual evapotranspiration estimates. Journal of Hydrology, 44(3/4).

Beven, K., 1989. Changing ideas in hydrology-the case of physically-based models. Journal of Hydrology, 105(1-2):157–172.

Beven, K., 1993. Prophecy, reality and uncertainty in distributed hydrological modelling. Advances in Water Resources, 16:41–41.

Beven, K., 2001. Dalton Medal Lecture: How far can we go in distributed hydrological modelling? Hydrology and Earth System Science, 5(1):1–12.

Beven, K., 2002. Towards a coherent philosophy for modelling the environment. Proceedings of the Royal Society of London-A-Mathem and Physical and Engin Sciences, 458(2026):2465–2484.

Beven, K., Lamb, R., Quinn, P., Romanowicz, R., Freer, J., Singh, V., 1995. TOPMODEL. Computer models of watershed hydrology., pages 627–668.

Bicknell, B., Imhoff, J., Kittle, J., Donigian, A., Johanson, R., 1993. Hydrological Simulation Program-FORTRAN (HSPF): User's manual for release 10.0. Environmental Research Laboratory, US Environmental Protection Agency, Athens, GA. PA, 600(3):84.

Birkinshaw, S., Ewen, J., 2000a. Modelling nitrate transport in the Slapton Wood catchment using SHETRAN. Journal of hydrology, 230(1-2):18–33.

Birkinshaw, S., Ewen, J., 2000b. Nitrogen transformation component for SHETRAN catchment nitrate transport modelling. Journal of Hydrology, 230(1-2):1–17.

Bredehoeft, J., 2003. From models to performance assessment: The conceptualization problem. Ground Water, 41(5):571–577.

Bronstert, A., Bardossy, A., 2003. Uncertainty of runoff modelling at the hillslope scale due to temporal variations of rainfall intensity. Physics and Chemistry of the Earth, 28(6-7):283–288.

Brooks, R., Corey, A., 1965. Properties of Porous Media Affecting Fluid Flow. Colorado Agricultural Experiment Station.

Brown, D., 1995. An analysis of transient flow in upland watersheds: interactions between structure and process. Ph.D. thesis, UNIVERSITY of CALIFORNIA.

Carsel, R., Parrish, R., 1988. Developing joint probability distributions of soil water retention characteristics. Water Resour. Res, 24(5):755–769.

Causape, J., 2002. Repercusiones medioambientales de la agricultura sobre los recursos hıdricos de la Comunidad de Regantes n V de Bardenas (Zaragoza). Ph.D. thesis, Tesis Doctoral. Departamento de Ciencias de la Tierra, Facultad de Ciencias Geologicas. Universidad de Zaragoza. 153 pp. Available in: http://www. cervantesvirtual. com.

Causapé, J., Quílez, D., Aragüés, R., 2004. Assessment of irrigation and environmental quality at the hydrological basin level I. Irrigation quality. Agricultural Water Management, 70(3):195–209.

Causape, J., Quilez, D., Aragues, R., 2006. Groundwater quality in CR-V irrigation district (Bardenas I, Spain): Alternative scenarios to reduce off-site salt and nitrate contamination. Agricultural Water Management, 84(3):281–289.

Cirpka, O., 2010. Class Notes: Numerical Methods in Subsurface Hydrology.

Conan, C., Bouraoui, F., Turpin, N., de Marsily, G., Bidoglio, G., 2003. Modeling Flow and Nitrate Fate at Catchment Scale in Brittany(France). Journal of Environmental Quality, 32(6):2026–2032.

Cooley, R., 1971. A finite difference method for unsteady flow in variably saturated porous media: Application to a single pumping well. Water Resources Research, 7(6):1607–1625.

Crawford, N., Glass, A., 1998. Molecular and physiological aspects of nitrate uptake in plants. Trends in Plant Science, 3(10):389–395.

Dawson, C., 2008. A continuous/discontinuous Galerkin framework for modeling coupled subsurface and surface water flow. Computational Geosciences, 12(4):451–472.

Delogu, G., Cattivelli, L., Pecchioni, N., De Falcis, D., Maggiore, T., Stanca, A., 1998. Uptake and agronomic efficiency of nitrogen in winter barley and winter wheat. European journal of agronomy, 9(1):11–20.

Dingman, S., 2002. Physical hydrology. v. 1. Prentice Hall.

Doherty, J., Hunt, R., 2009. Two statistics for evaluating parameter identifiability and error reduction. Journal of Hydrology, 366(1-4):119–127.

Downer, C., Ogden, F., 2004. Appropriate vertical discretization of Richards' equation for two-dimensional watershed-scale modelling. Hydrological Processes, 18(1):1–22.

Dunne, T., Black, R., 1970. Partial area contributions to storm runoff in a small New England watershed. Water Resources Research, 6(5):1296–1311.

Ebel, B., Mirus, B., Heppner, C., Vanderkwaak, J., Loague, K., 2009. First-order exchange coefficient coupling for simulating surface water–groundwater interactions: parameter sensitivity and consistency with a physics-based approach. Hydrological Processes, 23:1949–1959.

Ebel, B., Loague, K., 2006. Physics-based hydrologic-response simulation: Seeing through the fog of equifinality. Hydrological Processes, 20(13):2887–2900.

Ewen, J., Parkin, G., O'Connell, P., 2000. SHETRAN: distributed river basin flow and transport modeling system. Journal of hydrologic engineering, 5(3):250–258.

Ferguson, I., Maxwell, R., 2011. Hydrologic and land–energy feedbacks of agricultural water management practices. Environmental Research Letters, 6:014006.

Fetter, C., 1999. Contaminant hydrogeology. Prentice hall NJ.

Foglia, L., Hill, M., Mehl, S., Burlando, P., 2009. Sensitivity analysis, calibration, and testing of a distributed hydrological model using error-based weighting and one objective function. Water Resources Research, 45(6):W06427.

Fowler, H., Kilsby, C., 2007. Using regional climate model data to simulate historical and future river flows in northwest England. Climatic Change, 80(3):337–367.

Freeman, K., Girma, K., Teal, R., Arnall, D., Tubana, B., Holtz, S., Mosali, J., Raun, W., 2007. Long-Term Effects of Nitrogen Management Practices on Grain Yield, Nitrogen Uptake, and Efficiency in Irrigated Corn. Journal of Plant Nutrition, 30(12):2021–2036.

Freeze, R., Cherry, J., 1979. Groundwater. Prentice-Hall, Englewood Cliffs.

Freeze, R., Harlan, R., 1969. Blueprint for a physically-based, digitally-simulated hydrologic response model. Journal of Hydrology, 9(3):237–258.

Furman, A., 2008. Modeling coupled surface-subsurface flow processes: A review. Vadose Zone Journal, 7(2):741.

Garcia-Garizabal, I., Valenzuela, J., Abrahao, R., 2009. Evolution of the efficiency and agro-environmental impact of a traditional irrigation land in the middle Ebro Valley (2001-2007). Spanish Journal of Agricultural Research, 7(2):465–473.

Garcia-Vera, M., Martinez-Cob, A., 2004. Revision de las necesidades hidricas netas de los cultivos de la Cuenca del Ebro. Technical report, Ministerio de Medio Ambiente. Confederacion Hidrografica del Ebro. Oficina de Planificacion Hidrologica.

Gayler, S., Wang, E., Priesack, E., Schaaf, T., Maidl, F., 2002. Modeling biomass growth, N-uptake and phenological development of potato crop. Geoderma, 105(3-4):367–383.

Gelhar, L., Welty, C., Rehfeldt, K., 1992. A critical review of data on field-scale dispersion in aquifers. Water resources research, 28(7):1955–1974.

Goderniaux, P., Brouyère, S., Fowler, H., Blenkinsop, S., Therrien, R., Orban, P., Dassargues, A., 2009. Large scale surface-subsurface hydrological model to assess climate change impacts on groundwater reserves. Journal of Hydrology, 373(1-2):122–138.

Gottardi, G., Venutelli, M., 1993. A control-volume finite-element model for two-dimensional overland flow. Advances in Water Resources, 16(5):277–284.

Hansen, J., Refsgaard, J., Hansen, S., Ernstsen, V., 2007. Problems with heterogeneity in physically based agricultural catchment models. Journal of Hydrology, 342(1-2):1–16.

Hansen, S., Jensen, H., Nielsen, N., Svendsen, H., 1991. Simulation of nitrogen dynamics and biomass production in winter wheat using the Danish simulation model DAISY. Nutrient Cycling in Agroecosystems, 27(2):245–259.

Harbaugh, A., et al., 2000. MODFLOW-2000, the US Geological Survey modular ground-water model: User guide to modularization concepts and the ground-water flow process. US Dept. of the Interior, US Geological Survey.

Hargreaves, G., Samani, Z., 1985. Reference crop evapotranspiration from temperature. Applied Engineering in Agriculture, 1(2):96–99.

Hill, M., 1992. A Computer Program(MODFLOWP) for Estimating Parameters of a Transient, Three-dimensional, Ground-water Flow Model Using Nonlinear Regression. Available from Books and Open Files Reports Section, USGS Box 25425, Denver, CO 80225. USGS Open File Report 91-484, 1992. 358 p, 17 fig, 3 tab, 80 ref, 3 append.

Hill, M., 2006. The practical use of simplicity in developing ground water models. Ground water, 44(6):775–781.

Hill, M., Osterby, O., 2003. Determining extreme parameter correlation in ground water models. Ground water, 41(4):420–430.

Hill, M., Tiedeman, C., 2007. Effective groundwater model calibration: With analysis of data, sensitivities, predictions, and uncertainty. Wiley-Interscience.

Horton, R., 1931. The role of infiltration in the hydrologic cycle. Trans. Am. Geophys. Union, 12:189–202.

Horton, R., 1933. The role of infiltration in the hydrologic cycle. Trans. Am. Geophys. Union, 14:446–460.

Horton, R., 1936. The role of infiltration in the hydrologic cycle. Trans. Am. Geophys. Union, 17:344–357.

Hutson, J., Wagenet, R., 1991. Simulating nitrogen dynamics in soils using a deterministic model. Soil Use and Management, 7(2):74–78.

Huyakorn, P., Thomas, S., Thompson, B., 1984. Techniques for Making Finite Elements Competitve in Modeling Flow in Variably Saturated Porous Media. Water Resources Research, 20(8):1099–1115.

Jansson, S., 1958. Tracer studies on nitrogen transformations in soil with special attention to mineralisation/immobilisation relationships. Kungliga Lantbrukshogskolans Annaler, 24:101–361.

Johnsson, H., Bergstrom, L., Jansson, P., Paustian, K., 1987. Simulated nitrogen dynamics and losses in a layered agricultural soil. Agriculture, Ecosystems & Environment, 18(4):333–356.

Jones, J., Sudicky, E., Brookfield, A., Park, Y., 2006. An assessment of the tracer-based approach to quantifying groundwater contributions to streamflow. Water Resources Research, 42(2):W02407.

Jones, J., Sudicky, E., McLaren, R., 2008. Application of a fully-integrated surface-subsurface flow model at the watershed-scale: A case study. Water Resources Research, 44(3):W03407.

Kirchner, J., 2006. Getting the right answers for the right reasons: Linking measurements, a advance the science of hydrology. Water Resour. Res, 42.

Kitanidis, P., 1997. The minimum structure solution to the inverse problem. Water Resources Research, 33(10):2264–2272.

Klemes, V., 1986. Operational testing of hydrological simulation models/Vérification, en conditions réelles, des modèles de simulation hydrologique. Hydrological Sciences Journal, 31(1):13–24.

Klemes, V., 1987. The modelling of mountain hydrology: the ultimate challenge. Hydrology of Mountainous Areas, page 29.

Kolditz, O., Delfs, J., Burger, C., Beinhorn, M., Park, C., 2008. Numerical analysis of coupled hydrosystems based on an object-oriented compartment approach. Journal of hydroinformatics, 10(3):227–244.

Kolditz, O., Du, Y., Burger, C., Delfs, J., Kuntz, D., Beinhorn, M., Hess, M., Wang, W., van der Grift, B., te Stroet, C., 2007. Development of a regional hydrologic soil model and application to the Beerze-Reusel drainage basin. Environmental Pollution, 148(3):855–866.

Kollet, S., Maxwell, R., 2006. Integrated surface–groundwater flow modeling: A free-surface overland flow boundary condition in a parallel groundwater flow model. Advances in Water Resources, 29(7):945–958.

Kollet, S., Maxwell, R., Woodward, C., Smith, S., Vanderborght, J., Vereecken, H., Simmer, C., 2010. Proof of concept of regional scale hydrologic simulations at hydrologic resolution utilizing massively parallel computer resources. Water Resources Research, 46(4):W04201.

Kollet, S., Zlotnik, V., 2003. Stream depletion predictions using pumping test data from a heterogeneous stream-aquifer system (a case study from the Great Plains, USA). Journal of hydrology, 281(1-2):96–114.

Kristensen, K., Jensen, S., 1975. A model for estimating actual evapotranspiration from potential evapotranspiration. Nordic Hydrology, 6(3):170–188.

Kumar, R., Samaniego, L., Attinger, S., 2010. The effects of spatial discretization and model parameterization on the prediction of extreme runoff characteristics. Journal of Hydrology.

Li, Q., Unger, A., Sudicky, E., Kassenaar, D., Wexler, E., Shikaze, S., 2008. Simulating the multi-seasonal response of a large-scale watershed with a 3D physically-based hydrologic model. Journal of Hydrology.

Lindstrom, G., Johansson, B., Persson, M., Gardelin, M., Bergstrom, S., 1997. Development and test of the distributed HBV-96 hydrological model. Journal of hydrology, 201(1-4):272–288.

Loague, K., Heppner, C., Ebel, B., VanderKwaak, J., 2010. The quixotic search for a comprehensive understanding of hydrologic response at the surface: Horton, Dunne, Dunton, and the role of concept-development simulation. Hydrological Processes, 24:2499–2505.

Loague, K., Kyriakidis, P., 1997. Spatial and temporal variability in the R-5 infiltration data set: Deja vu and rainfall-runoff simulations. Water Resources Research, 33(12):2883–2895.

Loague, K., VanderKwaak, J., 2004. Physics-based hydrologic response simulation: platinum bridge, 1958 Edsel, or useful tool. Hydrological Processes, 18(15):2949–2956.

Maier, U., DeBiase, C., Baeder-Bederski, O., Bayer, P., 2009. Calibration of hydraulic parameters for large-scale vertical flow constructed wetlands. Journal of Hydrology, 369(3-4):260–273.

Maxwell, R., Chow, F., Kollet, S., 2007. The groundwater–land-surface–atmosphere connection: Soil moisture effects on the atmospheric boundary layer in fully-coupled simulations. Advances in Water Resources, 30(12):2447–2466.

Maxwell, R., Kollet, S., 2008. Quantifying the effects of three-dimensional subsurface heterogeneity on Hortonian runoff processes using a coupled numerical, stochastic approach. Advances in Water Resources, 31(5):807–817.

Monteith, J., 1965. Evaporation and environment. In Symp. Soc. Exp. Biol, volume 19, pages 205–234.

Mualem, Y., 1976. A new model for predicting the hydraulic conductivity of unsaturated porous media. Water Resources Research, 12(3):513–522.

Navidi, W., 2008. Statistics for engineers and scientists. McGraw-Hill Higher Education.

Neuman, S., 1990. Universal scaling of hydraulic conductivities and dispersivities in geologic media. Water Resour. Res, 26(8):1749–1758.

Panday, S., Huyakorn, P., 2004. A fully coupled physically-based spatially-distributed model for evaluating surface/subsurface flow. Advances in Water Resources, 27(4):361–382.

Penman, H., 1948. Natural evaporation from open water, bare soil and grass. Proceedings of the Royal Society of London. Series A, Mathematical and Physical Sciences, 193(1032):120–145.

Penman, H., 1956. Estimating evaporation. American Geophysical Union, 4:9–29.

Perez, A., Abrahao, R., Causape, J., Cirpka, O., Buerger, C., 2010. Implications of diffusive wave cascading plane simulations for the study of surface water - groundwater interaction with a 3-d fully-integrated catchment model. In XVIII International Conference on Water Resources.

Perez, A., Abrahao, R., Causape, J., Cirpka, O., Buerger, C., In review. Simulating the Transition of a Semi-Arid Rainfed Catchment towards Irrigation Agriculture. Journal of Hydrology.

Perez, A., Cirpka, O., Buerger, C., In Preparation. Implications of a Hillslope Equivalent Simulations on the Calibration of Physics-Based Models. Advances in Water Resources.

Poeter, E., Hill, M., 1997. Inverse Models: A Necessary Next Step in Ground-Water Modeling. Ground Water, 35(2):250–260.

Refsgaard, J., 1997. Parameterisation, calibration and validation of distributed hydrological models. Journal of Hydrology, 198(1-4):69–97.

Refsgaard, J., Knudsen, J., 1996. Operational validation and intercomparison of different types of hydrological models. Water Resources Research, 32(7):2189–2202.

Refsgaard, J., Storm, B., 1995. MIKE SHE In: Computer models of Watershed Hydrology, VP Singh ed. Water Resources, Highlands Ranch, Colo, pages 809–846.

Refsgaard, J., Storm, B., 1996. Construction, calibration and validation of hydrological models. Distributed hydrological modelling, pages 41–54.

Refsgaard, J., Storm, B., Refsgaard, A., 1995. Recent developments of the Systeme Hydrologique Europeen(SHE) towards the MIKE SHE. International Association of Hydrological Sciences, Publication, (231):427–434.

Refsgaard, J., Thorsen, M., Jensen, J., Kleeschulte, S., Hansen, S., 1999. Large scale modelling of groundwater contamination from nitrate leaching. Journal of Hydrology, 221(3-4):117–140.

Richards, L., 1931. Capillary conduction of liquids through porous media. Physics, 1(10):318–333.

Rijtema, P., Kroes, J., 1991. Some results of nitrogen simulations with the model ANIMO. Nutrient Cycling in Agroecosystems, 27(2):189–198.

Roche, M., 1963. Hydrologie de surface. Gauthier-Villars et ORSTOM , Paris, France. Gauthier-Villars et ORSTOM, Paris, France.

Sainju, U., Singh, B., Whitehead, W., 2001. Comparison of the effects of cover crops and nitrogen fertilization on tomato yield, root growth, and soil properties. Scientia horticulturae, 91(3-4):201–214.

Saltelli, A., 2008. Global sensitivity analysis: the primer. Wiley-Interscience.

Scanlon, B., Jolly, I., Sophocleous, M., Zhang, L., 2007. Global impacts of conversions from natural to agricultural ecosystems on water resources: Quantity versus quality. Water Resources Research, 43(3):W03437.

Schaap, M., Leij, F., 1998. Database-related accuracy and uncertainty of pedotransfer functions. Soil Science, 163(10):765.

Schaap, M., Leij, F., van-Genuchten, M., 2001. Rosetta: a computer program for estimating soil hydraulic parameters with hierarchical pedotransfer functions. Journal of Hydrology, 251(3-4):163–176.

Shiklomanov, I., 2000. Appraisal and assessment of world water resources. Water international, 25(1):11–32.

Smerdon, B., Mendoza, C., Devito, K., 2007. Simulations of fully coupled lake-groundwater exchange in a subhumid climate with an integrated hydrologic model. Water Resources Research, 43(1):W01416.

Stapleton, A., Wagenet, R., Turner, D., 1983. Corn growth and nitrogen uptake under irrigated, fertilized conditions. Irrigation Science, 4(1):1–15.

Sturges, H., 1926. The choice of a class interval. J. Amer. Statist. Assoc, 21:65–66.

Styczen, M., Storm, B., 1993. Modelling of N-movements on catchment scale-a tool for analysis and decision making. Nutrient Cycling in Agroecosystems, 36(1):7–17.

Sudicky, E., Jones, J., Park, Y., Brookfield, A., Colautti, D., 2008. Simulating complex flow and transport dynamics in an integrated surface-subsurface modeling framework. Geosciences Journal, 12(2):107–122.

Sun, N., Sun, N., Elimelech, M., Ryan, J., 2001. Sensitivity analysis and parameter identifiability for colloid transport in geochemically heterogeneous porous media. Water resources research, 37(2):209–222.

Therrien, R., McLaren, R., Sudicky, E., Panday, S., 2008. A three-dimensional numerical model describing fully integrated subsurface and solute surface flow and solute transport. Technical report.

Therrien, R., Sudicky, E., 1996. Three-dimensional analysis of variably-saturated flow and solute transport in discretely-fractured porous media. Journal of Contaminant Hydrology, 23(1-2):1–44.

Thompson, T., Doerge, T., Godin, R., 2002. Subsurface drip irrigation and fertigation of broccoli: I. Yield, quality, and nitrogen uptake. Soil Science Society of America Journal, 66(1):186–192.

van-Genuchten, M., 1980. A closed-form equation for predicting the hydraulic conductivity of unsaturated soils. Soil Sci. Soc. Am. J, 44(5):892–898.

van Griensven, A., Meixner, T., Grunwald, S., Bishop, T., Diluzio, M., Srinivasan, R., 2006. A global sensitivity analysis tool for the parameters of multi-variable catchment models. Journal of Hydrology, 324(1-4):10–23.

VanderKwaak, J., 1999. Numerical Simulation of Flow and Chemical Transport in Integrated Surface-Subsurface Hydrologic Systems. Ph.D. thesis, University of Waterloo.

VanderKwaak, J., Loague, K., 2001. Hydrologic-response simulations for the R-5 catchment with a comprehensive physics-based model. Water Resources Research, 37(4):999–1013.

Vogel, H., Ippisch, O., 2008. Estimation of a Critical Spatial Discretization Limit for Solving Richards' Equation at Large Scales. Vadose Zone Journal, 7(1):112.

Weill, S., Mazzia, A., Putti, M., Paniconi, C., 2011. Coupling water flow and solute transport into a physically-based surface-subsurface hydrological model. Advances in Water Resources, 34(1):128–136.

Xu, M., Eckstein, Y., 1995. Use of Weighted Least-Squares Method in Evaluation of the Relationship Between Dispersivity and Field Scale. Ground Water, 33(6):905–908.

Zhang, D., 2002. Stochastic Methods for Flow in Porous Media: Coping with Uncertainties. Academic Press.

Zheng, C., Wang, P., 1998. MT3DMS: A Modular Three-Dimensional Multispecies Transport Model for Simulation of Advection, Dispersion, and Chemical Reactions of Contaminants in Groundwater Systems; Documentation and User's Guide.

Zubillaga, M., Aristi, J., Lavado, R., 2002. Effect of phosphorus and nitrogen fertilization on sunflower (Helianthus annus L.) nitrogen uptake and yield. Journal of Agronomy and Crop Science, 188(4):267–274.

Appendix A

HydroGeoSphere Main Input File

```
!--------------------------  Problem description
Lerma Basin
ZAG, Tue., Mar 12, 2009 at 14:00
end title
!Lerma Basin: Rainfall Cola del saso + Kc= 5.e-5 m/s + 0.5ETP
!With corrections from Young-Jin and 4 hr Irrigation
!--------------------------  Grid generation
read gb 2d grid
../gb/lerma_ref

!3D mesh generation
generate layers interactive
    zone by layer

!Define the bottom of the domain
Base elevation
elevation constant
300.0
end

!Define the bottom layer of the "buro"
new layer
layer name
Middle layer
uniform sublayering
5
elevation from gb file
```

```
../gb/lerma_ref.nprop.hard
end

!Define a dummy layer to ensure 0.1 m vertical resolution for the
!first meter
new layer
layer name
Middle layer
uniform sublayering
10
elevation from gb file
../gb/lerma_ref.nprop.elevation -1.0 m
end

!Define the surface layer
new layer
layer name
Top layer
uniform sublayering
5
elevation from gb file
../gb/lerma_ref.nprop.elevation
end

end ! generate layers interactive
end grid generation

!Generate a file containing the geometry of the grid for verification
mesh to tecplot
lerma_grid.dat

!-------------------------  General simulation parameters
!Define units used in the simulation
units: kilogram-metre-second

transient flowrill storage height
0.002000

!Define the surface-subsurface coupling approach
```

```
dual nodes for surface flow

!Define extra simulation parameters
remove negative coefficients
finite difference mode
no nodal flow check

!-------------------------  Porous media properties
!Define the subsurface zonation
use zone type
porous media

!define de zones based on chosen nodes
clear chosen elements
choose elements gb
../gb/lerma_ref.echos.wzone1
6,21
new zone
1

clear chosen elements
choose elements gb
../gb/lerma_ref.echos.wzone2
6,21
new zone
2

clear chosen elements
choose elements gb
../gb/lerma_ref.echos.wzone3
6,21
new zone
3

clear chosen elements
choose elements gb
../gb/lerma_ref.echos.wzone4
6,21
new zone
```

```
4

clear chosen elements
choose elements gb
../gb/lerma_ref.echos.wzone5
6,21
new zone
5

clear chosen elements
choose elements gb
../gb/lerma_ref.echos.wzone6
6,21
new zone
6

clear chosen elements
choose elements gb
../gb/lerma_ref.echos.wzone7
6,21
new zone
7

clear chosen elements
choose elements gb
../gb/lerma_ref.echos.wzone8
6,21
new zone
8

clear chosen elements
choose elements by layer
1,3
new zone
9

!Give properties to the previously defined zones
properties file
lerma_multi_estimated.mprops
```

```
clear chosen zones
choose zone number
1
choose zone number
2
choose zone number
3
choose zone number
5
choose zone number
7
read properties
clay loam

clear chosen zones
choose zone number
8
read properties
sandy clay loam

clear chosen zones
choose zone number
4
choose zone number
6
read properties
clay

clear chosen zones
choose zone number
9
read properties
duro

!-------------------------  Overland flow properties
!Define surface properties for all of the surface elements
use zone type
surface
```

```
properties file
lerma_sec.oprops

!Create zones and give surface properties, i.e. roughness coefficient,
!obstruction and rill heights, for the 55 irrigated plots
include plot_distribution_2006.txt

!Give properties to the pinetrees
clear chosen faces
choose faces top gb
../gb/lerma_ref.echos.pinetrees
new zone
56

clear chosen zones
choose zone number
56
X friction
0.04
Y friction
0.04
obstruction storage height
0.002
rill storage height
0.002

!Give properties to the streams
! Main streams
clear chosen faces
choose faces top gb
../gb/lerma_ref.echos.mainstreams
new zone
57

clear chosen zones
choose zone number
57
X friction
```

```
0.025
Y friction
0.025
obstruction storage height
0.0005
rill storage height
0.0005

! Main streams
clear chosen faces
choose faces top gb
../gb/lerma_ref.echos.secstreams
new zone
58

clear chosen zones
choose zone number
58
X friction
0.03
Y friction
0.03
obstruction storage height
0.0005
rill storage height
0.0005

! Give the coupling length for the whole surface domain
clear chosen zones
choose zones all
coupling length
0.01

!-------------------------  Overland flow

!initial Conditions
use zone type
porous media
```

```
choose nodes all
initial head from output file
! Result from 20 years of simulation
../initial condition/lerma_dynwb.head.072


use zone type
surface
!default initial depth for overland
clear chosen nodes
choose nodes top
initial water depth
1.0d-4

!.............................. Boundary conditions

!Climatological Forcing

!Rainfall - Evapotranspiration
include Input2006.txt !hourly data

!Irrigation
include Irrigation2006.txt !daily data


!Critical depth
critical depth boundary all around

!No flow is the default subsurface boundary condition in HydroGeoSphere

!------------------------  Numerical Parameters
Newton maximum iterations
12
Jacobian epsilon
1.0d-6
Newton absolute convergence criteria
1.0d-2
Newton residual convergence criteria
1.0d-2
```

```
!--------------------------  Timestep controls
newton iteration control
10
water depth control
0.25
saturation control
0.05

maximum timestep
86400.
initial timestep
0.01
maximum timestep multiplier
2.0
minimum timestep multiplier
0.5

compute underrelaxation factor

Newton maximum update for head
1.0
Newton maximum update for depth
0.05
minimum relaxation factor allowed
0.1

flow solver maximum iterations
1000
flow solver convergence criteria
1.0e-8
!--------------------------  Output

!Adding file containing the dumping time (when the 3-D variables are
!printed)
include outtimes_1year.txt


!Defining the basin outlet
```

```
clear chosen nodes
choose nodes top gb
../gb/lerma_ref.nchos.outlet_corrected

set hydrograph nodes
Outlet


!Defining the piezometers
make observation point
well1
654746.21 4658636.27 342.00
make observation point
well2
655020.53 4658886.67 346.00
make observation point
well3
655514.66 4658738.65 347.00
make observation point
well4
656673.88 4658352.06 374.00
make observation point
well5
656198.23 4658222.68 366.00
make observation point
well6
656877.02 4656693.52 395.00
make observation point
well7
655152.77 4657989.73 347.00
make observation point
well8
655747.13 4657616.19 358.00
```

Appendix B

Computational Grid

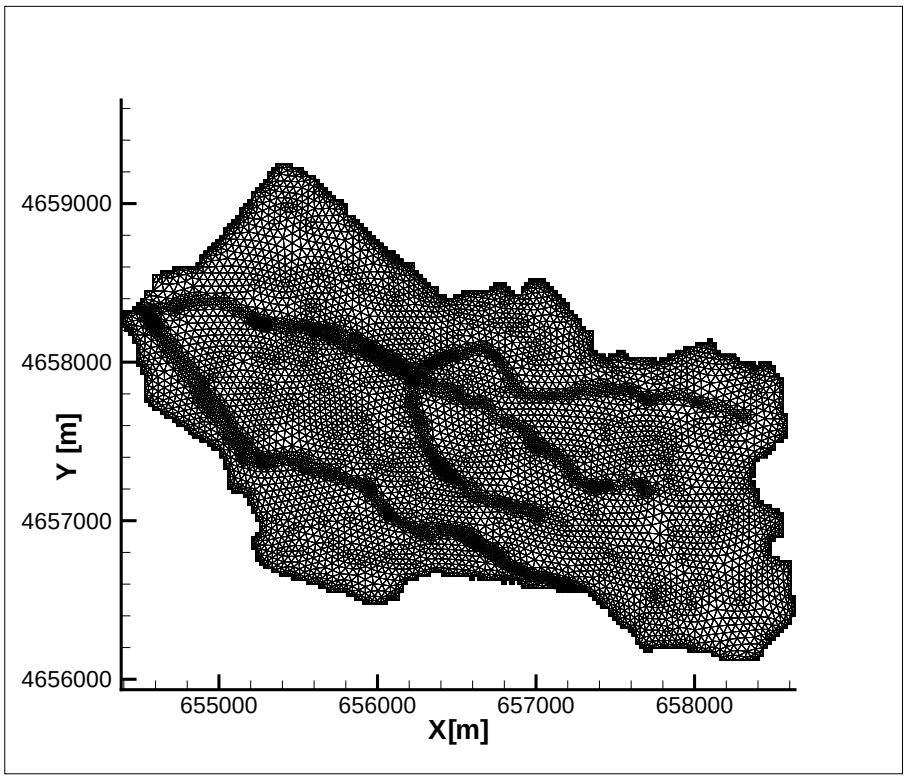

Figure B.1: Computational Grid of the Lerma basin including refinements